

# Cooperative surmounting of bottlenecks

D. Hennig<sup>1</sup>, C. Mulhern<sup>2</sup>, L. Schimansky-Geier<sup>3</sup>, G.P. Tsironis<sup>4,5</sup>, and P. Hänggi<sup>2,6,7</sup>

*1 Dept. Math., University of Portsmouth, Portsmouth, PO1 3HF, UK*

*2 Max Planck Institute for the Physics of Complex Systems, Nöthnitzer Str. 38, 01187 Dresden, Germany*

*3 Institut für Physik, Humboldt-Universität zu Berlin, Newtonstraße 15, 12489 Berlin, Germany*

*4 Dept. Phys., University of Crete, and IESL, FORTH, P. O. Box 2208, 71003 Heraklion, Greece*

*5 Dept. Phys., Nazarbayev University, 53 Kabanbay Batyr Ave., Astana 010000, Kazakhstan*

*6 Institut für Physik, Universität Augsburg, Universitätsstr. 1, D-86135 Augsburg, Germany*

*7 Nanosystems Initiative Munich, Schellingstr. 4, D-80799 München, Germany*

---

## Abstract

The physics of activated escape of objects out of a metastable state plays a key role in diverse scientific areas involving chemical kinetics, diffusion and dislocation motion in solids, nucleation, electrical transport, motion of flux lines superconductors, charge density waves, and transport processes of macromolecules and astrophysics, to name but a few. The underlying activated processes present the multidimensional extension of the Kramers problem of a single Brownian particle. In comparison to the latter case, however, the dynamics ensuing from the interactions of many coupled units can lead to intriguing novel phenomena that are not present when only a single degree of freedom is involved. In this review we report on a variety of such phenomena that are exhibited by systems consisting of chains of interacting units in the presence of potential barriers.

In the first part we consider recent developments in the case of a deterministic dynamics driving cooperative escape processes of coupled nonlinear units out of metastable states. The ability of chains of coupled units to undergo spontaneous conformational transitions can lead to a self-organised escape. The mechanism at work is that the energies of the units become re-arranged, while keeping the total energy conserved, in forming localised energy modes that in turn trigger the cooperative escape. We present scenarios of significantly enhanced noise-free escape rates if compared to the noise-assisted case.

The second part of the review deals with the collective directed transport of systems of interacting particles overcoming energetic barriers in periodic potential landscapes. Escape processes in both time-homogeneous and time-dependent driven systems are considered for the emergence of directed motion. It is shown that ballistic channels immersed in the associated mixed high-dimensional phase space are at the source for the directed long-range transport. Open problems and future directions are discussed in order to invigorate readers to engage in their own research.

*Keywords:*

---

## Contents

<b>1</b>	<b>Introduction</b>	<b>2</b>
<b>2</b>	<b>Deterministic dynamics and self-organised cooperative escape dynamics</b>	<b>5</b>
2.1	Crossing one-dimensional anharmonic potential barriers . . . . .	5
2.1.1	Escape of a one-dimensional chain . . . . .	5
2.1.2	Transition states . . . . .	6
2.1.3	Modulational instability and spontaneous localisation . . . . .	7
2.1.4	The formation of breathers . . . . .	9
2.1.5	Thermally activated escape . . . . .	11
2.2	Deterministic escape dynamics of two-dimensional coupled nonlinear chains . . . . .	13

2.2.1	Two-dimensional coupled unit chain model . . . . .	14
2.2.2	Energy redistribution process . . . . .	15
2.2.3	Transition states and collective escape . . . . .	15
2.3	Mexican hat potential . . . . .	17
2.3.1	Wave modes and escape dynamics . . . . .	18
2.4	Surmounting collectively oscillating bottlenecks . . . . .	22
2.5	Escape assisted by entropic localisation . . . . .	24
2.6	Cooperativity in molecular dissociation . . . . .	26
2.6.1	Mechanism of a triatomic dissociation . . . . .	26
2.6.2	Cooperative reaction paths . . . . .	27
<b>3</b>	<b>Collective transport</b>	<b>30</b>
3.1	Transport in general . . . . .	30
3.1.1	Individual particles . . . . .	30
3.1.2	Transport with two or more degrees-of-freedom . . . . .	31
3.1.3	Anomalous transport . . . . .	32
3.1.4	Transport in irregular domains . . . . .	33
3.1.5	Properties that determine transport features . . . . .	33
3.1.6	Ballistic transport . . . . .	35
3.1.7	Beneficial role of chaos . . . . .	35
3.1.8	Cooperative transport mechanism . . . . .	35
3.2	Transient-chaos induced transport in autonomous systems . . . . .	36
3.2.1	Symmetric Model . . . . .	38
3.2.2	Asymmetric model . . . . .	41
3.2.3	Symmetry breaking and emergence of a current . . . . .	44
3.2.4	The emergence of a non-zero current in the symmetric case . . . . .	45
3.2.5	Time-reversal symmetry manifolds . . . . .	46
3.2.6	The effect of broken symmetries . . . . .	47
3.3	Non-autonomous systems . . . . .	50
3.3.1	Collective periodic running states in coupled particle dynamics . . . . .	50
3.3.2	Features of collective driven transport . . . . .	52
3.3.3	Interaction-induced negative mobility . . . . .	53
3.3.4	Adiabatic driving and directed transport in many unit systems . . . . .	57
3.3.5	The driven chain system of interacting units . . . . .	57
3.3.6	Extremely long transients of directed transport . . . . .	58
<b>4</b>	<b>Summary and outlook</b>	<b>59</b>
<b>5</b>	<b>Acknowledgements</b>	<b>61</b>
<b>6</b>	<b>References</b>	<b>62</b>

## 1. Introduction

Ever since the seminal work by Kramers (for a comprehensive review see Ref. [1]) there has been significant interest in the dynamics of escape processes of single particles, of coupled degrees of freedom or of chains of coupled objects out of metastable states. To accomplish the escape the considered objects must cross an energetic barrier, separating the local potential minimum from a neighbouring attracting domain. From the perspective of statistical physics it is predominantly the thermally activated escape, based on the permanent interaction of the considered system with a heat bath, which is being investigated [1, 2]. The coupling to the heat bath causes dissipation and local energy fluctuations and consequently the escape process is conditioned on the creation of a rare, optimal fluctuation which in turn triggers an escape process.

To put it differently, an optimal fluctuation transfers sufficient energy to the system so that the system is able to statistically surmount the energetic bottleneck associated with the transition state. Characteristic time-scales of such a process are determined by the inverse of the corresponding rates of escape out of the domain of attraction. Within this topic, numerous extensions of Kramers escape theory and of first passage time problems have been widely investigated [1, 2, 3, 4]. Early generalisations to multi-dimensional systems date back to the late 1960's [5]. This method is by now well established and is commonly put to use in biophysical contexts, and for a great many other applications occurring in physics and chemistry and related areas [6, 7, 8, 9, 10, 11, 12, 13, 14, 15, 16, 17, 18, 19, 20, 21, 22]. More modern developments of rate theory address escape under time-dependent driving, typically being of periodically varying nature [23, 24, 25, 26, 27] so that a time periodic asymptotic state emerges as the most stable state. Applications of such time-dependent driven escape problems involve the objective of escape across sloshing potential barriers or wells or also the stochastic neural dynamics involving a time-periodically varying threshold to “firing events”.

Distinct from the numerous studies of thermally induced escape processes driven by the coupling of the system to an external heat bath is the *microcanonical situation*; i.e., when only the internal total fixed energy of a many-particle system is available to perform structural transitions – a situation which been studied to a much lesser extent. The underpinning key question is: how is it possible that many degrees of freedom subject to a deterministic and conservative dynamics can overcome a potential barrier given that initially its energy is almost equally shared among the units so that the system is far away from the critical equilibrium configuration related with a saddle point in configuration space. The latter configuration is commonly referred to as a localised transition state [28].

Concerning the attainment of localised structures it is by now an established fact that nonlinearity and diffusion in extended systems may cooperate to give rise to the formation of coherent structures that emerge even from an initial, almost homogeneous state [29]. The concentration of an originally distributed physical quantity to a few degrees of freedom in confined regions of a spatially extended and homogeneous systems proceeds typically in a self-organised manner. In recent years the concept of intrinsic localised modes (LMs), or discrete breathers, as time-periodic and spatially localised solutions of nonlinear lattice systems has proved to present the archetype of excitations describing localisation phenomena in numerous physical situations [30, 31, 32, 33, 34, 35]. For the creation of localised structures, modulational instability, leading to a self-induced modulation of an initial linear wave with a subsequent generation of localised pulses, has proven to be an effective mechanism. In this way energy localisation in a homogeneous system is achievable. For example, breathers have been successfully applied to describe localised excitations which reproduce typical features of the thermally induced opening dynamics of DNA duplex molecules such as the magnitude of the amplitude and the time-scale of the oscillating bubble preceding full strand separation (denaturation) [36, 37, 38, 39, 40]. The appearance of LMs in damped, driven deterministic nonlinear lattice systems has been the subject of the investigations in [41, 42, 43, 44]. Furthermore, the spontaneous formation of LMs (breathers) from thermal fluctuations in lattice systems, when thermalised with the Nosé-method [45] has been demonstrated in [46, 37, 47].

The objective of this review is to elaborate on the scenario of possible escape from a metastable domain of attraction; the main mechanism being based on the cooperativity between the interacting units of *purely deterministic* systems. Thus, no additional coupling to a thermal bath assists the escape. We consider macroscopic discrete, coupled nonlinear oscillator chains with typically 100 links, as these may appear as realistic models in neuroscience, in various biophysical contexts or also in networks of coupled superconductors, e.g. see in Refs. [32, 48, 49, 50]. An efficient deterministic escape that is driven in absence of noise is particularly important when dealing with low temperatures for which the activated escape becomes far too slow, or also for situations with many coupled nonlinear units in presence of non-thermal intrinsic noise that scales inversely with the square root of the system size.

We demonstrate how *cooperative behaviour* in systems of interacting units facilitates the task performance of surmounting potential barriers, which individual units, due to sheer limiting energetic reasons, would never be able to accomplish. In fact, it is the self-organised directed energy redistribution among the units of the coupled chain, leading to the formation of the critical LM, that makes the collective barrier crossing of the chain in a microcanonical situation possible. Moreover, in the deterministic context the barrier crossing of

a chain turns out to be (by far) more efficient compared with a thermally activated chain for small ratios between the total energy of the chain and the barrier energy. Also directed particle transport in metastable (multiple-well) periodic potential landscapes necessitates appropriately coordinated energy transfer processes among the interacting units enabling consecutive barrier crossings. While there exists a vast literature on directed transport of single particles moving mainly in periodic potentials based on the so-called ratchet effect (for a reviews see [19, 22, 51] and cited references therein), by far less is known regarding the transport of systems coupled particles through periodic landscapes. Especially, the effects stemming from the coupling between the particles on the emergence of a current require a reinforced study. Moreover, in contrast to the driven one-dimensional case, with its three-dimensional phase space, the dynamics of coupled units evolve in a higher-dimensional phase space, of which the details of its structure remain more elusive. Thus, an additional goal of the current review is to present also the state of the art relating to such collective transport.

The review is organised as follows: In Sec. 2.1 the cooperative escape dynamics of a one-dimensional chain from the metastable state of cubic external potential is considered. As an extension to the one-dimensional chain system, in Sec. 2.2 follows the investigation of a two-dimensional chain model with pairwise nonlinear Morse interaction. The special focus will be on the influence of the additional degree of freedom on the self-organised escape process. Escape from metastable states in a system of higher (geometrical) complexity in the form of a ring of interacting units evolving in a Mexican hat two-dimensional potential landscape is studied in the subsequent section.

In view of controlling the process of barrier crossing we consider in the next section the collective escape dynamics of a chain of coupled units in the presence of thermal noise and friction. In addition, the application of a weak external ac-field leads to periodically oscillating landscape of bottlenecks. We show that the formation of the critical LM can be distinctly accelerated via the application of a weak external ac-driving. By use of optimally oscillating barrier configurations it is feasible that a far faster escape can be promoted, leading to a drastic enhancement of the escape dynamics. Particularly at low temperatures, where the rate of thermal barrier crossing is exponentially suppressed, such a scenario can be very beneficial.

That even a very weak driving force suffices to trigger fast escape for a chain situated initially extremely close to the bottom of the potential well and thus containing a vanishingly small amount of energy is demonstrated in Sec. 2.5.

The chaos-assisted mechanism of dissociation of interacting molecules related to an organised barrier crossing is studied in Sec. 2.6.

Regarding collective transport we distinguish between the *time-independent* (autonomous) and the *time-dependent* (non-autonomous) Hamiltonian systems. Beginning with autonomous Hamiltonian systems modeling two coupled particles moving in a periodic washboard potential the guiding aim is to understand the conditions under which directed transport in phase-space is supported. Novel mechanisms pertaining to directed transport that are a direct consequence of the interaction between the particles are discussed.

Subsequent augmentation of the system by the inclusion of time-dependent driving and damping terms adds further complexity to the coupled dynamics. For directed particle transport mediated by periodically driving forces we derive exact results regarding the collective character of the running solutions.

Interaction-induced absolute negative mobility [52, 53, 54, 55, 56] of two coupled particles evolving in a symmetric and periodic substrate potential which is subjected to a static bias force is the subject of the next section. The bias force of magnitude  $F_0$  serves to tilt the potential landscape such that particle motion in the direction of the bias is favoured. It is shown that within a range of coupling strengths, the coupled particles can become self-organised and go, as periodic running states, frequency locked with the driving, against the direction of the bias force.

Regarding features of transport exhibited by systems with many degrees of freedom we consider the Hamiltonian dynamics of a one-dimensional chain of linearly coupled particles in a spatially periodic potential which is subjected to a time-periodic mono-frequency external field. For a chain escaping collectively from a potential, the possibility of the successive generation of a directed flow based on large accelerations is illustrated.

We conclude the review with a discussion of open questions and point out promising directions which may invigorate readers to undertake their own future studies in this research area.

## 2. Deterministic dynamics and self-organised cooperative escape dynamics

### 2.1. Crossing one-dimensional anharmonic potential barriers

#### 2.1.1. Escape of a one-dimensional chain

Consider first a one-dimensional chain of  $N$  linearly coupled units of mass  $m$  [57, 58, 59]. The chain is positioned in a cubic external potential where its equally spaced units perform one-dimensional motion with elongations  $q_n(t)$ ,  $n = 1, \dots, N$ , in parallel directions. That is, the  $q_n$  describe transversal elongations that are perpendicular to the direction of the potential valley (see Fig. 1). Each unit of mass unity experiences a nonlinear force caused by the potential

$$V(q_n) = \frac{\omega_0^2}{2}q_n^2 - \frac{a}{3}q_n^3. \quad (1)$$

The parameter  $a > 0$  controls the strength of the nonlinearity in the system. This potential possesses a metastable equilibrium at  $q_{min} = 0$  corresponding to the rest energy  $E_{min} = 0$  and the maximum is located at  $q_{max} = \omega_0^2/a$  with barrier energy  $E_{max} \equiv \Delta E = \omega_0^6/6a^2$ . Furthermore, there are coupling forces acting between neighbouring units with coupling parameter  $\kappa$  regulating the strength of the interactions. Moreover, each unit possesses a corresponding momenta  $p_n(t)$  that are canonically conjugate to  $q_n(t)$ . Unless otherwise stated, periodic boundary conditions are imposed throughout this report. First, we consider the deterministic dynamics in a micro-canonical situation with a Hamiltonian set-up. This implies that the *total* energy of the whole chain,  $E$ , is conserved.

Passing to dimensionless quantities by the following rescalings,  $\tilde{q}_n = a/(\omega_0^2)q_n$ ,  $\tilde{p}_n^2 = a^2/(\omega_0^6)p_n$ , and  $\tilde{t} = \omega_0 t$ , we obtain a Hamiltonian with only a single remaining parameter, the effective coupling strength  $\tilde{\kappa} = \kappa/(\omega_0^2)$ . In what follows we omit the tilde notation.

The Hamiltonian of the considered chain thus reads:

$$\mathcal{H} = \sum_{n=1}^N \left[ \frac{p_n^2}{2} + \frac{\kappa}{2} (q_n - q_{n+1})^2 + V(q_n) \right], \quad V(q_n) = \frac{q_n^2}{2} - \frac{q_n^3}{3}. \quad (2)$$

The resulting equations of motion become

$$\ddot{q}_n + q_n - q_n^2 - \kappa (q_{n+1} + q_{n-1} - 2q_n) = 0, \quad q_{N+1} = q_1. \quad (3)$$

For the study of escape we initially place the units of the chain close to the bottom of the external potential, i.e. nearby  $q_{min} = 0$ , providing each unit with very little energy compared to the barrier energy of the external potential. Due the system dynamics the chain is able to generate a critical state – a critical elongation – in a self-organised manner, thereby surpassing the potential local maximum. This initiates a transition of the chain into the unbounded regime  $q_n > q_{max} = 1$ , for all  $n = 1, \dots, N$ , which we refer to as an escape event. Fig. 1 illustrates various transition states which will be described in more detail below. For a single particle to overcome the potential barrier it needs to be supplied with an energy in excess of  $\Delta E = V(1) - V(0) = 1/6$ .

In what follows we make evident that the generation of these critical states proceeds within a highly efficient manner, even in cases where the total chain energy  $E$  is small compared to the cumulative barrier energy of all units; i.e.,  $E \ll N \cdot \Delta E$ . This low-energy regime is provided by the following initial preparation of the system: (i) First, the whole chain is placed at a fixed position  $q_n(0) = q_0$ ,  $n = 1, \dots, N$ , near the bottom of the potential well. (ii) Then, the position and momenta of all units are iso-energetically randomised while keeping the total energy a constant – i.e.,  $E = const..$  The random position and momentum values are uniformly distributed in intervals

$$|q_n(0) - q_0| \leq \Delta q \quad |p_n(0)| \leq \Delta p.$$

The value of  $q_0$  is chosen in such a way that the average excitation energy of a single unit is small compared to the depth,  $\Delta E$ , of the potential well. For our numerical simulations we consider chains comprising  $N = 100$  units.

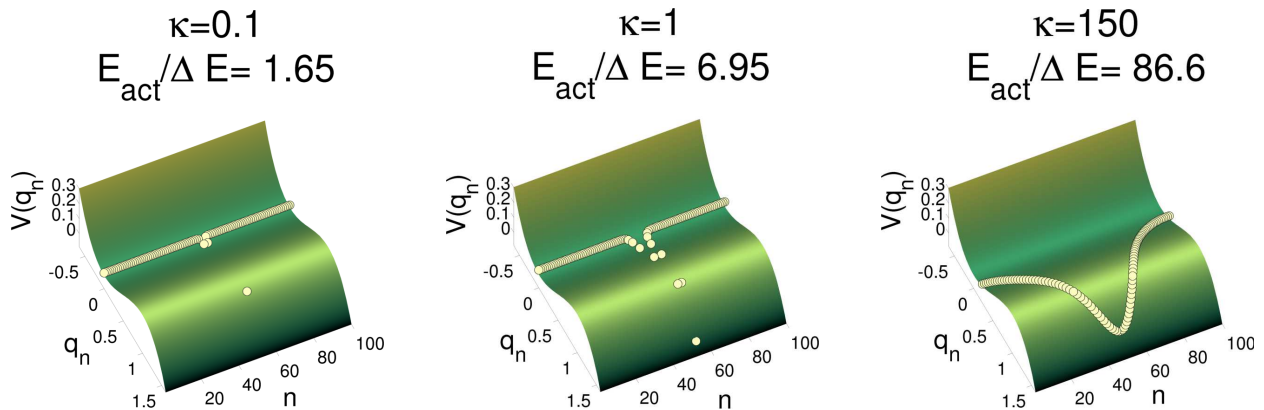


Figure 1: (Colour online) Transition state configurations for a chain placed in a cubic potential for three different values of coupling strength  $\kappa$ . The chain consists of  $N = 100$  units, whose dynamics obey Eq. (3). With increasing coupling strength, more units are required for the chain to adopt the transition state. Moreover, the ratio  $E_{act}/\Delta E$ , (see text) of the activation energy required for the chain to adopt the transition state and the barrier height, increases with  $\kappa$  – that is, more energy is required in the transition state configuration, as the interactions between the units become stronger. Source: Figure taken from Ref. [57].

### 2.1.2. Transition states

For conservative Hamiltonian systems local minima of the energy surface,  $H = E = const.$ , are Lyapunov stable. That is, orbits in the vicinity of a local elliptic equilibrium point never leave it as their associated energy is conserved. Only those orbits with energies exceeding the energy associated with a neighbouring saddle point are no longer bound to the basin. Thus, the saddle point is referred to as a transition state, as it separates bounded from unbounded orbits. Concerning our objective, the system's energy has to exceed the transition state energy to make an escape event possible. To determine this transition state, we have to solve  $\nabla U(q_1, q_2, \dots) = 0$ , where  $U$  denotes the potential energy (thus the transition state is a fixed-point) and the solution is such that all eigenvalues of the Hessian matrix of  $U$  are positive, except for a single negative one.

In the one-dimensional chain model the transition state configurations solve the stationary equation<sup>1</sup>

$$q_n^* - q_n^{*2} - \kappa (q_{n+1}^* + q_{n-1}^* - 2q_n^*) = 0, \quad (4)$$

and satisfy the above mentioned condition on the eigenvalues,  $\lambda^H$ , of the Hessian  $H$

$$H_{i,j} = \delta_{i,j} (2\kappa + 1 - 2q_i^*) - \kappa (\delta_{i,j+1} + \delta_{i,j-1}).$$

In the case of a vanishing coupling strength the units decouple. Therefore, the fixed points of the system consist of all the configurations where each unit is placed either on the maximum of the potential barrier or the potential valley, that is  $q_n^* = \{0, 1\}$ . In this case also the Hessian matrix,  $H$ , becomes diagonal and we can directly read off its eigenvalues,  $\lambda_n^H = 1 - 2q_n^*$ . Demanding that all but one of the eigenvalues be negative, the transition states are found to be all the configurations where all unit are positioned in the potential valley except for one that is placed on top of the potential barrier. The according energy is  $E_{act}(\kappa = 0) = \Delta E = 1/6$ .

In contrast, a very large coupling strength corresponds to a situation where the chain becomes effectively homogeneous and can be considered as a single unit. Therefore, the transition state corresponds to a chain configuration where all units are placed at the maximum of the potential. This can be seen by taking the limit  $\kappa \rightarrow \infty$  in Eq. (4). If we want  $q_n^*$  to take on values within an energetically bounded regime we must

<sup>1</sup>An alternative approach for the one-dimensional chain model is presented in [59]. It casts the stationary equation into a two-dimensional map and links the localised lattice solutions to its homoclinic orbits.

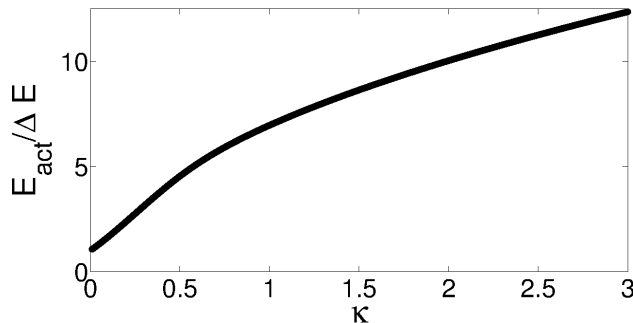


Figure 2: Activation energy (energy of transition state configurations) as a function of the coupling strength  $\kappa$ , for chains consisting of  $N = 100$  units. Each unit evolves in a cubic potential and is linearly coupled to its nearest neighbours. There is a clear tendency for the activation energy of the chain to increase with increasing coupling strength  $\kappa$ . Source: Figure taken from Ref. [57].

have  $q_{n+1}^* + q_{n-1}^* - 2q_n^* = 0$  in order to satisfy Eq.(4) in this limit. In the case of periodic boundary conditions this becomes equivalent to  $q_n^* = q^*$  so that Eq.(4) becomes  $q^*(1 - q^*) = 0$ . Which of its two roots corresponds to the transition state becomes clear from the linear stability analysis of Eq.(3) for this effective one unit problem

$$\ddot{q} = -q + q^2 \approx -q^* + q^{*2} + (-1 + 2q^*)q = (-1 + 2q^*)q. \quad (5)$$

Only the case  $q_n = q^* = 1$  is associated with the inherent instability of a transition state. Accordingly, the transition state energy is found to be  $E_{\text{act}}(\kappa \rightarrow \infty) = N \Delta E = N/6$ .

To determine the transition state in the intermediate coupling strength regime we used the dimer method, first introduced in [60], which is a minimum-mode following method that solely makes use of gradients of the potential surface. The obtained transition states together with their energy are represented in Fig. 1 and Fig. 2, respectively. The latter is computed by substituting the solutions  $q_n^*$  to Eq. (4) into the energy function given in Eq. (2) together with  $p_n^* = 0$ . The maximal amplitude of the hair pin-like transition state configuration grows with increasing  $\kappa$  until it reaches a critical elongation from which it decreases until the entire chain approaches the maximum of the potential barrier as described above. Further, the stronger the coupling is the higher the activation energy, which is presented in Fig. 2 in terms of the barrier height  $\Delta E$ .

### 2.1.3. Modulational instability and spontaneous localisation

The energy that is initially almost homogeneously distributed along the entire chain quickly concentrates into local excitations of single oscillators. This process is governed by the formation of regularly shaped wave patterns, so-called breathers which are spatially localised and time-periodically varying solutions. Their emergence is due to a mechanism known as *modulational instability*. In the following we elaborate on the onset of this modulational instability by applying it to the above situation. Further details are contained in [61] and [62].

As an approximation for small oscillation amplitudes we can neglect the nonlinear term in Eq. (3). The resulting equation in linear approximation exhibits phonon solutions with frequency  $\omega$  and wave number  $k = 2\pi k_0/N$  (with  $k_0 \in \mathbb{Z}$  and  $-N/2 \leq k_0 \leq N/2$ ) related by the dispersion relation

$$\omega^2 = 1 + 4\kappa \sin^2\left(\frac{k}{2}\right).$$

We make an Ansatz that only takes into account the first harmonics (rotating wave approximation)

$$q_i = F_{1,i}(t) e^{-it} + F_{0,i}(t) + F_{2,i}(t) e^{-2it} + c.c.$$

The amplitudes of the harmonics are expected to be of a lower order of magnitude ( $|F_{0,i}| \ll |F_{1,i}|, |F_{2,i}| \ll |F_{1,i}|$ ). Furthermore, we assume our envelope functions to vary slowly ( $|\dot{F}_{m,i}| \ll |F_{m,i}|$ ) as well as the

phonon band to be small ( $1 > 4\kappa$ ). Within the limits of these assumptions we obtain a discrete nonlinear Schrödinger equation (DNLS) for the amplitudes of the first harmonic.

$$2i\dot{F}_{1,i} = \kappa((F_{1,i-1} + F_{1,i+1}) + 2F_{1,i}) - \frac{10}{3} |F_{1,i}|^2 F_{1,i}. \quad (6)$$

We want to study the stability of this equation's plane wave solutions in the presence of small perturbations  $|\delta B_i(t)| \ll 1$  and  $|\delta \Psi_i(t)| \ll 1$ , leading to a new Ansatz for the envelope function

$$F_{1,n}^{pert.} = (A + \delta B_n(t)) e^{i((kn - \Delta\omega t) + \delta \Psi_n(t))}. \quad (7)$$

The perturbations are sufficiently small so that we can expand the envelope function up to the first order in  $\delta$  and neglect all terms of higher order. Using the Ansatz Eq. (7) in Eq. (6) leads to a complex differential equation for the perturbation functions  $B(t)$  and  $\Psi(t)$ . The real and imaginary part of this equation are independent. Hence, collecting all terms of first order in  $\delta$  results in two linear relations.

$$-A\dot{\Psi}_i = -\frac{\kappa}{2} \{A \sin k (\Psi_{i-1} - \Psi_{i+1}) + \cos k (B_{i+1} + B_{i-1})\} - \frac{10}{3} A^2 B_i \quad (8)$$

$$2\dot{B}_i = -\kappa \{A \cos k (\Psi_{i+1} + \Psi_{i-1} - 2\Psi_i) + \sin k (B_{i+1} - B_{i-1})\}. \quad (9)$$

Again, the solution to those coupled equations are plane waves

$$\Psi_n = \Psi^0 e^{i(Qn - \Omega t)} \quad B_n = B^0 e^{i(Qn - \Omega t)} \quad (10)$$

with the dispersion relation

$$(\Omega - \kappa \sin k \sin Q)^2 = \kappa \cos k \sin^2 \left( \frac{Q}{2} \right) \left( 4\kappa \cos k \sin^2 \left( \frac{Q}{2} \right) - \frac{20}{3} A^2 \right) \quad (11)$$

which describes the stability of the  $Q$ -mode perturbation on the  $k$ -mode carrier wave.  $Q$  and  $k$  have a  $2\pi$  periodicity and can therefore be chosen to be in the first Brillouin zone. Furthermore, we can restrict the range of  $k$  and  $Q$ :  $k, Q \in \{0, \pi\}$ , because negative values correspond to waves with the opposite direction of propagation.

The perturbations are stable for  $\Omega \in \mathbb{R}$  which is the case when the right hand side of Eq. (11) is positive. Therefore, all carrier waves with  $k \in \{\pi/2, \pi\}$  are stable with respect to all perturbation modes. For  $k \in \{0, \pi/2\}$  perturbations will grow, provided that

$$\cos k \sin^2 \left( \frac{Q}{2} \right) \leq \frac{5A^2}{3\kappa}. \quad (12)$$

We can then find an according growth rate

$$\Gamma(Q) = |\text{Im}(\Omega)| = \sin \left( \frac{Q}{2} \right) \sqrt{\frac{20}{3} \kappa \cos k \left( A^2 - \frac{3}{5} \kappa \sin^2 \left( \frac{Q}{2} \right) \cos k \right)} \quad (13)$$

which, for the case that  $A^2 \leq \frac{6}{5} \kappa \cos k$ , has its maximum at

$$Q_{\max} = 2 \arcsin \sqrt{\frac{5A^2}{6\kappa \cos k}}. \quad (14)$$

Otherwise the maximum growth rate is found at  $Q = \pi$ . The corresponding growth rates become

$$\Gamma_{\max} = \begin{cases} \Gamma(Q_{\max}) = \frac{5}{3} A^2 & \text{if } A^2 \leq \frac{6}{5} \kappa \cos k \\ \Gamma(\pi) = \sqrt{\frac{20}{3} \kappa \cos k (A^2 - \frac{3}{5} \kappa \cos k)} < \Gamma(Q_{\max}) & \text{if } A^2 > \frac{6}{5} \kappa \cos k \end{cases} \quad (15)$$

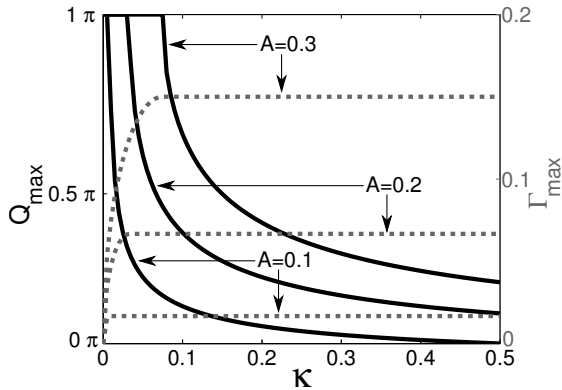


Figure 3: Fastest growing plane wave modes (solid line, left axis) - Eq. (14), and their growth rates (dashed line, right axis) - Eq. (15), for a wave number  $k = 0.0$ , both as a function of the coupling strength  $\kappa$ . The parameter  $A$  controls the amplitude of the envelop function Eq. (7). Source: Figure taken from Ref. [57].

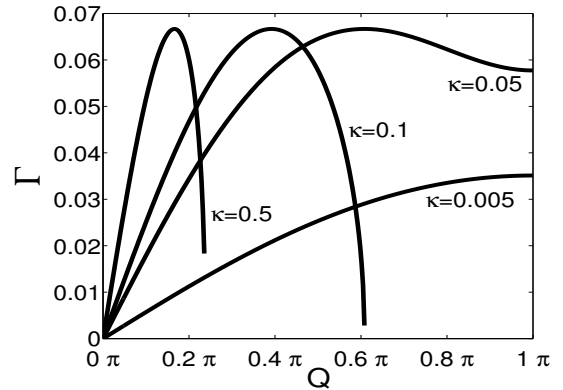


Figure 4: Growth rates  $\Gamma$  of perturbations to the derived Discrete Nonlinear Schrödinger equation - Eq. (6), as a function of the unstable plane wave  $Q$ -modes according to Eq. (13) from a  $k = 0$  carrier mode with  $A = 0.2$ . Each curve is obtained for a different value of the coupling strength  $\kappa$ , as indicated in the figure. Source: Figure taken from Ref. [57].

We recall that our system is initially prepared in a slightly perturbed  $k = 0$  mode. This is thus the only possible carrier wave mode; a result which follows because of the amplitudes,  $A$ , required for the other modes (which scale with the amplitude of the perturbation). The reason being that either the amplitudes are likely too small to generate growing modes – note the inequality given by Eq. (12) – or the arising maximal growth rates are suppressed. Evaluating the growth rate of instabilities of the  $k = 0$  carrier mode for different values of  $\kappa$  (Fig. 4), we find that the modulational instability becomes more mode selective upon increasing  $\kappa$ . Hence, for large values of  $\kappa$  the only relevant unstable modes are near the fastest growing mode depicted in Fig. 3. In such a situation we expect the emergence of a regular wave pattern (an array of breathers) that efficiently does localise energy and thereby enhances the escape of the chain.

#### 2.1.4. The formation of breathers

The mean values of (postive amplitudes)  $q_0$  are taken in such a way that the average excitation energy of a single unit,  $E_0$ , is small compared to the depth,  $\Delta E$ , of the potential well. Due to the choice of sufficiently small detunings  $\Delta q$  the initial lattice state,  $q_n(0) = q_0 + \Delta q$ , is close to an almost homogeneous state and yet such disturbed that there result very small – but non-vanishing – initial interaction terms. More precisely, Eq. (16) determines the energy of a unit

$$E_n = \frac{p_n^2}{2} + V(q_n) + \frac{\kappa}{4} ((q_{n+1} - q_n)^2 + (q_{n-1} - q_n)^2). \quad (16)$$

The last term in Eq. (16) represents the interaction energy of an individual unit. The initial set-up discussed above allows for weak, non-vanishing, interactions between neighbouring units. Thus an energy exchange between the coupled units is entailed. The initial energy per unit obeys  $E_n \ll \Delta E$ , but is still sufficiently large to initiate the excitation of nonlinear modes. In this realm the formation of localised excitations can be explained by the above discussed modulational instability. This mechanism initiates an instability of a plane wave when small perturbations of non-vanishing wavenumbers are imposed on the almost homogeneous state close to  $q_n(0) = q^* = 0$  for all  $n \in [1, N]$ . The instability – giving rise to an exponential growth of the perturbation – destroys the initial configuration at a critical wavenumber. Eventually, a pattern of localised humps gets formed, virtually with equal distance between them distributed on the chain [15–17]. A detailed study of the parameter's influences on the creation of the localised humps and in consequence on the escape process can be found in [17].

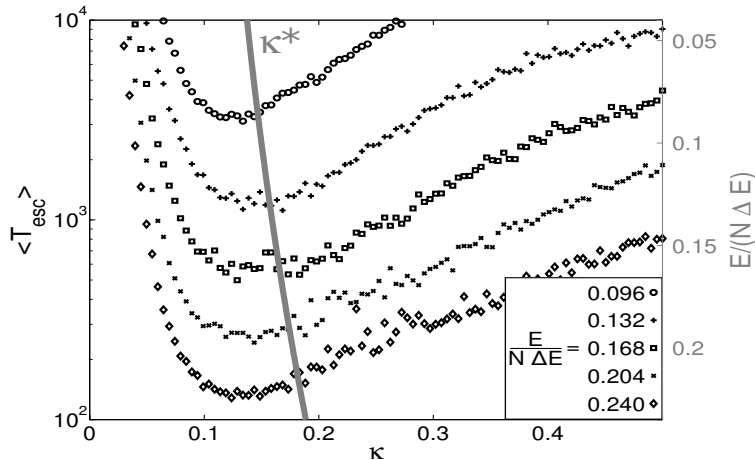


Figure 5: Semi-logscale plot showing the mean escape times (marker symbols) for chains, consisting of  $N = 100$  units, initially confined to the metastable minimum of a cubic potential. The averaging was done over 500 realisations of randomised initial conditions, each of which obey the relations  $|q_n(0) - q_0| \leq \Delta q$  and  $|p_n(0)| \leq \Delta p$  with  $\Delta q = 0.05$ ,  $\Delta p = 0.05$ . The different symbols represent different ratios of the total energy  $E$  and  $N$  times the barrier height, as indicated in the key. The solid grey line represents the analytical approximation for the optimal coupling strength for energy values given by the right-hand axis. Source: Figure taken from Ref. [57].

For a chain situated near the bottom of the potential the system is initially prepared in a slightly perturbed  $k = 0$  mode. In such a situation analytical considerations establish the emergence of a regular wave pattern (an array of breathers) that efficiently localises energy and thereby enhances the escape of the chain [58, 59].

Regarding the strength of the interaction between the units we note that in the limit  $\kappa \rightarrow 0$ , leading to uncoupled units, as well as the opposite limit of very strong couplings leading to a rigid rod-like chain, the chain behaves like a single particle, and so the escape is prevented on the grounds of too little energy available in each unit. In between these two limiting cases there exists a value of the coupling strength  $\kappa$  that optimises the escape rate. The latter can be approximated analytically [58].

The escape time of a unit is defined as the time instant when the unit passes across a coordinate value far beyond the potential barrier. Setting this value to  $q = 20q_{max}$  no likely recrossing back into the potential valley occurs. The mean escape time of the chain is then determined by the average of the escape times of all of its units. For the numerical evaluation of mean escape times in dependence of  $\kappa$  (see Fig. 5) the system - Eq. (3) - was integrated using a fourth order Runge-Kutta scheme. Numerical accuracy was obtained by ensuring the energy deviation to remain smaller than the order of  $10^{-12}$ . The mean escape times were determined from 500 realisations of randomised initial conditions at a given energy. The maximal integration time is  $5 \cdot 10^5$  time units.

Fig. 5 demonstrates the resonance behaviour of the mean escape time as a function of  $\kappa$  and also reveals a fairly good accordance of the analytical approximation of the optimal  $\kappa = \kappa^*$  with the simulation results (for details see [58],[57]). Regarding the pronounced variation of the mean escape times (ranging over several orders of magnitude) for different energies we remark that a low system energy does not supply single breathers with an energy sufficient to trigger an escape event. For example, for  $\kappa = 0.15$  and  $E/(N\Delta E) = 0.1$  typically an array with ten or more breathers forms so that each one can hold only an energy  $E/N_B < \Delta E$ , with  $N_B$  being the number of breathers. Nevertheless, an escape takes place, eventually. This implies a further concentration of energy due to breather coalescence taking place at later times after the initial creation of the breather array. The time evolution of the energy distribution defined in Eq. (16), shown in Fig. 6, illustrates this feature.  $E_n$  was monitored in time (upwards) for two exemplary cases. Energy is localised in both cases starting from an initially almost homogeneous state. In Fig. 6a, corresponding to a relatively high energy, we see the appearance of a regular breather pattern.

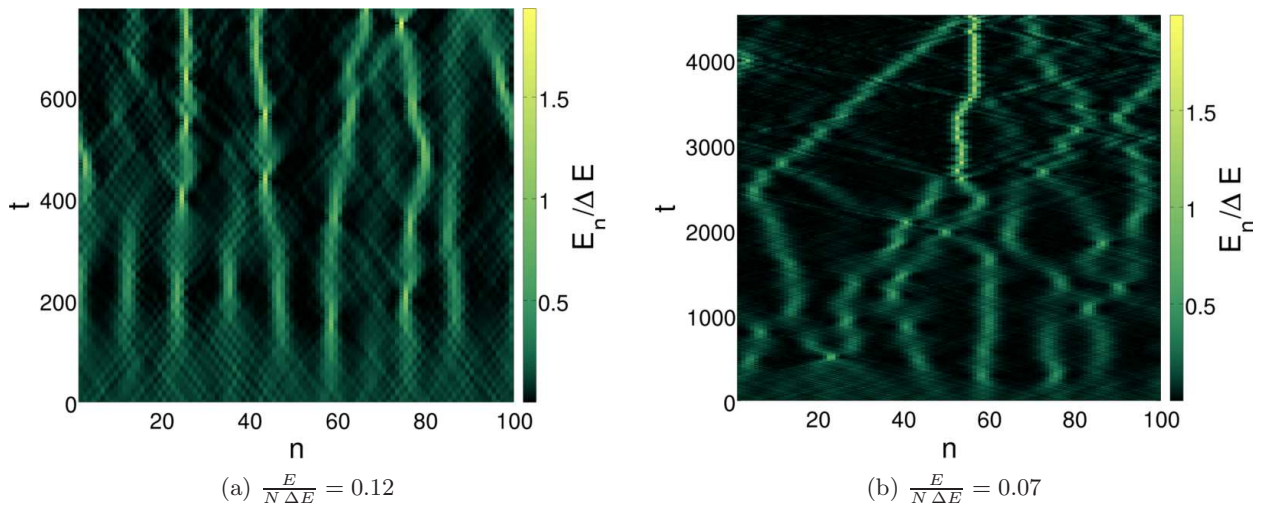


Figure 6: (Colour Online) Heat maps showing the temporal evolution of the energy distribution  $E_n(t)$  for linear chains evolving in a cubic potential - Eq. (3). Panels a) and b) represent different ratios of the total energy  $E$  and  $N$  times the barrier height. The localisation of energy from an initially homogeneous state causes in both cases an escape at the end of the depicted time frame. While the chain's energy in Fig. 6a is sufficiently high to let an individual breather from the early breather array to surpass the potential barrier, the lower energy in Fig. 6b necessitates a merging of breathers to cause the critical chain elongation. The parameter values are:  $\kappa = 0.15$ ,  $\Delta q = 0.05$ ,  $\Delta p = 0.05$ ,  $N = 100$ . Note the different time scales. Source: Figure taken from Ref. [57].

Every breather concentrates enough energy to certain units in order to trigger an escape, which in this case happens at  $t \approx 700$ . In contrast, the lower system energy in Fig. 6b does not allow for a direct escape of the initially formed breathers. Instead, breathers start an erratic movement. After an inelastic interaction they merge and can thereby eventually result in a configuration exceeding the critical chain elongation, see also [46]. However, this secondary process is slow compared to the (direct) breather formation which explains the different orders of magnitude of the escape times scale, in dependence of the energy content, seen in Fig. 5.

### 2.1.5. Thermally activated escape

The previous investigations dealt with a deterministic chain dynamics governing an escape event. In this part we study how a thermal bath with a temperature  $T$  assists the transition over the barrier, cf. in Ref. [59]. For this purpose we consider the associated Langevin equation driven by additive thermal noise,

$$\ddot{q}_n + q_n - q_n^2 - \kappa(q_{n+1} + q_{n-1} - 2q_n) + \gamma\dot{q}_n + \xi_n(t) = 0, \quad (17)$$

with a common damping parameter  $\gamma$  and uncorrelated Gaussian white noise terms  $\xi_n(t)$ . In order to be able to compare the deterministic situation to the thermally activated setting, the associated conserved energy  $E$  in the Hamiltonian case and the average energy  $\overline{E}$  transferred from the bath need to be equal. The latter is governed by the correlation function of the noisy force  $\xi(t)$  given by

$$\langle \xi_n(t)\xi_{n'}(t') \rangle = 2\gamma\overline{E}/N \delta_{n,n'} \delta(t-t'), \quad (18)$$

expressing that the mean energy of all particles is given by  $\overline{E}$ . If expressed by the bath temperature, every particle assumes on average  $k_B T$ , i.e.  $\overline{E} = N k_B T$  with  $k_B$  being the Boltzmann constant.

We measure the mean escape time for the system described by Eq. (17). The latter is numerically integrated using an second-order Heun stochastic solver scheme, again with a maximal integration time of  $5 \cdot 10^5$  time units. The system is initialised with all units set to the minimum of the potential and zero momenta. The system thermalises and the moment when its energy reaches  $\overline{E}$  is taken as the initial time for our studies of escape.

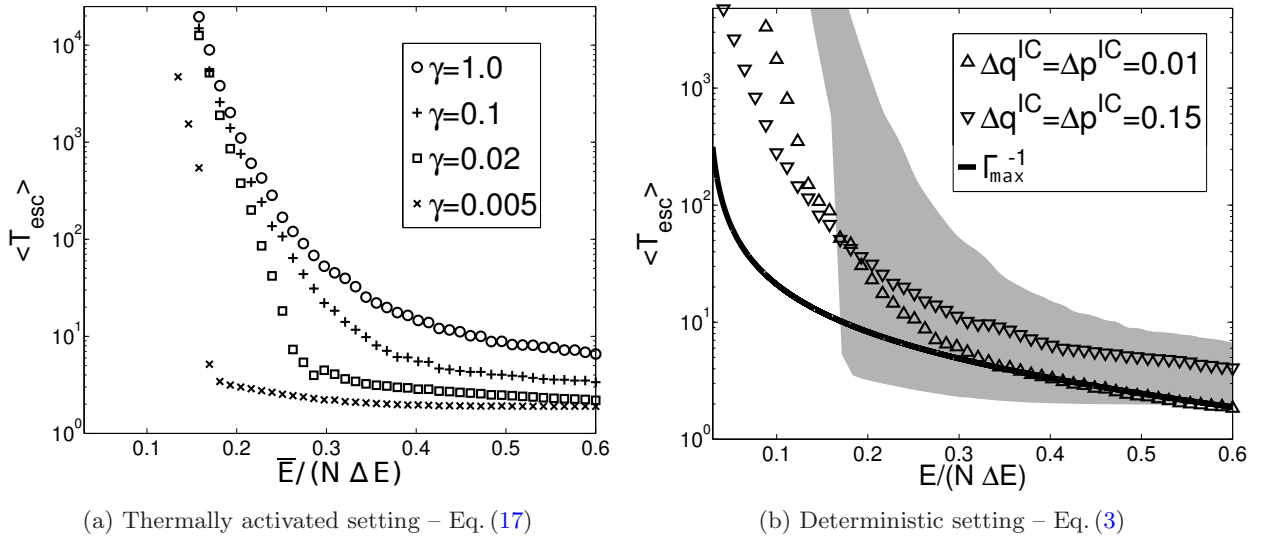


Figure 7: Lin-log plot showing the mean escape times in the thermally activated case – Eq. (17) – for different values of the damping constant, Fig. 7a, and their comparison to the deterministic setting, Fig. 7b, for 500 realisations each. The grey area in Fig. 7b sketches the mean escape times for the thermally activated case for  $0.005 < \gamma < 1.0$  as shown in Fig. 7a, whereas the symbols show results from the deterministic set-up with initial conditions given in the inset. The solid black line in Fig. 7b is the inverse of the maximal growth rate,  $\Gamma_{max}$ , obtained from Eq. (15). The parameter values are:  $\kappa = 0.15$ ,  $N = 100$ . In both panels  $\bar{E}$  and  $E$  are expressed in units of  $N$  times the barrier energy, with  $\bar{E} = Nk_bT$  and  $E$  being the total system energy in the deterministic case. Source: Figure taken from Ref. [57].

We study the system for the optimal coupling constant,  $\kappa = 0.15$ . Fig. 7a shows the mean escape times of 500 realisations for different values of the damping constant in dependence of  $\bar{E}$ . Fig. 7b compares these times (depicted as the grey surface) to the corresponding mean escape times of the deterministic system. It additionally shows the characteristic time constant for the formation of breathers due to modulational instability, given by Eq. (13), where the  $k = 0$  phonon amplitude,  $A$ , is related to the system energy via  $E(A) = N V(A)$ , with  $V(\cdot)$  is defined in Eq. (2).  $Q$  is the wave number of the perturbation-mode acting on the  $k$ -mode carrier wave.

Especially for smaller energies the deterministic escape is considerably faster than the thermally activated one. Notably for  $\bar{E}/(N \Delta E) < 0.1$  and quite contrary to the deterministic setting, escape events are practically absent during our simulations time in the thermal case. For larger mean energy values this picture can change to a higher efficiency of the thermal escape process when damping is weak. Also two deterministic settings with different magnitudes of the random initial perturbations swap their features of escape upon passing from low to high energies.

How can the speedy escape in the deterministic system, in comparison to the thermally activated escape, be explained? For small values of  $\gamma$  the system approaches the deterministic setting. This entails a tendency towards a more efficient and pronounced localised energy distribution as seen when comparing Fig. 8a (low damping strength  $\gamma = 0.005$ ) and Fig. 8b (high damping strength  $\gamma = 1.0$ ). The relaxation time of the chain scales with the inverse of the damping constant. Correspondingly, the life times of local excitations grow with decreasing  $\gamma$ . The outcome is a more heterogeneous energetic structure where thermal fluctuations are more likely to cause critical chain elongations. This explains the faster escape comparing small with large damping constants. But even in the case of very small  $\gamma$  the relaxation time is still much shorter than the time needed for the coalescence of multiple breathers (which is of the order of several hundred time units, see Fig. 6b). Therefore, the long term cumulative concentration of energy is generally inhibited in the thermal case. This explains the virtual impossibility of a thermal escape for small energies.

For higher energies the deterministic escape is mostly assisted by arrays of breathers that are formed

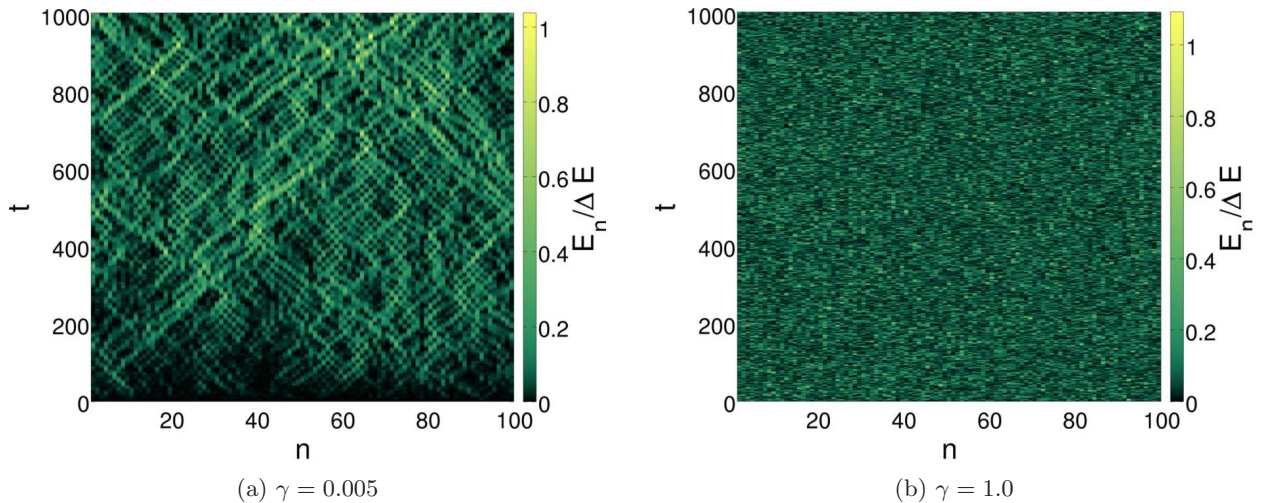


Figure 8: (Colour Online) Heat maps showing the temporal evolution of the energy distribution  $E_n(t)$  in the thermally activated case - Eq. (17) - for chains consisting of  $N = 100$  units. The two panels were obtained using different values of the damping parameter  $\gamma$ : A smaller damping constant leads to a higher degree of energy localisation. The remaining parameter values are:  $\overline{E}/(N \Delta E) = 0.15$ ,  $\kappa = 0.15$  with  $\overline{E} = Nk_bT$  and  $\Delta E$  being the barrier height. Source: Figure taken from Ref. [57].

as the result of modulational instability (referred to as initial breathers). The formation time of the initial breather array can be estimated by the inverse of the maximal growth rate,  $\Gamma_{\max}$  from Eq. (15). Fig. 7b shows the expected convergence of  $\Gamma_{\max}^{-1}$  to the deterministic escape times for large energies. We recall that  $\Gamma_{\max}$  was determined on the basis of a linear expansion in the perturbations. This explains the better match of  $\Gamma_{\max}^{-1}$  and  $\langle T_{esc} \rangle$  in the case of smaller initial perturbations. The divergence of  $\Gamma_{\max}^{-1}$  with the mean escape time for small energies again gives evidence to the fact that the initial breather array does not induce an escape and other mechanisms enhancing the degree of localisation are required.

In the thermally activated case with large energy the mobility of the breathers becomes amplified if noise acts. If the breathers possess longer life times, *i.e.* for smaller damping, a few (usually not more than two) breathers can temporarily merge and approach a critical chain elongation. Starting with a heterogeneous energy structure after its thermalisation then leads to shorter escape times in the presence of noise compared to the deterministic setting that first has to re-allocate energy from an initially almost homogeneous state. Conversely, for stronger damping, the life times of breathers is too short and the energy distribution remains mostly homogeneous (see Fig. 8b). The escape of the chains over the potential barrier then rely entirely on rare, strong enough, spontaneous fluctuations of the noise term and so the mean escape times generally become comparatively large.

Regarding the impact of the initial perturbations,  $\Delta q, \Delta p$ , of a homogeneous state on the escape time (cf. right panel, Fig. 7) in the deterministic case we note that, as the initial conditions for smaller perturbations are closer to the  $k = 0$  phonon mode, the initial breather array emerges more quickly so that the escape times are smaller when the energy is high enough for initial breathers to initiate the escape. Contrarily, when low energy necessitates coalescence, stronger perturbations lead to a higher breather mobility which speeds up the breather coalescence so that the escape times become smaller.

## 2.2. Deterministic escape dynamics of two-dimensional coupled nonlinear chains

As an extension to the one-dimensional chain system, as discussed in the previous section, we consider next a two-dimensional chain model with pairwise nonlinear Morse interaction between neighbouring units and study the role of the additional degree of freedom on the self-organised escape process [63]. In distinct contrast to the previous study taking into account solely motion in the transition direction, in this case dynamical motion is also allowed *transverse* to the barrier along the well of the external potential. As a

consequence, in addition to the formation of localised large amplitude breathers, with amplitudes evolving in transition direction, global oscillations of the chain transverse to the barrier are observed. Eventually a few chain links accumulate locally sufficient energy to cross the barrier. This mechanism is shown to take place for both linear rod-like and for coil-like configurations of the chain in two dimensions.

### 2.2.1. Two-dimensional coupled unit chain model

Our study treats a spring mass chain model. The chain consists of  $N$  units which are pairwise connected through nonlinear springs. The motion of these units takes place in the  $x - y$ -plane. We denote by  $q_{xn}$  the displacement of the  $n$ th unit in the  $x$ -direction, also referred to as the transition coordinate, while in the transverse  $y$ -direction displacements from the rest position are denoted by  $q_{yn}$ . The local on-site potential  $U$  reads as

$$U(q_{xn}) = \frac{m\omega_0^2}{2}q_{xn}^2 - \frac{a}{3}q_{xn}^3, \quad (19)$$

with  $n = 1, \dots, N$ . We assume a nonlinear interaction potential of Morse type between adjacent units of the chain

$$U_M(r_{n+1,n}) = D_0 [1 - \exp(-d(r_{n+1,n} - l)^2)]^2, \quad (20)$$

with depth  $D_0$ , range parameter  $d$ ,  $l$  the equilibrium distance of the units (also referred to as bond length), and  $r_{n+1,n}$  the Euclidean distance of two neighbouring units,

$$r_{n+1,n} = \sqrt{(q_{xn+1} - q_{xn})^2 + (q_{yn+1} - q_{yn})^2}, \quad (21)$$

with  $n = 1, \dots, N$ . The corresponding Hamiltonian of the two-dimensional chain model reads as

$$H = \sum_{n=1}^N \left( \frac{p_{xn}^2}{2} + \frac{p_{yn}^2}{2} + U(q_{xn}) \right) + \sum_{n=1}^{N-1} U_M(r_{n+1,n}). \quad (22)$$

Passing to dimensionless quantities is achieved with the following rescaling procedure:  $\tilde{q} = qd$ ,  $\tilde{p} = pd/(m\omega_0)$ ,  $\tilde{t} = \omega_0 t$ ,  $\tilde{a} = a/(dm\omega_0^2)$ . Furthermore, we use  $\kappa = 2D_0d^2/(m\omega_0^2)$ . In what follows we omit the tilde notation. The intrinsic length scale

$$s = q_x^{max} - q_x^{min} = \frac{1}{a}, \quad (23)$$

where  $q_x^{max} = m\omega_0/a^2$  and  $q_x^{min} = 0$  denote the position of the potential maximum and minimum respectively, plays an important role. To be precise, small ratios  $l/s$ ; i.e., the ratio of the bond length  $l$  and the intrinsic length scale  $s$  of the system, cause coil-like chain configurations, while rodlike states appear for ratios of the order of one or above. Note that in the limit of vanishing  $a$  the barrier disappears and the intrinsic length scale diverges.

The equations of motion derived from the Hamiltonian read:

$$\begin{aligned} \ddot{q}_{xn} &= -q_{xn} + aq_{xn}^2 \\ &- \kappa [1 - \exp(-d(r_{n+1,n} - l))] \exp(-d(r_{n+1,n} - l)) \frac{q_{xn} - q_{xn+1}}{r_{n+1,n}} \\ &- \kappa [1 - \exp(-d(r_{n,n-1} - l))] \exp(-d(r_{n,n-1} - l)) \frac{q_{xn} - q_{xn-1}}{r_{n,n-1}} \end{aligned} \quad (24)$$

$$\begin{aligned} \ddot{q}_{yn} &= -\kappa [1 - \exp(-d(r_{n+1,n} - l))] \exp(-d(r_{n+1,n} - l)) \frac{q_{yn} - q_{yn+1}}{r_{n+1,n}} \\ &- \kappa [1 - \exp(-d(r_{n,n-1} - l))] \exp(-d(r_{n,n-1} - l)) \frac{q_{yn} - q_{yn-1}}{r_{n,n-1}}, \end{aligned} \quad (25)$$

for  $n = 2, \dots, N - 1$ . Moreover, open boundary conditions are imposed.

Like in the study of the one-dimensional case, initially the chain is in a flat state of amplitude  $q_{x0}$  on which small perturbations are exerted by taking random initial amplitudes which are uniformly distributed

in an interval  $|q_{xn}(0) - q_{x0}| \leq \Delta q_x$ . The mean values of  $q_{x0}$  are taken in such a way that the average excitation energy of a single unit,  $E_0$ , is small compared to the depth,  $\Delta E$ , of the potential well. Due to the choice of sufficiently small displacements  $\Delta q_x$  the initial lattice state,  $q_{xn}(0) = q_{x0} + \Delta q_{xn}$ , is close to an almost homogeneous state and yet sufficiently disturbed that there result small but non-vanishing initial interaction terms. Thus an energy exchange between the coupled units is instigated. The initial momenta  $p_{xn} = 0$  are set zero. The initial amplitudes in the transverse direction are  $q_{yn}(0) = nl$  and the momenta  $p_{yn}(0) = 0$ , entailing the conservation of the centre of mass in the  $y$ -direction.

### 2.2.2. Energy redistribution process

In the beginning, the system energy is essentially equally shared among all units in the chain, expressed by a homogeneous elongation of the whole chain in the transition direction, and the escape scenario proceeds as follows: Just like for the one-dimensional study (see previous Section) the process of modulational instability governs the dynamics of the system during an early phase of the evolution. In particular this triggers the formation of an array of localised solutions (large-amplitude breathers) in the  $x$ -direction. Later on, the influence of the – compared to a purely one-dimensional unit model – second, transverse, degree of freedom crucially affects the dynamical processes of the coupled unit chain. Interestingly, we observe that in the cases of both very short bond lengths  $l/s \ll 1$  and bond lengths obeying  $l/s > 1$  the structure, which is formed by a modulational instability, persists for very long times, whereas it disappears rather fast for intermediate values of the bond length. Such a decrease of the amplitudes of the localised structures in the  $x$ -direction comes along with the excitation of motions in the transverse degree of freedom. As one measure of the energy content in the  $x$ - and the  $y$ -direction the respective kinetic energy can be taken. Initially the mean of the  $x$ -kinetic energy of the  $x$ -motion is  $E_{kin}^x = 0.5E$ , whereas  $E_{kin}^y = 0$ . Induced by the breather formation in the  $x$ -direction an enhanced interaction of neighbouring units is caused and since the interaction force couples the motion in the  $x$ - and in the  $y$ -direction an energy transfer is initiated. In fact, one observes that a state of equipartition is reached for which  $E_{kin} = 0.25E$  in both the  $x$ - and the  $y$ -direction, respectively. The time until equipartition is attained decreases with increasing coupling strength. We underline, that the energy transfer described above constitutes a purely nonlinear effect. We could never observe a complete back transfer of energy from the  $y$ - to the  $x$ - motion. Rather a breathing-like behaviour, for which the chain contracts and relaxes along its axis periodically in time results. This behaviour of global oscillations of the chain as a whole along the transverse direction appears in addition to the large-amplitude breathers evolving in the transition coordinate direction involving fairly strong energy localisation at certain sites.

### 2.2.3. Transition states and collective escape

Whether an unit involved in a large amplitude breather state is able to escape from the region of bounded motion inside the potential well or is held back depends on the corresponding amplitude pattern as well as on the coupling strength. The associated critical chain configuration – called the transition state – is determined as the solution of the corresponding stationary system which represents a force-free configuration corresponding to a first-order saddle point in configuration space. There appear two scenarios: The peak of the localised amplitude profile of the critical configuration is situated either at one free end of the chain (referred to as boundary critical localised mode – BCLM), or somewhere in between the free ends (referred simply to as CLM).

Regarding CLMs it is found that, for a given coupling strength  $\kappa$ , the transition state is represented by a thin needle shape with the central unit situated beyond the barrier if  $l < s$  (akin to the one-dimensional situation). In general, the smaller the bond length  $l$  the larger is the extension of the critical localised mode along the  $x$ -direction and the more units are elongated from the potential minimum. In contrast, for  $l > s$ , the central unit is always situated at the barrier, while its neighbours are arranged in such a way that there remains no stress arising from the bonds. We underline that the ends of the chain are free and there act thus no restoring forces. Hence, in order to reduce the stress arising from the elongation of the central unit over the barrier, its neighbours can be displaced force free along the  $y$ -axis. Furthermore, due to the strong degree of localisation the obtained structures remain the same when increasing the number of units in the chain. It should be stressed that the alignment of the units along the potential minimum situated at

$q_{min}^x = 0$  is completely arbitrary, as long as next neighbours keep their equilibrium distance  $l$ . In particular, completely coiled configurations can be critical transition states, too.

For the BCLMs, the qualitative dependencies on the system's parameters  $\kappa$  and  $l$  remain – compared to the situation when the critical peak is formed between the ends – the same. But – since the unit beyond the barrier is now connected to only one neighbour inside the potential well and thus the acting back-pulling forces are smaller – the force-free critical state is less elongated.

Concerning the dependence of the activation energy on the bond length, we observe a decay of  $E_{act}$  with enlarging bond length. In the limit  $l \rightarrow s$  its value approaches  $E_{act} = \Delta E$ . We remark that in the case of  $l \geq s$  we always find a critical stationary solution with activation energy  $E_{act} = \Delta E$ . Surprisingly, in the limit of long bonds the activation energy becomes independent of the coupling strength and is equal to the net barrier height. As long as  $l < s$ , the activation energy grows with an increasing value of the coupling strength. The growth is the stronger the smaller is  $l$ . In the case of BCLMs the activation energies are remarkably lower compared to transition states with a peak somewhere in between the loose ends. A detailed analysis of the energetic contributions to the activation energy reveals that the major part of  $E_{act}$  is stored as deformation energy of the springs. Since a BCLM contains fewer stretched springs, the value of activation energy is lower. Crucially, the process of barrier crossing of the chain is not only influenced by the amount of energy provided to the system. It also depends on the ratio of different length scales, since the geometry plays a vital role for motions in a two-dimensional potential landscape. Thus, the rate of escape will be significantly affected by the choice of the parameters.

The escape time of a chain is as defined in the one-dimensional case (see Sec. 2.1). In Fig. 9 a typical escape process is illustrated by showing the escape times  $t_{esc}$  versus the position of the escaping unit when the corresponding unit passes  $q_x^{thresh}$ . First, one unit moves directly beyond the barrier (since the underlying dynamics is irregular for different realisations of initial conditions the incident escape can happen at an arbitrary location in the chain), and therefore adjacent units are subjected to pulling forces and a cascade of escapes is initiated in a relatively short time interval.

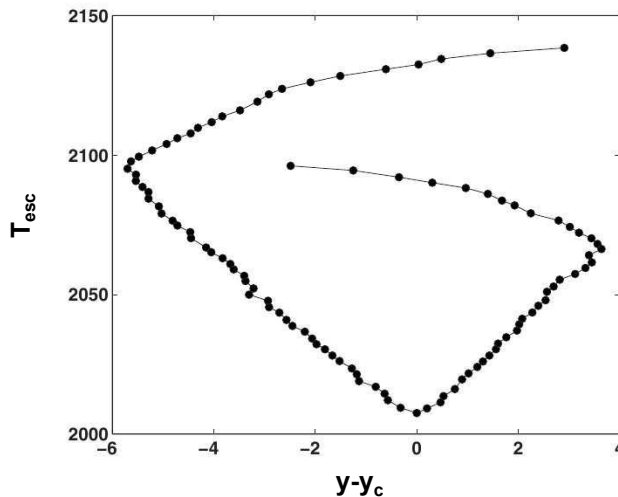


Figure 9: Escape process for one realisation of initial conditions for the two-dimensional chain model - Eqs. (24)-(25): Escape times  $t_{esc}$  of the units versus the  $y$  position when the corresponding unit passes the threshold value  $q_x^{thresh}$  far beyond the barrier. The position of the unit which overcomes the barrier first is denoted by  $y_c$ , all other positions are shifted by this value. The initial conditions are  $q_{x0} = -0.05$  and  $\Delta q_x = 0.001$ , yielding  $E_0/\Delta E = 0.219$ . The parameter values are  $a = 5$ ,  $\kappa = 0.9$ ,  $l/s = 1.25$ , and  $N = 100$ . Source: Figure adapted from Ref. [63].

Regarding the dependence of the escape time on the coupling strength  $\kappa$ , the fraction of escape events, as a function of  $\kappa$ , has been calculated. Numerically 200 different realisations of initial conditions, each with a simulation time set to  $t_{sim} = 10^4$ , corresponding to more than 1500 periods of linear ground-state oscillations, were considered. Since not all simulations lead to escape events during  $t_{sim}$  the mere calculation

of the mean escape time alone is not suitable.

Fig. 10 depicts the fraction of successful exits of the entire chain for two different bond lengths as a function of the coupling strength  $\kappa$ . The values of the bond lengths are chosen in such way that one is smaller and one is larger than  $s$ . For  $\kappa = 0.45$  one observes the first rare events of escape of the complete unit chain. The fraction of successful escape events of the entire chain further increases with enhanced coupling strength. Whereas for the larger bond length at  $\kappa = 0.75$  the curve saturates to 1 – i.e., all initial preparations lead to an escape of the whole chain – the curve for the smaller bond length reaches there a maximum of 0.835. With further increasing of the coupling strength the latter curve descends reaching a value of 0.345 at  $\kappa = 1.5$ .

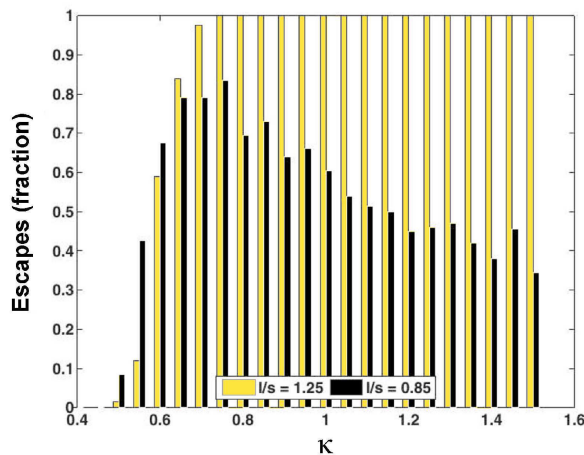


Figure 10: (Colour online) Fraction of completed escapes of the chain as a function of the coupling strength  $\kappa$  for the two-dimensional chain model - Eqs. (24)-(25), with chains consisting of  $N = 100$  units. The value of the bond length  $l$  is given in the legend, in units of the intrinsic length scale of the system  $s$  - Eq. (23). The initial conditions are  $q_{x0} = -0.05$  and  $\Delta q_x = 0.001$ , amounting to  $E_0/\Delta E = 0.219$ . The remaining dimensionless parameter, which regulates the barrier height of the cubic potential, is  $a = 5$ . Source: Figure taken from Ref. [63].

The different shape of the curves can be explained by the dependence of the activation energy on the value of the coupling strength for  $l < s$ . Here, the effective potential barrier that must be surmounted during the escape process grows with  $\kappa$ . As a result we observe a drastic reduction of the successful exit events for shorter bond lengths.

Regarding a study of the influence of the bond length on the mean escape time of the unit chain the coupling strength was fixed to  $\kappa = 0.9$ , guaranteeing an exit of the entire chain without fragmentation. The results are shown with Fig. 11. For small bond lengths up to  $l/s = 1$  the curve drops continuously and at  $l/s \approx 1.1$  a minimum is reached. With further increase of the bond length the mean escape time slightly increases. The rise of the curve for enlarging bond length can be explained with the smaller growth rates of the localised structures created during the process of modulational instability. The effective interaction is weaker. Thus the process of energy localisation is slower and thereby all subsequent exchange processes induced by the modulational instability are slowed down, too. The reason for the absence of escape for  $l/s \lesssim 0.75$  is that the limit of  $l/s \rightarrow 0$ , i.e. small bonds compared to the width of the local potential, and a fairly weak coupling, the chain tends to fragment.

### 2.3. Mexican hat potential

Extending the previous studies of escape from metastable states to systems of higher (geometrical) complexity we investigate a ring of interacting units evolving in a two-dimensional potential landscape of the form of a Mexican hat [64].

Besides the conceptual interest in this work, the results can be applied to the description of micro bubble surface modes which can be modelled by a closely related system in which breather modes were verified

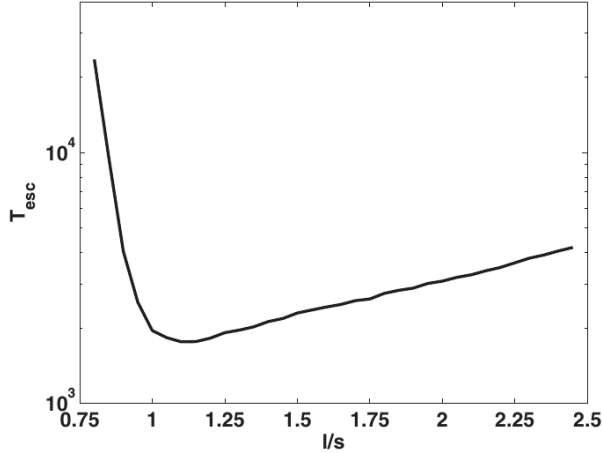


Figure 11: Mean escape time as a function of the bond length  $l$ , in units of the intrinsic length scale of the system  $s$  - Eq. (23). 500 realisations of the random initial conditions, for chains consisting of  $N = 100$  units, have been used in the averaging. The parameters regulating the initial conditions are  $q_{x0} = -0.05$  and  $\Delta q_x = 0.001$ , yielding  $E_0/\Delta E = 0.219$ . The remaining dimensionless parameter, which regulates the barrier height of the cubic potential, is  $a = 5$ . Source: Figure taken from Ref. [63].

experimentally [65]. These results demonstrate the potential relevance of resonant wave modes, as well as the escape behaviour in such topological set ups.

We study a Hamiltonian system consisting of a two dimensional ring of  $N$  linearly coupled units subjected to an external Mexican-hat-like, anharmonic potential; i.e.,

$$V(\mathbf{q}_i) = -\sqrt{\mathbf{q}_i^2} + \cos\left(\frac{\sqrt{\mathbf{q}_i^2}}{\lambda}\right) \quad (26)$$

with (conserved) Hamiltonian in dimensionless units given by

$$\mathcal{H} = \sum_{i=0}^{N-1} \left[ \frac{\mathbf{p}_i^2}{2} + \frac{\kappa}{2} (\mathbf{q}_i - \mathbf{q}_{i+1})^2 + V(\mathbf{q}_i) \right], \quad (27)$$

where  $\kappa$  is the coupling strength between neighbouring units and the parameter  $\lambda$  regulates the width of the Mexican hat potential  $V(\mathbf{q}_i)$ . Moreover,  $\mathbf{q}_i = (q_{xi}, q_{yi})$  and  $\mathbf{p}_i = (p_{xi}, p_{yi})$ . A typical setup is shown in Fig. 12.

The corresponding equations of motion read

$$\begin{aligned} \ddot{\mathbf{q}}_i = & -\kappa (2\mathbf{q}_i - \mathbf{q}_{i+1} - \mathbf{q}_{i-1}) + \frac{\mathbf{q}_i}{\sqrt{\mathbf{q}_i^2}} \\ & + \sin\left(\frac{\sqrt{\mathbf{q}_i^2}}{\lambda}\right) \frac{\mathbf{q}_i}{\lambda \sqrt{\mathbf{q}_i^2}} \quad i \in 0 \dots N-1. \end{aligned} \quad (28)$$

### 2.3.1. Wave modes and escape dynamics

We elucidate the influence of different wave modes on the escape dynamics of the ring from the metastable state over the potential barrier when the ring is initially situated in a metastable state in the vicinity of the potential's bottom corresponding to a local minimum energy configuration. Given the rotational symmetry of the Mexican hat potential polar coordinates, i.e.  $(r_i, \varphi_i)$ , can be introduced accounting for the motions of the radial and angular degree of freedom of each unit. The local minimum energy configuration is determined

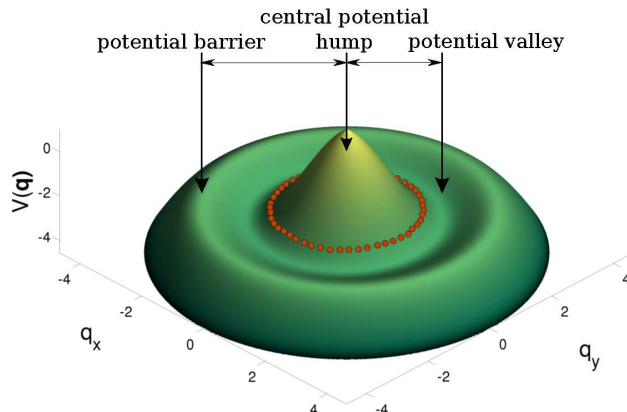


Figure 12: (Colour online) A typical initial preparation of a chain in the Mexican hat potential  $V(\mathbf{q}_i)$  - Eq. (26). The key features of the potential are indicated in the figure. Source: Figure taken from Ref. [64].

by  $r_i = r_0$  and  $\varphi_i = i\Delta\Theta$  with  $\Delta\Theta = 2\pi/N$  complemented with a conditional equation for the radial position, reading

$$-2\kappa r_0(1 - \cos(\Delta\Theta)) + 1 + \frac{1}{\lambda} \sin\left(\frac{r_0}{\lambda}\right) = 0. \quad (29)$$

Initially, the units are placed in a slightly perturbed ring-like structure around the central potential hump, see Fig. 12,

$$\mathbf{q}_i(0) = r_0 \cdot \begin{pmatrix} \cos(i\Delta\Theta) \\ \sin(i\Delta\Theta) \end{pmatrix} + \begin{pmatrix} \Delta q_i^x \\ \Delta q_i^y \end{pmatrix}, \quad \mathbf{p}_i(0) = \begin{pmatrix} \Delta p_i^x \\ \Delta p_i^y \end{pmatrix},$$

where  $\Delta q_i^x$  and  $\Delta q_i^y$  as well as  $\Delta p_i^x$  and  $\Delta p_i^y$  are random perturbations taken from a uniform distribution within the intervals

$$\Delta q_i^x, \Delta q_i^y \in [-0.01, 0.01]; \quad \Delta p_i^x, \Delta p_i^y \in [-0.01, 0.01].$$

In this setting, the angular distance between any pair of neighbouring units is almost equal (i.e. being close to  $\Delta\Theta$ ) so that the initial angular acceleration is small. Thus, for short time periods after the system's preparation, virtually no variations of the angular variables, *viz.*  $\varphi_i(t) = \varphi_i^0 = i\Delta\Theta$ , are expectable. Furthermore each unit's initial radius is close to  $r_0$ . Thus, (at least) for short periods of time after the initialisation of the system, the angular components remain fixed and the units can only move along equally spaced rays that all emerge from the origin.

In more detail, the initial ring-like setup entails that the chain will first oscillate in a  $k = 0$  phonon-like manner. For appropriate parameter values the mechanism of modulational instability triggers the formation of a regularly spaced array of breathers as shown in Fig. 13. These localised excitations, forming a transversal wave pattern, play a crucial role because they concentrate energy in single radial degrees of freedom and therefore substantially influence the escape behaviour.

Generally, at an early stage the dynamics is characterised by the transversal wave pattern. However, later on the angular components experience changes as well. Remarkably, for most of the parameter choices the angular movement is far from being erratic but instead consists of regular and pronounced longitudinal wave patterns, as shown in Fig. 14. As will be seen below, these patterns are fundamental for the characterisation of the system's dynamics and its escape behaviour.

The escape can be realised via two escape channels which are related to different transition states depicted in Fig. 15. The escape through each of these channels is driven by breather modes. They efficiently accumulate energy into single radial degrees of freedom.

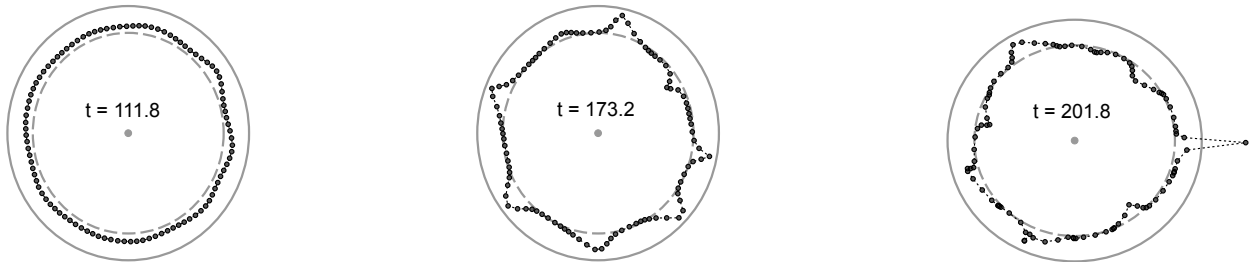


Figure 13: Simulation snapshots of a chain in a Mexican Hat potential evolving according to Eq. (28). The snapshots show the growth of a radial breather array from an almost homogeneous initial state due to modulational instability. The ongoing amplification of this pattern eventually drives an individual unit over the potential barrier and thus triggers an escape of type I as described below. The parameter values are:  $\kappa \Delta\Theta^2 = 0.79 \cdot 10^{-4}$ ,  $\lambda = 0.85$ . Source: Figure adapted from Ref. [64].

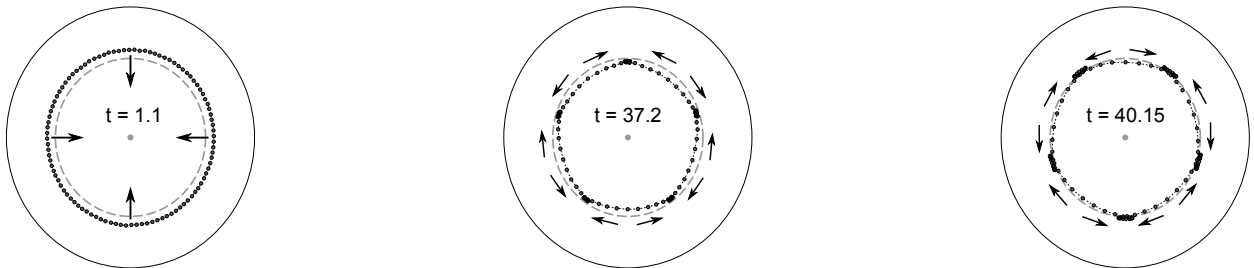


Figure 14: Simulation snapshots for a chain in a Mexican hat potential evolving according to Eq. (28). The snapshots show the emergence of a longitudinal wave pattern. Arrows indicate the chain movement. The parameter values are:  $\kappa \Delta\Theta^2 = 0.06$ ,  $\lambda = 0.4$ . Source: Figure adapted from Ref. [64].

The escape related to transition state type I, as depicted in Fig. 16, indicates a process in which a few units surmount the potential barrier, are driven further down the outer slope of the potential barrier and thereby pull out the entire chain from the meta-stable state. An escape of type II, depicted in Fig. 17, describes the process in which the chain first surmounts the central potential hump, passing the transition state of type IIa as a bundle, and then overcomes the potential barrier in the way indicated by transition state type IIb.

In both of these cases successful escape events occur already for energy values in the order of a few times of the associated activation energy.

Concerning the dynamics on longer time scales, we can identify three dynamical regimes characterised by how the energy is transferred into different degrees of freedom depending on the parameter values. This has a crucial impact on typical escape times.

(I) If longitudinal wave modes are absent or when the angular displacements of the units remain small the system's behaviour is dominated by transversal wave modes. When the system's dynamics comprises a dominant transversal wave mode, it forms breathers that promote an escape of type I, as shown in Fig. 16.

(II) In the opposite case, when radial wave modes are absent (viz. the  $k = 0$  phonon mode is not affected by modulational instability), longitudinal (angular) wave modes arise due to a resonant excitation from the initial phonon mode. Eventually, the system attains a state of periodic energy exchange between the phonon mode and the longitudinal mode. Both the phonon and longitudinal mode cause a synchronous oscillation between kinetic and potential energy for each unit. In general, an escape of type I is not expected because of the lack of energy concentration into critical radial elongations. However, we see an enhancement of an escape of type II. In such a case the chain is strongly stretched in between two wave nodes. It tends to reduce the tension by decreasing the length of the stretched sections, rendering them more straight and they thereby surmount the central potential hump. The initial perturbations can break the symmetry of the

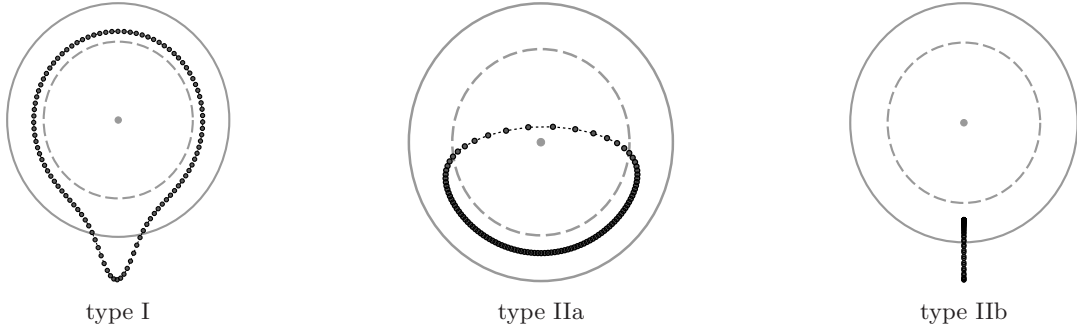


Figure 15: Relevant transition state types for chains in a Mexican hat potential. The chains, by passing through a transition state, can escape from the metastable potential minimum. The states differ by the way in which the chain overcomes the central potential hump, and also the potential barrier (see also Fig. 12). Snapshots of an escape of type I (type II) can be seen in Fig. 16 (Fig. 17). Source: Figure taken from Ref. [64].

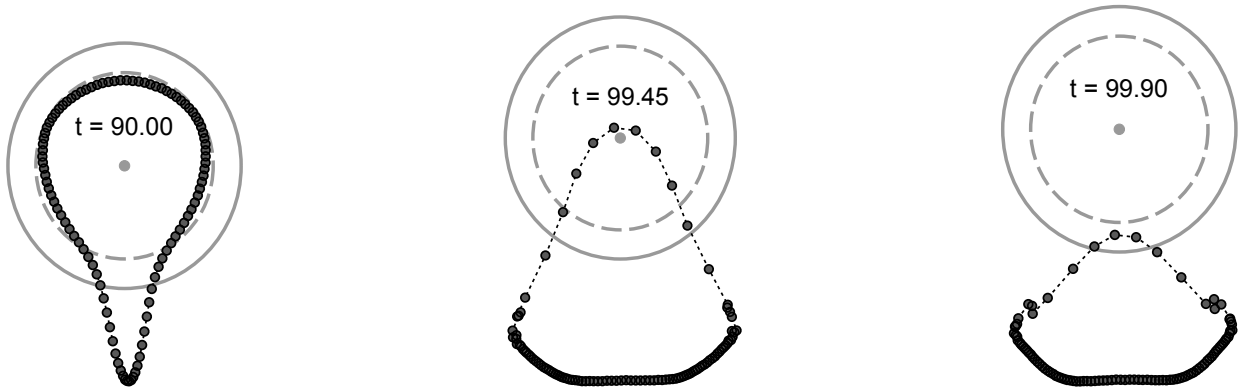


Figure 16: Snapshots of an escape process of type I for a chain in a Mexican hat potential evolving according to Eq. (28). Notice that a few units surmount the potential barrier, are driven further down the outer slope of the potential barrier and thereby pull the entire chain, first over the central potential hump, and subsequently from the potential valley. Parameters:  $\lambda = 0.8$  and  $\kappa \Delta\Theta^2 = 0.08$ . Source: Figure taken from Ref. [64].

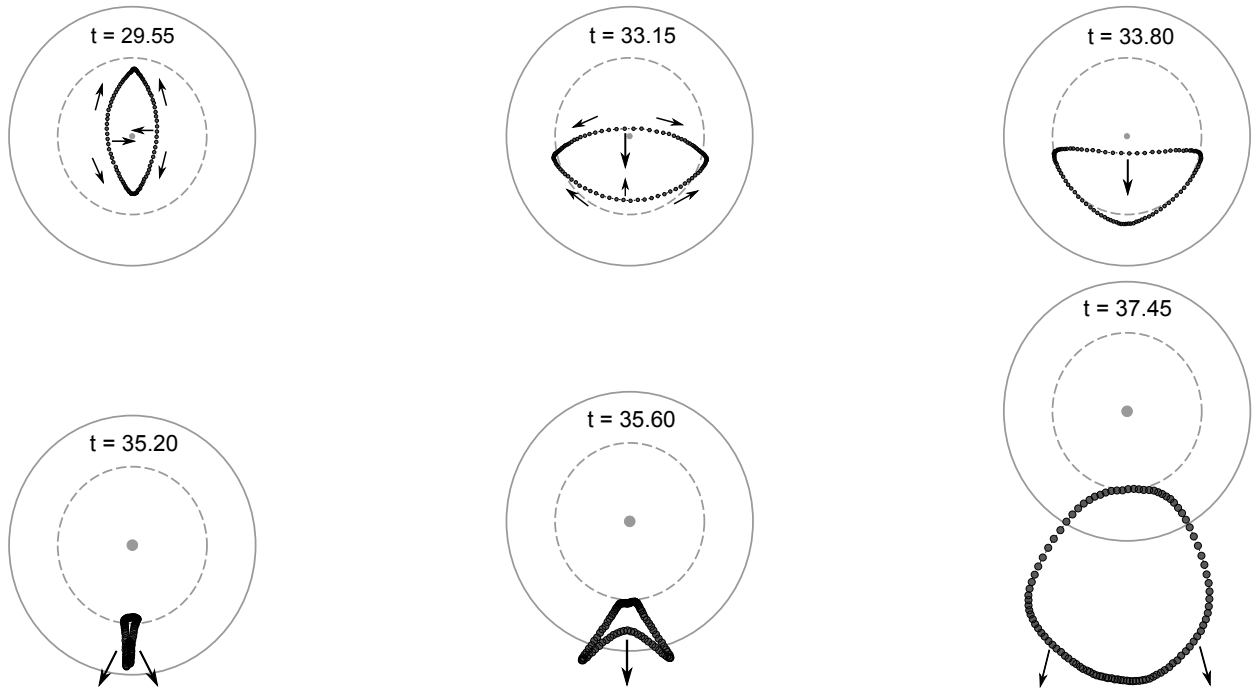


Figure 17: Snapshots of an escape process of type II for a chain in a Mexican hat potential evolving according to Eq. (28). Arrows indicate the direction of chain movement. In contrast to a type I escape, in a type II escape the chain first overcomes the central potential hump, and then the potential barrier. The parameter values are:  $\lambda = 0.4$  and  $\kappa\Delta\Theta = 1.00$ . Source: Figure adapted from Ref. [64].

longitudinal pattern which can cause one of the two stretched segments to overcome the potential hump. Exactly this can be observed in the first three snapshots of Fig. 17. The first two snapshots show the two wave nodes (first vertically then horizontally aligned) and the third displays how the upper part of the stretched chain segment is carried over the potential hump.

(III) In the simultaneous presence of radial (transversal) and angular (longitudinal) wave modes the system will evolve into a chaotic state as the two modes mix in such a way that the system develops irregular long-term behaviour. In fact, once the initial wave patterns have ceased, the resulting irregularity leads to an on average almost homogeneous distribution of the system energy into all degrees of freedom. Compared to case (I) the escape events proceed with a reduced overall efficiency.

#### 2.4. Surmounting collectively oscillating bottlenecks

We next consider the collective escape dynamics of a chain of coupled units in the presence of a weak external ac-field, rendering periodically oscillating barriers [66]. To be precise, the escape dynamics for the system of coupled Langevin equations (Eq. (17)) augmented by a external time-periodic modulation field is considered. The driving field of amplitude strength  $f$ , frequency  $\omega$  and phase  $\theta_0$  globally acts upon the system, with a temporal dynamics obeying:

$$\ddot{q}_n + \gamma\dot{q}_n + \omega_0^2 q_n - aq_n^2 + \xi_n(t) - \kappa[q_{n+1} - 2q_n + q_{n-1}] - f \sin(\omega t + \theta_0) = 0, \quad (30)$$

For the deterministic system it is shown in Ref. [66] that for a chain situated initially at the bottom of the potential well, i.e. there is no net energy contained in the chain, that for certain values of the frequency  $\omega$  of the weak external driving field  $F(t) = f \sin(\omega t + \theta_0)$ , energy is now pumped resonantly into the chain, resulting in a plane wave excitation. Notably, the energy that a unit gains on average from the external

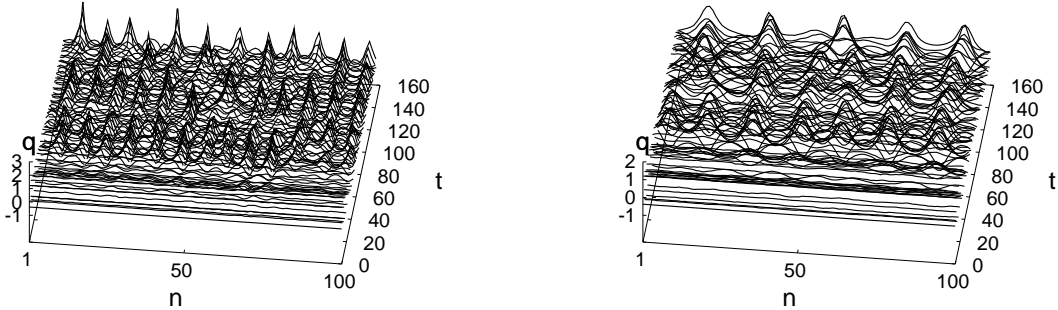


Figure 18: Spatio-temporal pattern of the solutions  $q_n(t)$  for chains consisting of  $N = 100$  units. These chains are driven by an ac-field, damped, and subjected to random fluctuations - see Eq. (30). The two panels correspond to coupling strengths  $\kappa = 0.5$  (left panel) and  $\kappa = 2$  (right panel), respectively, for the same realisation of Gaussian white noise with thermal energy  $k_B T = 0.001 \times \Delta E$ . The remaining parameter values are set at  $f = 0.15$ ,  $\omega = 1.295$ ,  $\theta_0 = 0$  and friction  $\gamma = 0.1$ . Source: Figure adapted from Ref. [66].

field, measured by the ratio  $E_n/\tilde{E}_{field}$ , can attain a remarkably large ratio of  $\sim 20$  where we denote by

$$E_n = \frac{p_n^2}{2} + U(q_n) \quad (31)$$

and

$$\tilde{E}_{field}(t) = -f \sin(\omega t + \theta_0) q_n \quad (32)$$

the energy of a unit and the field energy respectively. Exerting a stationary flat state, represented by a plane wave, additionally to weak spatially periodic perturbations of certain critical wave numbers the deterministic system responds by means of parametric instability such that a pattern of localised states forms.

In the context of the driven Langevin system Eq. (30) the energy is introduced in the lattice coherently in the form of a plane-wave excitation as the response to the external ac-field and non-coherently through thermal fluctuations. The stochastic source and the external ac-field conspire to produce such an instability mechanism of the stationary flat-state (plane-wave) solution yielding a spatially localised system state.

In fact, the additional stochastic term provides perturbations of all wave numbers and a pattern emerges from the low-energy homogeneous flat state. (The energy contained in the chain at  $t = 0$  is vanishingly small compared to the barrier energy, i.e.  $E/\Delta E \ll 1$ .) That is, perturbations provided by the thermal noise grow and induce a localised mode (LM) consisting of several humps. This is demonstrated in Fig. 18 which shows the spatio-temporal evolution of the amplitudes  $q_n(t)$  for couplings  $\kappa = 0.5$  and  $\kappa = 2$ . The Langevin equations were numerically integrated using a second-order Heun stochastic solver scheme. We note the formation of a LM of certain wave length arising from the homogeneous state soon after a short time span (after  $t \sim 60$ ) and we find that the period duration for oscillations near the bottom of the potential is around  $2\pi/\omega_0 \simeq 4.4$ .

The fastest growing perturbations are those associated with the critical wave number (see Sec. 2.1). Each of these humps resembles the hairpin shape of the transition state as the critical escape configuration possessing an energy  $E_{act}$  through which the coupled units have to pass in order to cross the barrier. The robustness of the LMs is remarkable: a LM is sustained, despite continuously impacting thermal noise of strengths up to values  $k_B T = 0.2 \times \Delta E$ . Moreover, the formed patterns maintain their distinct wavelength determined by the critical wave number at which the parametric resonance occurs.

When the noise strength is increased the growth rate of the humps becomes enhanced, being reflected in the statistics of the barrier crossing of the chain in the presence of weak ac-driving. The amplitude and frequency of the latter are chosen such that the dynamics exhibits parametric resonance. The dependence

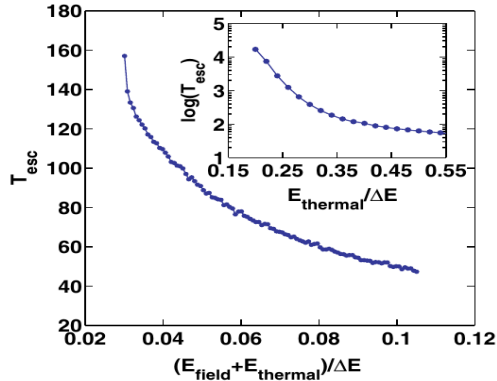


Figure 19: (Colour online) Mean escape time in the one-dimensional Langevin setting - Eq. (30). Shown is the mean escape time vs. the mean injected energy  $E = E_{field} + k_B T$ , for chains consisting of  $N = 100$  units, averaged over ensembles. The injected energy is measured in units of  $\Delta E$  with fixed field energy  $E_{field} = 0.03 \times \Delta E$  provided by an external modulation field with  $\omega = 1.295$ ,  $\theta_0 = 0$  and  $f = 0.15$ . Here we vary the thermal energy  $E_{thermal} = k_B T$ . The inset depicts the unforced case with  $f = 0$  in semi-logscale. The remaining parameter values are  $N = 100$ ,  $\kappa = 0.28$  and  $\gamma = 0.1$ . Source: Figure adapted from Ref. [66].

of the mean escape time of the chain on the injected average energy  $E = E_{field} + E_{thermal}$ , with  $E_{field} = \langle \tilde{E}_{field}(t) \rangle_t$  and  $E_{thermal} = k_B T$  (measured in units of the barrier energy  $\Delta E$ ) is displayed in Fig. 19. The thermal energy  $E_{thermal}$ , supplied non-coherently by the heat bath, is varied within the range  $[(10^{-4} - 0.11) \times \Delta E]$ .

We observe that the underlying irregular dynamics serves for self-averaging and thus the choice of the phase,  $\theta_0$ , of the coherent, external forcing does not affect the mean escape time. In the forced as well as unforced case there occurs a rather rapid decay of  $T_{esc}$  with growing  $E_{thermal} = k_B T$  at low temperatures. This effect weakens gradually upon further increasing  $k_B T$ . Most strikingly, for the forced system the escape times become drastically shortened in comparison with the unforced case with  $f = 0$ . Moreover, for the forced system escape takes place also at very low temperatures for which in the undriven case not even the escape of a single unit has been observed during the simulation time (taken here as  $t = 10^5$ ) implying a giant enhancement of the rate of escape as compared to the purely thermal-noise-driven rate. This emphasises the collective mechanism of this resonance effect which occurs for finite interaction strength  $\kappa \neq 0$  only.

### 2.5. Escape assisted by entropic localisation

In a deterministic (noise-free) setup the escape problem of a chain of harmonically coupled units over the barrier of a metastable potential was studied in [67]. Energy is injected into the system by means of an applied external time-periodic field. The corresponding system is given by

$$\ddot{q}_n + \omega_0^2 q_n - a q_n^2 - \kappa [q_{n+1} - 2q_n + q_{n-1}] - f \sin(\omega t + \theta_0) = 0. \quad (33)$$

Notably, even for a very weak driving force there results fast escape for a chain situated initially extremely close to the bottom of the potential well and thus containing a vanishingly small amount of energy. For a suitably chosen driving frequency, almost coinciding with the frequency at the lower edge of the phonon band of linear oscillations, as a start, an almost uniform oscillating state of the chain is excited. The amplitude of the latter rises (slowly) in time, and upon entering the weakly nonlinear regime the almost uniform state becomes unstable with respect to spatial perturbations. This triggers the formation of a few localised humps (standing breathers) coexisting with a phonon “bath” background in between them. Due to the effect of entropic localisation for the standing breathers, their energy-reduction process is impeded. In more detail, once a unit has acquired a sufficiently high energy, it is retained for a fairly long time due to the fact that in a soft unit the energy dwells relatively more time in the potential part rather than in its kinetic form. The reason for this is that in soft potentials the oscillation frequency decreases with

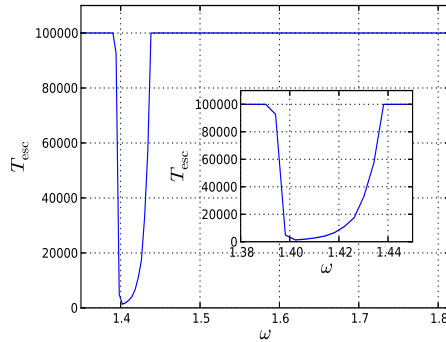


Figure 20: (Colour online) Mean escape time for ensembles as a function of the driving frequency  $\omega$ . Each chain in the ensemble, consisting of  $N = 100$  units and evolving in a cubic potential, has deterministic dynamics and is subjected to a weak periodic driving force with a fixed driving strength  $f = 0.003$ . The values of the remaining parameters are  $\omega_0 = 2$  and  $a = 1$ , regulating the depth and width of the valley in the cubic potential respectively,  $\theta_0 = 0$  controlling the phase of the external driving, and  $\kappa = 0.1$  regulating the strength of the nearest-neighbour interactions. Note that  $T_{esc} = 10^5$  in fact implies that no transitions for any initial condition in the ensemble were observed in our simulations. Source: Figure taken from Ref. [67].

increasing amplitude. In conjunction with the fact that the density of states increases with increasing amplitude, attaining and preserving higher amplitudes becomes entropically more favourable. Thus, during the major part of an oscillation period of a unit, after it has gained energy from the external field, its neighbours, or impacting moving breathers, the displacement of this unit remains large while the velocity is low. Therefore, this entropic localisation mechanism impedes the energy exchange of a higher-amplitude unit with the surroundings. Conclusively, localisation of energy minimises the free energy as it is favoured, with respect to maximisation of entropy, that the energy gaining units populate regions in phase space where the density of states is higher.

In contrast, the process in the other direction is entropically favoured. That is, due to the fact that the driving frequency lies just below the phonon band, further resonant energy pumping by the external field into standing breathers is possible, provided a proper phase relation is retained between them. In fact, the associated growth of the amplitude of the breathers enhances even entropic localisation. However, as with growing amplitude, the frequency of a breather diminishes, and there results a frequency mismatch between the external field and the standing large-amplitude breather hampering direct substantial energy feeding from the external field into it. Therefore, at this stage the only way a breather can gain more energy is by processes of internal energy redistribution along the chain. Conclusively, choosing the frequency of the external driving just below the phonon band is advantageous for two reasons: First, emerging standing breathers can become amplified by direct energy gain from the (almost) resonant external field. At the same time, externally driving with a frequency almost equal to that of harmonic oscillations near the bottom of the potential well generates permanently a phonon “bath” background between the standing breathers forming the source for the emergence of mobile chaotic breathers. The emergence of the itinerant chaotic breathers, and the merging with these standing breathers, contributes to their growth. Eventually, for overcritical amplitudes a standing breather adopts the shape and energy content of the transition state, and by passing across the latter, escape of the chain over the barrier is instigated.

In Fig. 20 the mean escape time  $T_{esc}$  of the chain versus the driving frequency for a small driving amplitude  $A = 0.003$  is displayed. The averages were performed over 1000 realisations of random initial conditions. There is a window of frequencies  $1.395 \lesssim \omega \lesssim 1.437$  for which speedy escape is accomplished, and outside of this window not a single event of escape takes place throughout the simulation time  $T_s = 10^5$ . The window of the driving frequencies associated with speedy escape has an overlap with the phonon band penetrating the latter from its lower edge, underlining the fact that permanently impinging phonons (the latter arise as the result of driving the system within this frequency range) are paramount for the creation

of breathers promoting eventually the escape process. The resulting breathers possess frequencies lying in the window of speedy escape just below the phonon band.

### 2.6. Cooperativity in molecular dissociation

The problem of molecular dissociation is usually looked upon in a stochastic context of Arrhenius or Kramers theory [68, 69, 3, 70, 1]. Nevertheless, it is well known that the bond breaking mechanism may appear within the context of nonlinear dynamics in the form of breaking up of a separatrix lines and the emerging chaotic dynamics [71]. This chaos induced dissociation constitutes a relatively slow process where the chaotic dynamics now take on the role of a stochastic dynamics that drives the dissociation in the Kramers escape regime. As an alternative, a ‘‘coherent’’ mechanism exists involving the organised dynamics of interacting molecules that leads to a cooperative barrier crossing [50], similar in nature to the topics treated in this review above. This is a non-perturbative approach of anharmonic molecular vibrations with a particular concern to the exploration of the general principles for large-amplitude molecular vibrations, leading eventually to molecular dissociation. Since generally the dissociation involves a small number of constituent parts, a reasonable minimal model involves a three-atom molecule composed of linearly arranged identical atoms.

#### 2.6.1. Triatomic dissociation

We consider here the vibrations of a linear molecule composed of three identical atoms A, B, C each with atomic masses  $m$  and respective displacements from their equilibrium position denoted as  $u_1, u_2$  and  $u_3$ , assuming only nearest-neighbour interactions. The interatomic potential  $U_i$ ,  $i = 1$  for the A-B interaction and  $i = 2$  for B-C interaction depend solely on relative distance; explicitly those are chosen as Morse potentials; i.e.,

$$U_i(|u_i - u_{i+1}|) = D_i(1 - \exp[-a_i|u_i - u_{i+1}|])^2, \quad i = 1, 2, \quad (34)$$

where  $D_i$  and  $a_i$  denote potential parameters. The equations of motion for the atoms in the molecule in relative displacements  $x_1 = u_1 - u_2$  and  $x_2 = u_3 - u_2$  read

$$\ddot{x}_1 = -\frac{1}{\mu} \frac{dU_1(x_1)}{dx_1} - \frac{1}{m} \frac{dU_2(x_2)}{dx_2} \quad (35)$$

$$\ddot{x}_2 = -\frac{1}{m} \frac{dU_1(x_1)}{dx_1} - \frac{1}{\mu} \frac{dU_2(x_2)}{dx_2} \quad (36)$$

where  $\mu = m/2$  denotes the reduced mass. Under the nearest neighbour approximation, the three-body problem reduces to a pair of coupled nonlinear differential equations, viz. Eqs. (35)-(36), that are generally non-integrable [50, 71]. For the further analysis of the energetics of the dissociation processes it is useful to introduce bond energy variables  $h_1(t)$ ,  $h_2(t)$  for the A-B, B-C bonds respectively, via the relations

$$h_i(t) \equiv h_i = \frac{\mu}{2} \dot{x}_i^2 + U_i(x_i) \quad i = 1, 2. \quad (37)$$

By use of the equations of motion one finds that [50]:

$$\frac{dh_1}{dt} = -\frac{\mu}{m} \frac{dU_2(x_2)}{dx_2} \dot{x}_1, \quad (38)$$

$$\frac{dh_2}{dt} = -\frac{\mu}{m} \frac{dU_1(x_1)}{dx_1} \dot{x}_2, \quad (39)$$

Upon multiplying the latter two relations we obtain that

$$\dot{h}_1 \dot{h}_2 = \frac{\mu^2}{m^2} \dot{U}_1 \dot{U}_2 . \quad (40)$$

From this relation it is seen that for identical oscillators and identical initial conditions the system of nonlinear oscillators decouples in which case the coefficients of the Morse potential become renormalised.

In the more general case, however, we may recast Eqs. (38)-(39) as [50]

$$\dot{h}_1 - \frac{\mu}{m} f(t) \dot{U}_1 = 0, \quad \dot{h}_2 - \frac{\mu}{m} \frac{1}{f(t)} \dot{U}_2 = 0, \quad (41)$$

where

$$f(t) = \frac{\mu}{m} \dot{U}_2 / \dot{h}_2 = \dot{h}_1 / \left( \frac{\mu}{m} \dot{U}_1 \right), \quad (42)$$

is some function of time. Eqs. (41) show that each unit experiences an effective force that involves both the intrinsic nonlinearity of the problem as well as the implied initial conditions. It is not obvious from the form of these equations alone whether any coherent processes may affect the dissociation process. This analysis may be done through the study of the potential landscape of the problem and the numerical solution of the equations of motion. We note that molecular dissociation of say bond 2 at a given time  $t_0$  signifies that with force  $F \rightarrow 0$  as  $t \rightarrow 0$  we have

$$h_2 \gg h_1 \quad \text{as} \quad t \rightarrow t_0 . \quad (43)$$

This in turn shows that bond breaking is generally associated with dissociation.

### 2.6.2. Cooperative reaction paths

We introduce the two-dimensional potential function and the potential energy surface

$$U(x_1, x_2) = U_1(x_1) + U_2(x_2) \quad (44)$$

and consider the various trajectories for different total energies that follow from the numerical solution of Eqs. (35)-(36) for the parameters  $a_1 = a_2 = D_1 = D_2 = 1$ , and with the initial conditions  $x_1(t=0) = x_2(t=0) = 0$  and  $\dot{x}_1(t=0) = 0.5$ ,  $\dot{x}_2(t=0) = v$ . It can be deduced from Figs. 21 and Fig. 22 that varying the initial velocity  $v$  we may access different regimes of the three unit problem. Three regimes can be identified and are discussed in the following.

In Fig. 21 we show the potential landscape projections for type-I motion with: (a)  $v = 0.4$ , (b)  $v = 0.8$ , and (c)  $v = 1.5$ , as well as a type-II motion for (d)  $v = 1.9$ . In contrast, in Fig. 22 we have a type-III motion with (a)  $v = 1.935$  and a type III-2 with (b)  $v = 1.95$ . It is seen that from case I (a) to (c) that the area covered by the trajectory around the origin at  $(0,0)$  changes from a cross section of a cone lying along the  $(1,1)$ -direction to a regime which covers almost the whole region enclosed by a potential-energy contour. In the separating type-II case, the domain covered by the orbit tends to extend almost equally in the direction of the rays of the potential function. In type-III motion shown in Fig. 22, the trajectory elongates indefinitely along the  $x_2$  direction, showing that a break-up of bond 2 occurs. This line is identified as a reaction path. Thus, only for type-I motion does normal mode theory apply with bond energy equipartition.

In Fig. 23 we depict the energy quantities  $h_1(t)$  and  $h_2(t)$  as a function of time for type-I (top and bottom figures on lhs) and type-II motion (top and bottom figures on rhs). The first pair clearly shows a rapid energy exchange between the bonds. For type-II motion we display the quantities  $h_1(t), h_2(t)$  for  $1250 \leq t \leq 1300$  and observe, in distinct contrast to the type-I regime an energy localisation in each bond that is subsequently transferred to the neighbouring one. The process of energy exchange proceeds in ‘‘packets’’ and not in a continuous manner as for the type-I linearised motion. This process of exchange of localised energy between the bonds continues indefinitely and, as a result, we may consider this case as the pre-bond breaking regime. The value  $v_c \approx 1.92$  is a critical value because for  $v$  slightly larger than  $v_c$ , the energy-versus-time relation in the two bonds becomes irregular. As  $v$  increases further, the system crosses over into type-III motion, as displayed with Fig. 24.

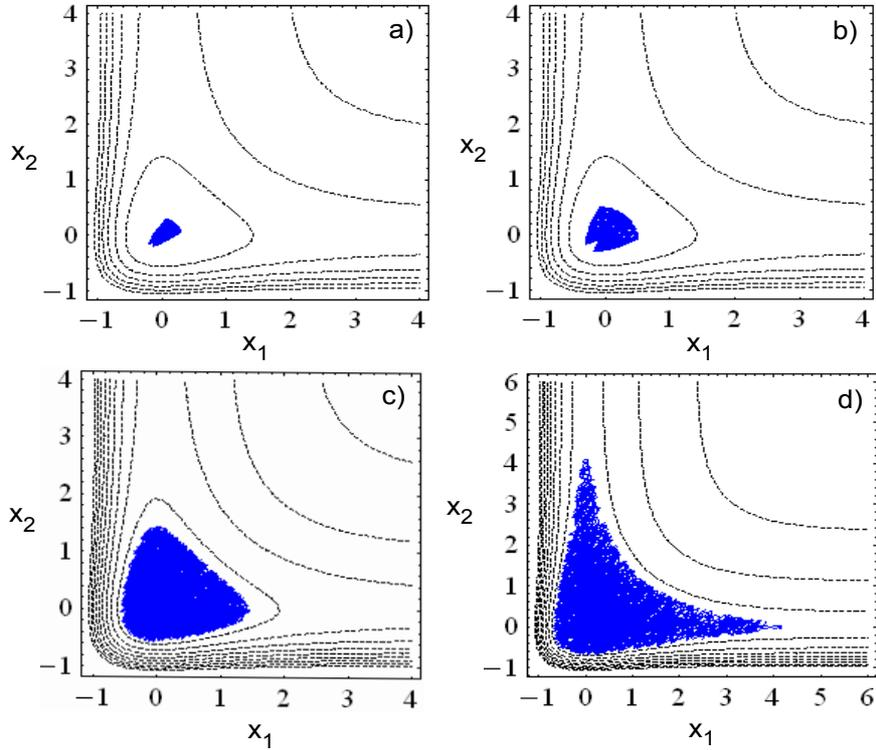


Figure 21: (Colour online) Molecular trajectories in the potential energy landscape of the linear three atom molecule for various initial relative velocities in bond 2. In (a)  $v = 0.4$ , (b)  $v = 0.8$ , (c)  $v = 1.5$  (Type-I trajectories: fast energy exchanges between bonds) (d)  $v = 1.9$  (Type-II trajectories: delimit stable linearised energy exchange between the units and unbounded motion). Source: Figure adapted from Ref. [50].

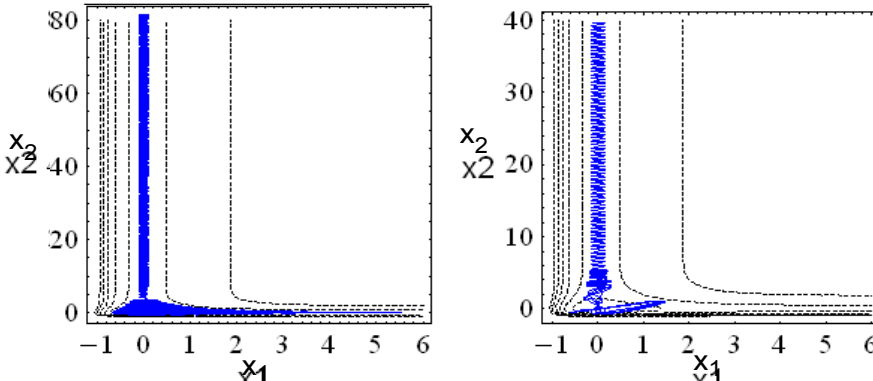


Figure 22: (Colour online) Molecular trajectories in the potential energy landscape for unbounded motion leading to bond breaking and dissociation. Type-III motion with  $v = 1.935$  (left panel) and  $v = 1.95$  (right panel). Source: Figure adapted from Ref. [50].

From the numerical calculation of  $h_1(t)$  and  $h_2(t)$  we observe that bond 2 breaks although almost complete transfer of energy from bond 2 to bond 1 may take place. These bouncing exchanges become less pronounced as  $v$ , and thus the initial energy, increases. Physically, breaking of a bond in chemical dissociation is equivalent to a transition from a bounded motion to an unbounded one. In the latter case equipartition of the system energy between kinetic energy and the potential energy breaks down and almost

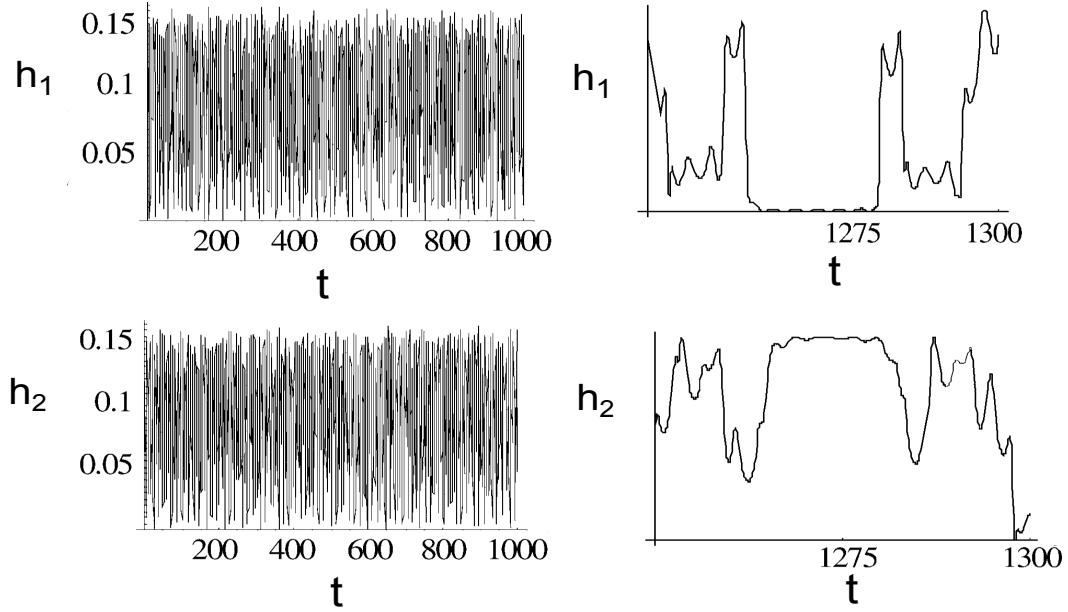


Figure 23: Total energies  $h_1(t)$  and  $h_2(t)$  accumulated in each bond as a function of time. The left two plots correspond to type-I motion ( $v = 0.8$ ) while the right two figures correspond to type-II, intermittent motion ( $v = 1.9$ ). The continuous energy exchange seen in the linearised regime is sharply contrasted by the intermittent yet coherent predissociative exchange in type-II motion. Source: Figure adapted from Ref. [50].

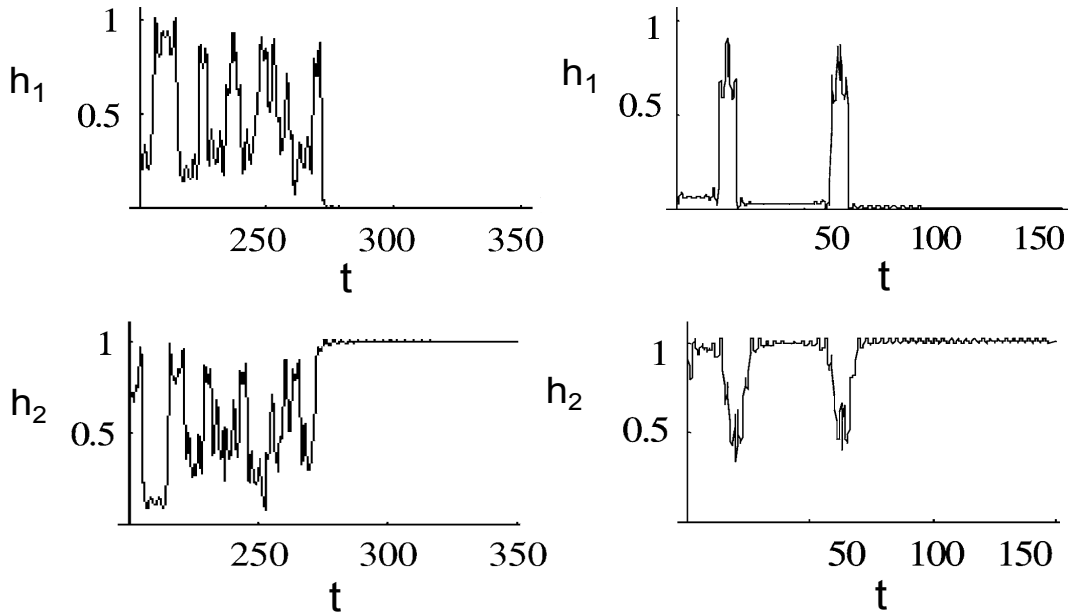


Figure 24: Total energies  $h_1(t)$  and  $h_2(t)$  accumulated in each bond as a function of time for type-III motion. The left panels correspond to  $v = 1.935$  while the right panels to  $v = 1.5$ . Dissociation occurs after coherent initial energy localisation and exchange of the localised energy between the two bonds. As initial energy increases, bond breaking occurs faster and with less or eventually no exchange of localised energy “packets”. Source: Figure adapted from Ref. [50].

all system energy is transformed into potential energy localised in the breaking bond. This accumulation of potential energy in bond 2 at the expense of kinetic energies and potential energy in bond 1 leads to molecular dissociation.

Molecular dissociation occurs here as a process that is induced by collective effects and nonlinear interactions; spontaneous energy accumulation in the form of discrete breathers [72] appears to play a role. In the simple three atom case one finds, in addition to a “trivial” low energy regime, a collective, yet intermittent regime that is predissociative and is characterised by spontaneous energy accumulation and non-continuous energy transfer. At yet higher energies a spontaneous dissociation regime also appears where motion becomes unbounded. Dissociation occurs through system energy concentration to potential energy of a given bond at the expense of kinetic energy; this resonant transfer is cooperative and possibly related to targeted energy transfer [73]. This resonant energy accumulation and exchange may take place for a substantially long time before leading to molecular dissociation. This process is dependent on the initial bond energy: as the initial kinetic energy becomes larger, localised energy oscillations become less frequent, leading to an almost instantaneous bond breaking at sufficiently large initial energies.

### 3. Collective transport

#### 3.1. Transport in general

The topic of particle transport is typically concerned with the movement of particles across potential landscapes. Studies of transport in such systems focus on how forces on the particles resolve themselves to allow for directed transport; i.e. net motion that is (on average) in one direction or another. Of particular interest is the *ratchet effect*: the possibility to obtain directed transport by using zero mean perturbations. The state of the art with respect to transport in spatially periodic systems out of thermal equilibrium was presented recently in [19, 22, 51].

Some of the earliest studies of particle transport were in the area of celestial mechanics, in an effort to understand, for example, the motion of planets orbiting a star. Since the advent of numerical computation [74], investigations into particle transport have increased at an almost exponential rate. This new tool has complemented analytical and experimental work already being carried out. In addition, the twentieth century saw the birth of new fields of research, fueled by application areas such as Josephson junctions, cold atom systems, and Bose-Einstein condensates, where transport properties shed light on the features of these systems. Thus the study of transport properties in the presence and absence of random perturbations or noise is a very active area of research [22, 51].

##### 3.1.1. Individual particles

A large portion of the literature has focused on the transport properties of individual particles. In [75] the authors carried out relevant work on transport in (autonomous) Hamiltonian systems (to be precise for area-preserving maps). In particular, they outlined the structures contained in a largely chaotic phase-space, most notably cantori and KAM-tori, that play a key role for the occurrence of transport. They showed that the particle flow through the partial barriers, created by cantori, was controlled by *turnstile*s that could trap particles in transporting channels. The phase-space of the standard map exhibits coexisting chaotic and regular regions (details of the standard map can be found in [76]). In fact, magnification of any of the boundaries between regular and chaotic regions will reveal more intricate structures embedded in the chaotic regions. In particular, the hierarchy of cantori will be revealed through successive magnifications of particular regions [77].

Analogous features would take prominence in time-dependent driven (i.e. non-autonomous) Hamiltonian systems (flows) [78, 79, 80]. In many studies it has been shown that the emergence of a directed current is triggered by an external time-dependent field of zero mean. Important in this respect are the spatio-temporal symmetries (cf. Section 3.1.5) of the system. With regard to the emergence of a non-zero current, all symmetries that, to each trajectory, generate a counterpart moving in the opposite direction need to be broken. Further, it has been shown that a *mixed phase-space* is required [81, 82, 80, 51]. The mixed phase-space, containing regular and chaotic components allows for directed transport in the chaotic component

of the phase-space. The regular and irregular components are separated by impenetrable KAM-tori which are in turn surrounded by a hierarchy of cantori. These cantori, although appearing to form closed curves, are interspersed by an infinite number of gaps, which allow particles to pass through and become stuck in *ballistic channels*<sup>2</sup> (similar to the turnstiles idea from maps). It is these sticking episodes that allow for directed transport. The general phenomena is sometimes called *intermittency* [83].

The observation of a non-vanishing current, as an average velocity in coordinate-space, based on the chaotic ratchet effect as discussed in [84, 79, 85, 86, 80] has even been extended to chaotic ratchet acceleration expressed in terms of an averaged velocity in momentum space [87]. In both cases the sum rule derived in [82] for the chaotic transport velocity in driven one-dimensional systems assures the existence of a persistent chaotic ratchet current.

The case of particles in non-Hamiltonian systems has also attracted considerable interest. While the Hamiltonian systems remain an active area of research, some have focused on less idealised systems that are dissipative (possibly including noise), and driven. Brownian motors extract work from thermal fluctuations in out-of-equilibrium conditions. With regard to transport under such thermal fluctuations, the ‘constructive role of Brownian motion’ is crucial [88, 20, 19, 22]. A particular type are Brownian motors which find applications in various fields such as physics, engineering, chemistry and biological transport [19, 22], to name but a few. Motion in such ratchet-like devices is confined to a periodic and asymmetric landscape. In the presence of out-of-equilibrium conditions they are able to rectify thermal fluctuations. Interestingly, under certain conditions, it is possible to derive analytical solutions pertaining to transport of Brownian particles via the *Gambler’s Ruin* model [89]. For Brownian ratchets, the broken spatial symmetry combined with external forces with time-correlations were shown to be sufficient ingredients for transport [90, 91]. The interdependence of the confining potential landscape and of the thermal fluctuations, for the emergence of transport, has further been studied in [92].

In general though, the dynamics of particle motion in periodic potentials at finite temperatures is an extensively studied field [93]. In a similar domain, [94] investigated the motions of driven, under-damped Brownian particles, evolving in a *washboard potential* (a spatially symmetric and periodic potential), under the influence of a time-delayed feedback term. They found that, at finite temperatures, the time-delayed feedback term can in fact enhance the transport features of the system such that there is an increase in the overall net motion of the system, which is not observed when the feedback term is switched off. These results were related to a desymmetrisation of the relevant attractors supporting directed transport.

Transport of particles in potentials with multiple wells, at its most fundamental level, is characterised by escape processes over potential barriers as discussed in the first part of the review.

### 3.1.2. Transport with two or more degrees-of-freedom

Increasing the number of degrees-of-freedom to two (two and a half), and by consequence the dimension of the phase-space to four (five), by coupling two individual particles together adds further complexity to the system’s dynamics. For those studies which look at the transport features of systems of coupled units, the objective is to investigate the conditions which lead to said transport features. In particular, for directed transport to occur, it is quite often the case that the two particles will work *cooperatively* to achieve this directed transport. Importantly, under the same conditions, a dimer (a compound made up of two particles) has distinct transport properties compared with those of the single particle [95].

Dimer systems have been shown to exhibit a complicated dependence, with respect to observables of interest, on the coupling between the subsystems making up the dimer. For example, the value of the net transport for a dimer system can change erratically as the coupling parameter is varied [96]. Similarly, [97] considered the conservative and deterministic escape dynamics of two coupled particles out of a metastable potential. The scenario considered is such that neither particle can escape independently (on energetic grounds), and thus cooperation is required. It was shown that the escape times of the dimer out of the

---

<sup>2</sup>Ballistic channels exist inside the chaotic component of a mixed phase space at the boundary with the regular regions. Motion inside a ballistic channel is characterised by long periods of non-zero average velocity. In contrast, motion that takes place inside the chaotic component, but not at the boundary of a regular region, will usually have vanishingly small average velocity.

metastable state become severely inhibited for coupling strengths that are either too large or too small. In [98] it was demonstrated that dynamical detrapping of a dimer from a potential well of a periodic potential followed by unidirectional motion, i.e. a running solution, depends critically on the coupling between the two subsystems.

Increasing the number of degrees-of-freedom further renders the analysis of these systems more cumbersome. Some of the already illusive phase-space structures become difficult, if not impossible, to detect. However, in spite of this, it is still possible to explore the transport properties in these higher dimensional systems in a fashion similar to the studies of escape in the first part of this review.

### 3.1.3. Anomalous transport

For systems modelling the dynamics of particles evolving in periodic potentials, the inclusion of driving and damping can produce some interesting and unexpected behaviours. For such a particle, where the underlying potential is of the ratchet type and the driving is of zero average, [99, 100, 101] observed a current reversal via an increase of the driving amplitude – that is, the current, going in one direction, passes through zero and changes direction as the driving amplitude is increased. A ratchet subjected to an unbiased external force that periodically modulates the inclination of the potential, is called a *rocking ratchet*. Current reversals in such a system are unexpected due to the inherent bias contained in the ratchet potential. In this situation, the current reversal, when it occurs, has been shown to coincide with a bifurcation from chaotic to regular motion [99, 100]. In a similar study [102] related current reversals to the basins of attraction for the system’s coexisting attractors that produce counter-propagating motion. This study differs from the previous two in that a current reversal is obtained through the appropriate selection of (completely symmetric) initial conditions, rather than through the modification of a control parameter. These studies have been extended to consider the case of two coupled driven and damped particles evolving in a ratchet potential [103]. Not surprisingly, the addition of the second particle can have important consequences for the current reversals observed in the case of the single particle. It appears that current reversals exist for coupling strengths below some critical value. However, beyond this critical coupling strength, the particles become synchronous – the single particle dynamics are restored – and no further current reversals are observed. Little explanation is given as to why no further current reversals appear. However, from the [100] study it is known that current reversals are restored, in the case of the single particle, for stronger driving amplitudes. In a separate study, [104] investigated the dynamics of a single particle evolving in a periodic and spatially symmetric potential landscape. In such a potential, there is no inherent bias with respect to transport. Thus, for a current to emerge at all, some symmetry of the system needs to be broken (see in Sec. 3.1.5). In [105, 104] this was achieved by using a bi-harmonic driving term, resulting in a system that is driven out of equilibrium by an asymmetric external force. The authors provide evidence that current reversals, in this situation, are induced by the symmetry-breaking effect of the system’s damping.

Other types of counter-intuitive transport can be collected under the term *negative mobility*. To motivate this, let us consider two examples. The first, coined the *Brazil nut effect* [106], occurs when granular media of different sizes are mixed. Applying a rocking force to the mixture can cause the unexpected result that the larger granules rise [107]. Secondly, an effect known as *induced demand* can help explain, for example, the counter-intuitive rise in traffic when new roads are created (explanations include people wanting shorter journey times, access to better roads, etc). For particle transport, a negative-valued mobility also plays an interesting role [52, 53, 55, 56]. The work in [54] gives an overview of this topic, together with a list of possible applications. In particular, they describe two types of motion of this kind; namely, *absolute negative mobility* (ANM) and *differential negative mobility* (DNM). For illustration, consider a simple system consisting of a single particle in equilibrium, which has a spatially static homogeneous force  $F$  applied. It is generally expected that the response of this system to the bias force  $F$  is in the direction of, and proportional to, this force. However, for systems driven out of equilibrium (and possibly with the inclusion of noise), these new types of motion can be observed. ANM refers to motion whose response, on average, to the sufficiently *small* bias force  $F$  around  $F = 0$  is in the opposite direction of  $F$ . DNM on the other hand refers to motion that, although in the same direction as  $F$ , slows down as the magnitude of  $F$  increases. These ideas have been expanded upon to further understand the response of these systems to noise [108, 55, 109, 110, 56].

The case of coupled particles has also been considered. For under-damped particles evolving in spatially periodic and symmetric potentials, subjected to periodic driving and an additional static bias force, [111] related the occurrence of negative mobility to a bifurcation from chaotic to regular motion. Further, a heuristic description of the mechanism that allows for such motion is outlined. In short, the particles must together work cooperatively in conjunction with the periodic driving so that ‘downhill’ motion is minimised, while ‘uphill’ motion is promoted. Thus, ‘uphill’ motion ensues. The corresponding solutions remain stable under low temperature fluctuations (see the discussion in Sec. 3.3.3). In contrast, outside the observed windows of negative mobility, it is the chaotic dynamics that emerge resulting in motion that is in the same direction as the bias. A later investigation by [112] can be considered as an extension of this study to the case of over-damped particles. Again, ANM was observed. They were able to prove that ANM is not possible for an over-damped dimer where the interaction potential is convex. That is, for a system of two coupled particles in the over-damped limit, subject to the forces discussed above, and with an interaction potential  $W(x)$  such that

$$W''(x) > 0 \quad \forall x, \quad (45)$$

the possibility of ANM is excluded.

#### 3.1.4. Transport in irregular domains

Extensions of the above concept address the case of autonomous Hamiltonian systems of one-dimensional billiard chains [113, 114]. The necessity of creating chaos requires at least two degrees-of-freedom. As an example for such a system, a classical magnetic billiard for particles carrying an electric charge has been studied in [113]. In order to break the time-reversal invariance, an external static magnetic field, penetrating the plane of motion perpendicularly, has been applied. In addition, achieving directed transport requires breaking of the remaining spatial symmetry which can be achieved, e.g. by properly placed asymmetric obstacles inside the billiard [113, 114]. Uni-directional motion in a serpent billiard chain has been reported in [115].

The work in [116] introduced a novel class of billiard systems which the author called the *Mushroom Billiard*. For an example we refer to Fig. 25. Its novelty comes from the fact that it has the remarkable property of having a phase-space consisting of a single (regular) KAM-island and a single (chaotic) ergodic region. Such billiards offer insight into the dynamics of Hamiltonian system with a more complicated phase-space. In fact [117, 118] looked at the stickiness of chaotic trajectories to the single KAM island, using recurrence time statistics, in mushroom billiards. It was shown that the sticking episodes are facilitated by orbits known as *marginally unstable periodic orbits*. Marginally unstable refers to the fact that perturbations grow linearly (rather than exponentially) in time. These orbits, even though being of measure zero, govern the main dynamical properties of the system. Most notably, they are responsible for a power-law behaviour observed in the recurrence time statistics – something that is often related to the partial barriers created by cantori in a mixed phase-space.

#### 3.1.5. Properties that determine transport features

A symmetry analysis of a system of equations can illuminate important transport properties. An important quantity related to transport is the time averaged, ensemble averaged, momentum. This is typically called the *current*. Let  $p(t)$  represent the momentum of a particle at time  $t$ , then the current is given by

$$J = \frac{1}{T_s} \int_0^{T_s} dt \left( \frac{1}{N} \sum_{n=1}^N p_n(t) \right), \quad (46)$$

with  $N$  being the number of initial conditions in the ensemble, and time  $T_s$  taken in the asymptotic limit  $T_s \rightarrow \infty$ . The direction and magnitude of the current is inextricably linked with a system’s symmetry properties.

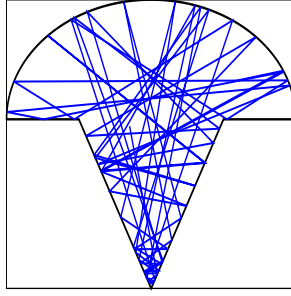


Figure 25: (Colour online) Transport in an irregular domain: A *mushroom billiard*, together with an example trajectory. Source: Figure taken from Ref. [119] and the corresponding data was obtained from [120].

To give an example, [84, 51] considered the symmetry properties of a system consisting of a particle evolving in a spatially periodic potential subjected to driving and damping. The equation of motion is given by

$$\ddot{X} + \gamma \dot{X} + f(X) + E(t) = 0. \quad (47)$$

Here  $E(t) = E(t+T)$  is a time-periodic external field of period  $T = 2\pi/\omega$  and frequency  $\omega$ , and  $f(X) = f(X + 2\pi)$  is a periodic potential function. Both  $E(t)$  and  $f(X)$  are assumed to be bounded, and  $\max(|f(X)|) \sim 1$ . The authors defined system symmetries related to the properties of the underlying potential and external field. These properties (shown in a modified form which allows for greater applicability – due to [121], for example) for a given function  $g(a)$  are

$$\begin{aligned} g_s &: g(a + \tau) = g(-a + \tau) && \text{for some } \tau && \text{(symmetric)} \\ g_a &: g(a + \tau) = -g(-a + \tau) && \text{for some } \tau && \text{(anti-symmetric)} \\ g_{sh} &: g(a) = -g(-a + \tau) && \text{for some } \tau && \text{(shift-symmetric)} \end{aligned}$$

where  $g(a)$  can represent either a spatial or temporal function, i.e. the potential or the time-dependent external field, respectively. If  $f(X)$  is anti-symmetric, and  $E(X)$  shift-symmetric ( $f_a$  and  $E_{sh}$ ), then Eq. (47) is invariant under the symmetry  $\hat{S}_a : X \mapsto (-X + 2\chi)$ ,  $t \mapsto t + T/2$  for some appropriate argument shift. In the dissipationless case,  $\gamma = 0$ , a second symmetry can be obtained. If  $E(t)$  possesses the shift-symmetry  $E_{sh}$  then Eq. (47) is invariant under the symmetry  $\hat{S}_b : t \mapsto -t + 2\phi$ , again for some appropriate argument shift.

It then follows that for a given trajectory  $X(t; t_0, X_0, P_0)$ ,  $P(t; t_0, X_0, P_0)$  with initial condition  $t_0, X_0, P_0$ , it is possible to generate new trajectories given by

$$\begin{aligned} \hat{S}_a &: -X(t + T/2; t_0, X_0, P_0) + 2\chi, -P(t + T/2; t_0, X_0, P_0) && \{\hat{f}_a, \hat{E}_{sh}\}, \\ \hat{S}_b &: X(-t + 2\phi; t_0, X_0, P_0), -P(-t + 2\phi; t_0, X_0, P_0) && \{\hat{E}_s, \gamma = 0\}. \end{aligned}$$

Importantly, these transformations change the sign of  $P$ . This has the consequence that the original trajectory, and the corresponding trajectory generated through the symmetry transformation yield time-averaged values of  $P$  that differ only by sign. Going further, for a system with  $\hat{S}_a$  or  $\hat{S}_b$  symmetry, the net current will be zero as each trajectory will have a counterpart that negates the others contribution to the current. The implication being that in order to generate a non-zero current, both the symmetries  $\hat{S}_a$  and  $\hat{S}_b$  need to be broken. Note that  $\hat{S}_a$  holds in both the dissipation and the dissipationless cases, whereas  $\hat{S}_b$  holds only for  $\gamma = 0$ . The work [79] identified an additional symmetry,  $\hat{S}_c$ , of Eq. (47), this time in the over-damped case where inertial effects become negligible, namely:

$$\hat{S}_c : X(-t; t_0, X_0, P_0) + \chi/2, -P(-t; t_0, X_0, P_0) \quad \{\hat{f}_{sh}, \hat{E}_a, m = 0\}.$$

It is worth noting that the symmetries  $\hat{S}_a$ ,  $\hat{S}_b$  and  $\hat{S}_c$  require that the time-dependent external field satisfies certain properties. Thus, an appropriate choice of  $E(t)$  can be sufficient to break all three symmetries.

The authors in Ref. [78] investigated the symmetry properties of the Hamiltonian version of Eq. (47) ( $\gamma = 0$ ), where the underlying potential is spatially periodic and symmetric. A lowering of the dynamical

symmetry, controlled by the phase of the external field, leads to a directed current.

### 3.1.6. Ballistic transport

Others have focused on the dynamical mechanisms that allow for a directed current in a mixed phase-space. While the appearance of a dc-output can be expected using symmetry analysis, its appearance and magnitude are due to dynamical mechanisms of motion inside the stochastic layer. The paper [122] looked at the structures in phase-space and considered how they influence the magnitude and direction of current. To ensure that the appropriate symmetries were broken, thus allowing for a directed current, they chose the external field

$$E(t) = E_1 \cos(t) + E_2 \cos(2t + \phi), \quad (48)$$

where  $E_2 \neq 0$  and  $\phi \neq 0, \pi$ . The phase-space of this system is characterised by a stochastic layer which emanates from the separatrix of the unperturbed system ( $E_1 = E_2 = 0$ ). Inside the stochastic layer there exists a hierarchical structure of resonance islands that are responsible for the creation of ballistic channels in phase-space. That is, the resonance islands form partial barriers such that when a particle enters a ballistic channel it may be stuck there for large durations, thus contributing to an overall non-zero net current. The authors relate the emergence of a directed current to a desymmetrisation of the ballistic channels bringing the particles in opposite directions. Going further, they analytically derive an expression for the current from the geometry of the phase-space. In particular, each resonance island has associated to it a winding number  $\omega_i$ , a probability of ‘sticking’ to the resonance island  $\rho_i$ , and mean sticking time  $\langle t_i \rangle$ . In addition the mean time between sticking episodes is  $\langle t_r \rangle$ . The authors in [122] define the current as

$$J = \sum_{i=1}^N \omega_i \rho_i \langle t_i \rangle / \left( \sum_{i=1}^N \rho_i \langle t_i \rangle + \langle t_r \rangle \right) \quad (49)$$

where  $N$  is the number of resonance islands. This definition of the current suffers two limitations. Firstly, the four unknowns in the equation will, in general, need to be computed numerically. The second is that there may be resonances of all orders. To even locate resonances of increasing order becomes computationally impractical. However, this does not pose much of a problem as it is only a few resonance islands that are relevant for obtaining the net current. Higher order resonances have sticking times that are close to zero and therefore their contribution to the net current is negligible.

### 3.1.7. Beneficial role of chaos

All of the studies discussed above look at systems with at least (effectively) three variables. Thus the dynamics of these systems then typically display a chaotic dynamics. Although chaotic motion seems to be inherently counter-productive with respect to net directed motion it can, for example, allow trajectories to visit (transporting) ballistic channels associated to resonance islands with non-zero winding numbers [82]. However, such ballistic channels will only exist in non-hyperbolic systems: systems that contain mixed regular and chaotic regions. These chaotic regions are born out of (nonintegrable) perturbations to an integrable system, with the strength of perturbations determining the prevalence of chaos. This is true in general; i.e. nonintegrable perturbations to an underlying integrable system are the source of chaos. The systems under investigation in the following exhibit several forms of chaotic motion, including transient chaos, permanent chaos and motion on strange attractors. In particular, transient chaos can be beneficial for current rectification.

### 3.1.8. Cooperative transport mechanism

This section explores the deterministic dynamics of systems of several *coupled* units. In particular, the focus of the review is concerned with the transport features which this complexity generates. Of interest is how particles work together, cooperatively, to achieve directed transport. For this reason, the strength of the coupling between the particles serves as the main control parameter. Further, ensemble dynamics serve to highlight some of the collective effects of these systems.

The section is split into two parts: The first part looks at a class of time-independent (autonomous) Hamiltonian systems, while the second part considers a class of time-dependent driven (non-autonomous) and damped systems. A common feature of these systems is that they contain a spatially open component that facilitates long range transport. More precisely, transport proceeds in a spatially symmetric and periodic multiple well potential. Thus transport is characterised by particles overcoming successive energetic barriers created by the potential landscape.

The cooperative effects between the particles becomes apparent in Sec. 3.2 when the autonomous Hamiltonian systems are considered. In the uncoupled limit the low dimensional systems decompose typically into two integrable subsystems and the dynamics are fully understood. However, the dynamics become more complicated when the particles are coupled. As these systems are conservative a coordinated energy exchange between the particles is often required for directed transport to ensue. Interestingly enough, these systems contrast well with the non-autonomous one-and-a-half degree-of-freedom Hamiltonian systems, where transport occurs through intermittent periods of directed motion in so-called ballistic channels. The autonomous two degree-of-freedom counterpart considered here relies on a rather different mechanism for directed transport that is provided solely by regular structures in phase-space.

With the inclusion of external driving and damping (Sec. 3.3) the transport dynamics are controlled by various coexisting attractors in phase-space. The nature and stability of these attractors is determined by the system parameters. As before, cooperative effects play a key role when it comes to particle transport. Notably, the coupling between the particles can result in a suppression of chaos that allows, for example, for collective periodic motion of rotational type.

### 3.2. Transient-chaos induced transport in autonomous systems

In this part we review the works on autonomous Hamiltonian systems modelling two coupled units. The guiding aim is to understand the conditions under which directed transport in phase-space is supported. In particular, analytical and numerical results are produced illustrating the effects that the interaction between the two units has on the direction and velocity of transport.

The focus of this section is on the deterministic transport properties of systems of two coupled particles or units. In particular, much attention is given to the relationship between various transport scenarios and the coupling between the units. Notably, the nature of the interaction between the units that allows for directed transport (on average) is scrutinised.

The work presented in the first part of this section serves as a bridge between single unit systems and many unit systems. Importantly, two unit systems are the first non-trivial step from the lower of these limits, bringing with it new types of motion, such as hyperchaos [123], that have important implications when it comes to transport. More than that, the work presented in this section explores novel mechanisms pertaining to directed transport that are a direct consequence of the interaction between the units.

In Sec. 3.2.1 the first example treated is a spatially symmetric system containing two open components allowing that either unit can undergo directed transport. By way of symmetry analysis, it is clear that if a constant energy surface is entirely populated by initial conditions then no current can emerge. However, this may not be the case for other, more physically relevant, sets of initial conditions. For one such set, some qualitatively different transport scenarios are outlined and their relation to the net current described. As a general point for the class of systems discussed in Sec. 3.2, the mechanism promoting directed transport in these systems is quite distinct from systems where transport proceeds over finite periods in so-called *ballistic channels*, each period being separated by an interval of chaotic motion. The novel mechanism for transport presented here, where chaos is required only in a transient period of the dynamics (after which transport is provided solely by regular structures), is illustrated and the implications discussed.

The Hamiltonian systems discussed here are of the form:

$$H(\mathbf{p}, \mathbf{q}) = \frac{p^2}{2} + \frac{P^2}{2} + U(q) + V(Q) + H_{\text{int}}(q, Q) , \quad (50)$$

where  $\mathbf{p} (= (p, P)) \in \mathbb{R}^2$ ,  $\mathbf{q} (= (q, Q)) \in \mathbb{R}^2$  are the canonically conjugated positions and momenta of coupled units. Further, we assume from now on that these units are of unit mass. The units evolve in a potential

given by  $U_{\text{eff}}(\mathbf{q}) = U(q) + V(Q) + H_{\text{int}}(q, Q)$ , where  $U(q)$  and  $V(Q)$  are positive semi-definite functions, and in addition, are coupled via an interaction potential  $H_{\text{int}}(q, Q)$ . It may be the case that  $U$  and  $V$  describe the same potential landscape. However, to keep the results as general as possible, we consider both cases, i.e. when the potential landscapes are the same, and also when they differ. Crucially, a prerequisite for the occurrence of transport is that these systems contain an open component. That is, on surfaces of constant energy the system must be unbounded in at least one of the spatial coordinates, thus allowing for the possibility of unbounded and directed transport. Therefore, we assume that all systems explored here contain an open component. The equations of motion, corresponding to this class of Hamiltonian systems, are given by

$$\ddot{q} = -\frac{\partial U_{\text{eff}}(\mathbf{q})}{\partial q} \quad \& \quad \ddot{Q} = -\frac{\partial U_{\text{eff}}(\mathbf{q})}{\partial Q}. \quad (51)$$

Before moving onto the first subsection in this part, it is worthwhile discussing a particular potential landscape that is used in all of the forthcoming sections. This potential, often called the *washboard* potential, is periodic (of period 1) and spatially symmetric. It is described by the equation

$$U(q) = U(q+1) = \frac{1 - \cos(2\pi q)}{2\pi}. \quad (52)$$

$U(q)$  has minima at  $q_{\text{min}} = n$ , with  $U(q_{\text{min}}) = 0$ , and maxima at  $q_{\text{max}} = n + 0.5$ , with  $U(q_{\text{max}}) = 1/\pi$  ( $\approx 0.318$ ), where  $n \in \mathbb{Z}$ . As mentioned, the potential is spatially symmetric, i.e.  $U(q) = U(-q)$ .

For now let us suppose that a single unit is evolving in a washboard potential with no external forces present. The occurrence of transport can then be viewed as a string of consecutive escape processes where the unit overcomes the potential barriers located at  $q_{\text{max}}^{n+0.5}$  ( $n \in \mathbb{Z}$ ) with increasing  $|n|$ . The only requirement for directed transport is that the system possesses a sufficient amount of energy so that the unit can overcome these barriers.

An analogous statement regarding transport can be made for the case of two coupled units. However, directed transport in this case may require not just a sufficient amount of system energy, but also a coherent energy exchange between the units. This is elaborated upon in the next section. To conclude this section an interaction potential used in the coming section is presented and its properties briefly discussed. The interaction potential is of the form

$$H_{\text{int}}(q, Q) = D \left[ 1 - \frac{1}{\cosh(q - Q)} \right], \quad (53)$$

which is dependent on the distance  $d = |q - Q|$ . The strength of this coupling is regulated by the parameter  $D$ . Like the washboard potential, the interaction potential is also spatially symmetric —  $H_{\text{int}}(q, Q) = H_{\text{int}}(-q, -Q)$ . It is important to note that the gradient  $dH_{\text{int}}(x)/dx$  goes to zero asymptotically; i.e. as the relative distance  $|q - Q|$  increases, the related interaction forces,  $\partial H_{\text{int}}/\partial q$  and  $\partial H_{\text{int}}/\partial Q$ , vanish asymptotically, allowing for transient chaos [124, 125, 126, 127]. That is, for large distance  $|q - Q| \gg 1$ , the interaction vanishes with the result that the two degrees-of-freedom decouple, rendering the dynamics regular. This is crucial for what is presented in the coming sections.

Transport in autonomous Hamiltonian systems is remarkable due to the fact that a system requires no additional input of energy, in the form of an external time-dependent drive for example, for said transport to occur. Rather an internal energy distribution must take place before transport can take place. This effect is even more remarkable in systems of coupled units when the system's energy does not suffice to allow that both units can undergo rotational motion<sup>3</sup> at the same time. In this case the subsystems, related to each unit, must work cooperatively to achieve transport. We next show that the strength of the coupling between the subsystems is crucial to the resulting dynamics. More than that, some general features of systems of coupled units are exposed.

---

<sup>3</sup>In this review *rotational motion* refers to motion where a unit(s) overcomes consecutive potential barriers in a periodic fashion.

### 3.2.1. Case of a spatially symmetric model

Let us introduce the model that is used in this section. This model is minimal in two respects. The first is that  $U$  and  $V$  describe the same potential landscape – the so-called *washboard potential*. The second is that this system contains only one parameter, namely the parameter that regulates the strength of the bond between the two units. Thus, there are two units evolving in the washboard potential (Eq. (52)) that are coupled via the interaction potential (Eq. (53)).

The equations of motion are given by [128]

$$\ddot{q} = -\sin(2\pi q) - D \left[ \frac{\tanh(q - Q)}{\cosh(q - Q)} \right], \quad (54)$$

$$\ddot{Q} = -\sin(2\pi Q) + D \left[ \frac{\tanh(q - Q)}{\cosh(q - Q)} \right]. \quad (55)$$

For the numerics in the coming sections the initial set-up is as follows. The two units are separated by a sufficient distance such that they are effectively uncoupled, i.e. the energy contained in the interaction potential saturates:  $E_{int} \approx D$ . One unit is situated at the origin, while the other unit is in a potential well that is sufficiently far from the origin, so that the effect of one unit on the other is almost negligible. Further, the unit at the origin is at rest. The additional unit is given an initial velocity that sees it move towards the unit at rest (these units are henceforth be called unit  $A$ , associated with the variables  $(p, q)$ , and unit  $B$ , associated with the variables  $(P, Q)$ , respectively). Of course, the energy supplied to unit  $A$  must be greater than that required to overcome potential barriers of the washboard potential – that is  $E_A(0) > E_b = 1/\pi$ , where  $E_A(0)$  is the energy possessed by unit  $A$  at time  $t = 0$  and  $E_b$  is the barrier height of the washboard potential. Thus, as the relative distance  $|q - Q|$  decreases, the energy exchange becomes more pronounced (depending on the value  $D$ ) and the system dynamics become more complex.

For  $D \neq 0$  the units can interact via the interaction potential and exchange energy. This exchange excites the additional (initially resting) unit and, to varying degrees, influences the motion of the unit that has entered the interaction region. Again, it is important to note that both components of this system are open and thus it is feasible that either unit escapes. For large  $|q - Q| \gg 1$  the interaction between the units vanishes, and again the dynamics is represented by regular rotational motion (assuming sufficient system energy). For the systems considered here, the energy is kept sufficiently low such that the possibility of both units escaping independently is excluded, and the cooperative effects between the units come to the fore.

As mentioned earlier, the initial conditions for unit  $B$  are  $Q = P = 0$ . The unit  $A$  starts as a virtually free unit in the *asymptotic* region, i.e. it approaches the interaction region from a far distance. The initial amount of energy  $E = 0.9$  lies above the highest possible energy of the saddle-centre points but, for not too low coupling, below almost all of the saddle-saddle points of the effective potential (see [129]). The initial positions of the units  $A$  are contained within the well whose minimum is located at  $q \simeq -25$  and the corresponding initial momenta are determined as those points populating, densely and uniformly, the level curve

$$E = \frac{1}{2}p^2 + U(q) + H_{int}(q, 0), \quad (56)$$

in the  $(q, p)$ -plane. Asymptotically, the interaction potential attains a value approaching  $D$ . Therefore, as the units begin in the asymptotic region and as the initial conditions depend explicitly on  $D$ , no two sets of initial conditions are the same. The energy is fixed at  $E = 0.9$ , which is less than three times the barrier height of the washboard potential,  $E_b = 1/\pi \approx 0.3183$ . It should be emphasised that for unit  $B$  to escape, it must gain a sufficient amount of energy from its interaction with unit  $A$ . With no interaction this system contains a strong positive current, as unit  $A$  can escape to infinity feeling no effect from unit  $B$ . It is worth adding that for these initial conditions with  $D \neq 0$  the problem becomes a unit scattering problem with the stationary unit playing the role of the scatter.

We illustrate some of the qualitatively different transport scenarios that are present in this system by varying the strength of the coupling parameter  $D$ . Before this however, it is useful to present a table of  $D$  values that are used in this section along with their respective currents. Unit current is assessed quantitatively by the mean momentum, which is defined by taking the averaged momentum of an ensemble of units, i.e.

$$\bar{p} = \frac{1}{T_s} \int_0^{T_s} dt \langle p(t) \rangle, \quad (57)$$

where  $T_s$  is the simulation time, and the ensemble average is given by

$$\langle p(t) \rangle = \frac{1}{N} \sum_{n=1}^N \sum_{i=1}^2 p_{i,n}(t), \quad (58)$$

with  $N$  being the number of initial conditions. The current, along with details of the calculation, is discussed in detail below. Below is a table of representative coupling strengths with their respective current values.

$D$	$\bar{p}$
0.3	0.925
0.5613	-0.239
0.5617	0.262
0.5672	0.009
0.58169	-0.0001

Fig. 26 contains plots showing the temporal evolution of the coordinates  $q$ ,  $Q$  for the five  $D$  values contained in the table. For comparison, for each  $D$  value, the initial positions of the pair of units are the same, i.e. with  $q(0) = -25.5$  and  $Q(0) = 0$ , and the initial momentum  $p(0)$  of unit  $A$  follows from the relation given in Eq. (56), while unit  $B$  has zero momentum,  $P(0) = 0$ . Slightly altering these initial conditions can have a large impact on the path that the units take, as for a large range of the coupling strength the dynamics is chaotic.

The  $D$  values in the table above have been chosen as they represent, in addition to typical system dynamics, transport scenarios with varying contributions to the net current. With  $D = 0.3$  (Fig. 26 a) ) we see that unit  $A$  is able to pass straight through the interaction region almost unscathed. Unit  $B$  does receive some energy from the interaction, but this energy only allows for small oscillations about its starting position. This set-up favours a strong, positive current. With regard to unit  $B$  leaving its initial potential well, there appears a blow-up at  $D \approx 0.562$ , after which we can expect both units to travel multiple potential wells together. As can be seen in Figs 26 b) & c), both with  $D < 0.562$ , unit  $B$  can largely influence the path of unit  $A$  without actually leaving its starting potential well. Setting  $D$  to 0.5613 (Fig. 26 b) ) we see that the dynamics of the system is quite different. The interaction between the units is such that unit  $A$  can pass through the interaction region (to a certain extent) and subsequently be pulled back, escaping in the negative  $q$  direction and thus contributing to *current reversal*. Again unit  $B$  receives little energy from the interaction. A similar phenomenon can be seen for  $D = 0.5617$  (Fig. 26 c) ). This time unit  $A$  oscillates around  $q = 0$  a number of times before escaping in the positive  $q$  direction maintaining the original direction of the current.

Some of the most interesting behaviour observed in this system can be seen in the remaining two figures. Figs. 26 d) show a trajectory with  $D = 0.5672$ . There are number of striking things that can be noted about this trajectory. Firstly, the duration of time that the trajectories ‘stick’ together before one escapes. In this case unit  $B$  escapes in the positive  $q$  direction. This is substantially longer than the escape times presented in the previous figures. Also, both units take excursions to the left and right before the escape of unit  $B$ . However, the most notable thing about this figure is that *it is unit B that escapes, not unit A* as for the previous  $D$  values. Thus, unit  $B$  is able to gain enough energy to escape from its starting potential well,

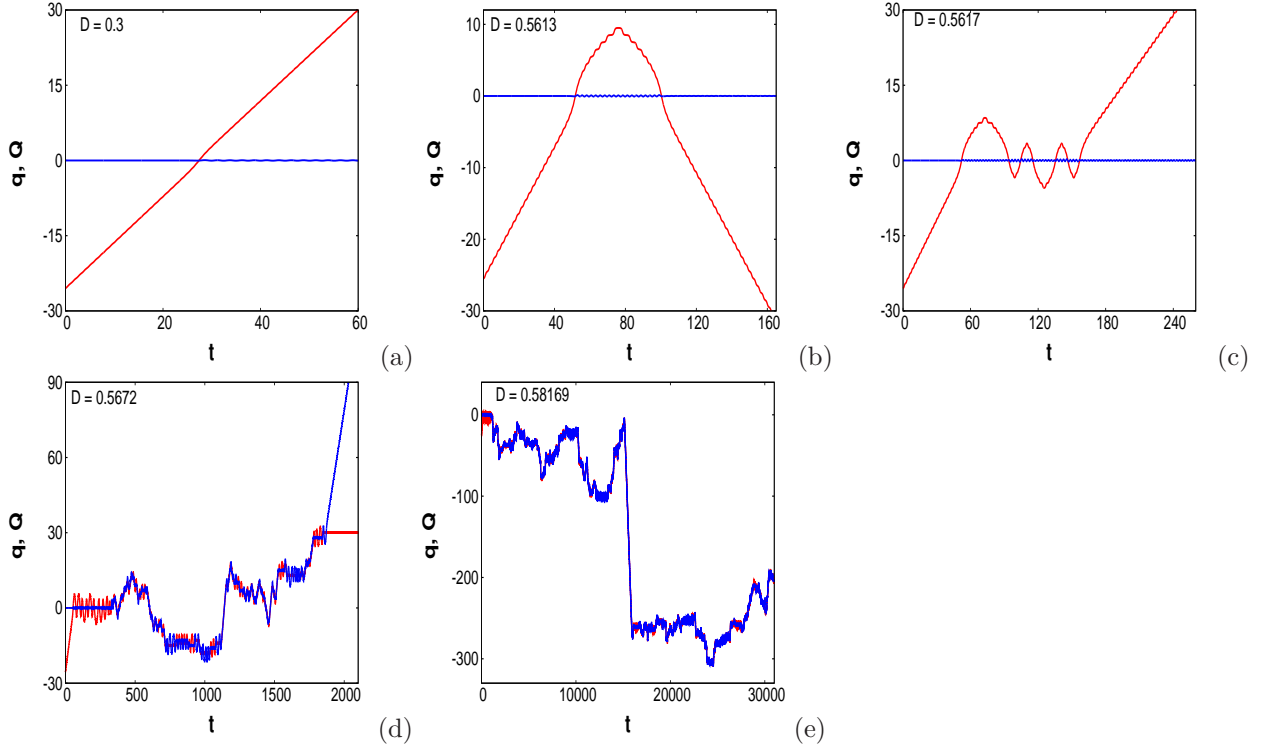


Figure 26: (Colour Online) Example trajectories for an autonomous system consisting of two nonlinearly coupled units, both evolving in a periodic and symmetric potential. Each panel differs by the strength of the parameter  $D$  regulating the strength of the coupling between the units. The red line shows the temporal evolution of Unit  $A$ , which has an initial condition  $q(0) = -25.5$  and  $p(0)$  as obtained from Eq. (56), while the blue line shows the time evolution of unit  $B$  with initial condition for each trajectory chosen as  $Q(0) = P(0) = 0$ . Note the different time-scales. Source: Figure adapted from Ref. [128].

and subsequently from any force that it feels from unit  $A$ . Unit  $A$  has sacrificed its energy and has become trapped. This situation describes an *interchange of the roles* played by the units, with the initially free unit becoming trapped and the initially trapped unit becoming free.

The final figure (Fig. 26 e), with  $D = 0.58169$ , show similar behaviour in that the units seem to ‘stick’ together. However, neither unit escapes, but instead are, in some sense, stuck to each other for the duration of the simulation. This is a process known as *dimerisation*, where the units, each initially acting as a monomer, form a bound unit. This process is evident in some of the previous figures, however in this case, the process is permanent. Both units undergo large excursions, closely following the line  $q = Q$ . For this particular  $D$  value, the units are in a continual and most importantly, a substantial energy exchange. This allows the units to travel together in an erratic fashion undergoing multiple changes of direction and visiting multiple potential wells. Although an independent escape for one of the units remains a statistical possibility, it requires an optimal energy fluctuation that sees one unit sacrifice all of its energy to the other. This is highly unlikely given the fairly strong coupling between the units.

This symmetric model, which consists of two washboard potentials that are coupled via an interaction potential, proves to be a rich source for complex dynamics which produces numerous interesting results. In fact, a number of transport scenarios are possible. The units can undergo independent motions: either, a single unit travels through the potential landscape (the other remaining trapped), or both units are transporting. Alternatively, the units can travel through this landscape in close proximity continuously exchanging energy (this includes the possibility of complete synchronisation where there is no energy exchange). The coupling strength determines which of these scenarios are possible. Furthermore, with fine

tuning of the system parameter which regulates coupling strength, unit scattering leading to the emergence of a non-zero net current, or bond formation (dimerisation) yielding a zero net current, are possible outcomes in this model.

A novel aspect of these autonomous Hamiltonian systems is that directed transport, when it occurs, is regular and permanent. Chaos is needed only in an initial phase of the dynamics to guide trajectories beyond separatrices into the range of unbounded motion. This contrasts with the transport observed in non-autonomous Hamiltonian systems where there is a mixed phase-space [122]. In these non-autonomous systems, finite bursts of almost regular transport are separated by periods of chaotic motion. Thus the autonomous systems, where directed transport is provided solely by regular motion, appear to be favourable with respect to directed transport. However, it should also be emphasized that the transport observed in this autonomous case is predominantly a cooperative effect which uses a favourable energy exchange between subsystems.

An interesting observation is that according to the theory of time-reversal symmetry, this symmetric model should produce a zero net current for all values of  $D$ . The explanation of why this case, and systems alike, can still produce a directed current is the subject of Sec. 3.2.2. This section looks at time-reversal symmetry for the class of systems whose equations of motion are given by Eq. (51) (of which our model is a member). It is explained in detail how this symmetry is broken in practice, thus allowing for the emergence of a non-vanishing net current. Further, a second model is introduced below that is similar to the case studied here but with the exception that one of the washboard potentials is replaced by a different potential. This new potential serves to break one of the spatial symmetries of the system. The consequences of this broken symmetry are also examined.

In systems that satisfy certain spatial and temporal symmetries it is possible to find, in phase-space, two trajectories that nullify each others contribution to the net current. That is to say, for each trajectory in phase-space there exists another complementary trajectory such that collectively both trajectories produce zero net current. Therefore, if a system is to express a non-zero net current, some of these symmetries must be broken. Quite often this is achieved through the addition of a periodic (but non-symmetric) time dependent drive to the system [22, 79, 51]. Analogously, in the autonomous case the introduction of a static bias force that penetrates the plane of motion, usually suffices when breaking the spatial symmetry, thus allowing for the emergence of a non-zero current [110].

We search for the mechanism that serves to break the spatio-temporal symmetries and thus allow for the possible occurrence of a non-zero current in autonomous systems modelling the interaction of coupled units. Crucially, in systems (with a mixed phase-space) that rely on regular interludes between periods of chaotic motion for directed transport, the chaotic periods are seen as destructive with regard to directed transport, in that the average velocity of trajectories in the chaotic component of phase-space will be close to zero. In contrast, the systems looked at here *require chaos* in an initial stage of the dynamics so that trajectories can be captured by hyperbolic structures allowing them to escape. The emergence of a non-zero net current is still dependent on other factors. Particular attention is given to the symmetry properties induced by the inclusion of an interaction potential. The symmetry properties derived are illustrated via an example model system. This model is introduced next.

### 3.2.2. Case of a spatially asymmetric model

The above discussed symmetric model was idealised in that both coordinates of the system obeyed a spatial symmetry; namely the system remains invariant under a change of sign of both coordinates. This is not true of the following asymmetric model were a new potential is introduced that has the effect of breaking a spatial symmetry for one of these two subsystems. Rather than having two units each evolve in a washboard potential, as in the symmetric model case, in this model only one unit evolves in a washboard potential. This unit is coupled to a second unit (which is unable to contribute to the net current due to energy constraints) that serves as an energy deposit from which the unit evolving in the washboard potential can draw energy. The second potential is an anharmonic unit and interactions with this unit are local in nature due to the type of interaction potential and the finite amount of energy injected into the system. It is defined by

$$V(Q) = \exp(-Q) + Q - 1. \quad (59)$$

Unlike the washboard potential which has bounded potential energy  $U(q) \leq E_b = 1/\pi$ , this anharmonic unit has unbounded potential energy for  $\pm Q$ ; i.e  $V(Q) \rightarrow \infty$  as  $Q \rightarrow \pm\infty$ . Note the asymmetry of this potential, i.e.  $V(Q) \neq V(-Q)$ , as this is important when the symmetry properties of this model are discussed. Before moving on to the main focus of this section it is worthwhile exploring some of the coupled system dynamics. The equations of motion are [130]

$$\ddot{q} = -\sin(2\pi q) - D \left[ \frac{\tanh(q-Q)}{\cosh(q-Q)} \right], \quad (60)$$

$$\ddot{Q} = \exp(-Q) - 1 + D \left[ \frac{\tanh(q-Q)}{\cosh(q-Q)} \right]. \quad (61)$$

Let us assume a finite system energy. For  $D = 0$ , the system decouples into two integrable subsystems and the dynamics is characterised by individual regular motions of the unit in the washboard potential, and bounded oscillations of the additional degree-of-freedom (due to the energetic constraints), respectively. For  $D \neq 0$ , the subsystems interact, thereby exchanging energy. While the  $Q$ -unit performs solely bounded motion there is the possibility that, for an escaping unit, the corresponding coordinate,  $|q|$ , attains large values and thus the related interaction forces,  $\partial H_{\text{int}}/\partial q$  and  $\partial H_{\text{int}}/\partial Q$ , vanish asymptotically, allowing transient chaos [126, 127, 131]. That is, for large distance  $|q - Q| \gg 1$ , the interaction vanishes with the result that the two degrees-of-freedom decouple, rendering the dynamics regular.

Looking at example trajectories for three representative coupling values reveals some of the system's dynamics. Fig. 27 presents the time evolution of the coordinates  $q$  &  $Q$  for  $D = 0.4, 0.75, 1.5$ . In addition, the corresponding partial energies of the unit and the deposit degree-of-freedom are presented. The partial energies for both units are given by

$$E_q = \frac{1}{2}\dot{q}^2 + U(q) + \frac{1}{2}H_{\text{int}}(q, Q), \quad E_Q = \frac{1}{2}\dot{Q}^2 + V(Q) + \frac{1}{2}H_{\text{int}}(q, Q), \quad (62)$$

where the interaction energy has been evenly divided between the two units.

Three qualitatively different transport scenarios are presented. Note that for the numerics the system's energy is fixed at  $E = 1.5$ . Further, the initial conditions have been chosen so that all the system's energy is initially in the deposit degree-of-freedom. For the low value  $D = 0.4$  (left column) the washboard unit undergoes small amplitude oscillations about a potential minimum. Crucially, with regard to transport, these oscillations are much lower than the barrier height  $E_b = 1/\pi$  of the washboard potential. In contrast, the deposit degree-of-freedom sees oscillations of much larger magnitude. Looking at the partial energies of the washboard unit and the anharmonic unit, it can be seen that there is an insufficient energy exchange to allow for the washboard unit to overcome the barrier height  $E_b$  – a prerequisite for the occurrence of transport. The dynamics changes drastically when the coupling strength is increased to  $D = 0.75$  (middle column). The early dynamics ( $t < 10$ ) is similar to the situation described above. Subsequently, the washboard unit escapes from its starting potential well and travels to multiple wells in both directions. At  $t \approx 40$  the washboard unit gains sufficient energy to allow it to undergo independent directed transport. That is, after a chaotic transient, the two subsystems decouple rendering the dynamics regular. The chaotic exchange of energy preceding the directed transport of the washboard unit is clearly visible in Fig. 27. It is also clear that after the chaotic transient, the energy exchange between the two units terminates. A further increase in the coupling strength to  $D = 1.5$  (right column) results in a third qualitatively different transport scenario. It appears that the washboard unit is free to travel multiple potential wells. However, for the duration of the simulation it is confined to potential wells in the range  $-2.5 < q < 2.5$ . The reasons for this are two-fold. Firstly, as is proven rigorously [119], with  $D = 1.5$  (and  $E = 1.5$ ) the possibility of directed transport for the washboard unit is excluded. Secondly, the system's (finite) energy means that oscillations of the anharmonic potential are bounded. Combined, this results in two units that remain in close contact and under constant chaotic energy exchange.

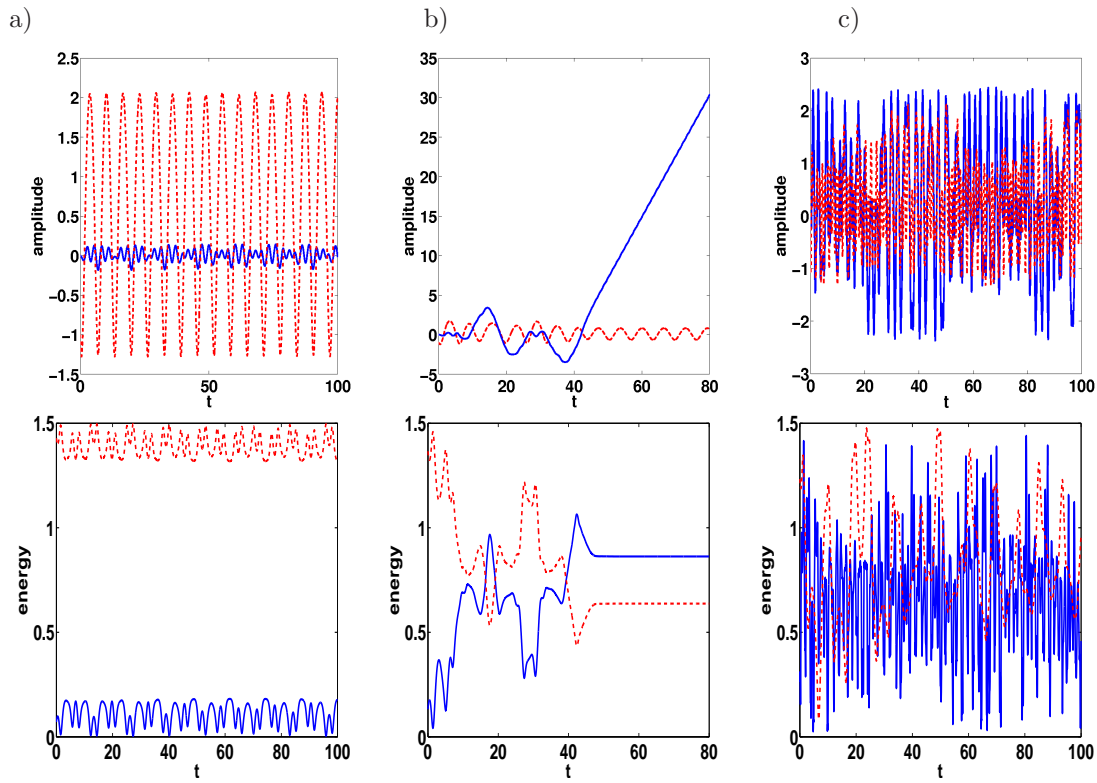


Figure 27: (Colour Online) Example trajectories in the spatially asymmetric model described by Eqs. (60)-(61). The top panels show the time evolution of the coordinates  $q$  (solid blue line) and  $Q$  (dashed red line) for three different values of the coupling strength  $D$ : (a)  $D = 0.4$ , (b)  $D = 0.75$ , and (c)  $D = 1.5$ . The bottom panels show the corresponding evolution of the energies. The unit with coordinate  $q$  has dynamics that take place in a periodic and symmetric potential, while the unit with coordinate  $Q$  has dynamics that take place in an asymmetric and anharmonic potential. The units are coupled via an symmetric anharmonic potential. Source: Figure taken from Ref. [130].

### 3.2.3. Symmetry breaking and emergence of a current

It was shown that with a suitable choice of parameters the second asymmetric model can exhibit directed transport, which is a necessary, but not sufficient, condition for a system to show a non-zero net current. However, the class of systems that this asymmetric model belongs to possesses time-reversibility symmetry and the implications of this with regard to the net current are extremely important. These implications, and a mechanism for destroying this symmetry, was discussed in Ref. [132] (and further in Ref. [119]) and will be the focus of this section.

The class of systems in question are Hamiltonian and of the form

$$H(\mathbf{p}, \mathbf{q}) = \frac{1}{2}\mathbf{p}^2 + U_{\text{eff}}(\mathbf{q}) \quad (63)$$

where  $\mathbf{p}, \mathbf{q} \in \mathbb{R}^n$ ,  $\mathbf{p}$  and  $\mathbf{q}$  are the canonically conjugated momenta and positions, and  $U_{\text{eff}}(\mathbf{q})$  is the potential function. With transport and directed current being of interest, it is assumed that  $U_{\text{eff}}(\mathbf{q})$  provides an open component. To reiterate, this means that on constant energy surfaces, the system may be unbounded in one, or more, of its coordinates.

The corresponding Hamiltonian equations  $\dot{p}_i = -\partial H/\partial q_i$  and  $\dot{q}_i = \partial H/\partial p_i$ ,  $1 \leq i \leq n$ , exhibit the time-reversibility symmetry, i.e. there exists a time-reversal operator  $\hat{\tau}$  such that if  $\mathbf{X}$  is a solution, then so is  $\hat{\tau}\mathbf{X}$ . In more detail, suppose that solutions take the form  $\mathbf{X}(t) = [\mathbf{p}(t), \mathbf{q}(t)]$ . Applying the time-reversal operator yields  $\hat{\tau}[\mathbf{p}(t), \mathbf{q}(t)] = [-\mathbf{p}(-t), \mathbf{q}(-t)]$ . This operation is involutory as  $\hat{\tau}^2[\mathbf{p}(t), \mathbf{q}(t)] = [\mathbf{p}(t), \mathbf{q}(t)]$ . As for the implication of time-reversibility with respect to the net current, consider a solution with initial condition (at  $t = 0$ ) given as  $\mathbf{X}(0)$ . Given a finite observation time  $T$  (relevant for numerical and experimental studies), let  $\mathbf{X}(t)$  evolve from  $\mathbf{X}(0)$  to  $\mathbf{X}(T)$ . This trajectory is called the *forward* trajectory. At this point the time-reversal operator is applied which switches the sign of the momenta and changes the direction of time. This creates a new initial condition  $\hat{\tau}\mathbf{X}(T)$  which can be evolved in (negative) time. This trajectory is called the *backward* trajectory. In fact, when the system is evolved from this new initial condition it traces over the forward trajectory in coordinate-space. Note that the forward and backward trajectories coincide in coordinate-space, but not in phase-space due to the change in the sign of momenta. Given the general nature of the above initial condition  $\mathbf{X}(0)$ , we can conclude that on constant energy surfaces, for each such initial condition there exists a corresponding initial condition  $\hat{\tau}\mathbf{X}(T)$  such that they cancel each others contribution to the net current. Therefore, for systems with time-reversibility symmetry there is no preferred direction of the flow thus preventing the emergence of a directed current.

The content of the above discussion is shown schematically in Fig. 28. Imagine  $q = \theta$  is the angle of rotation of a pendulum, and  $p = \dot{\theta}$  is the corresponding angular velocity. Then the top half of the figure (in red) shows the phase portrait of a pendulum, with initial condition  $X(0) = (p(0), q(0))$ , undergoing rotational motion. The trajectory terminates at  $X(T) = (p(T), q(T))$ . The bottom half of the figure (in blue) is the time-reversed counterpart of this trajectory,  $X(T-t)$ , with the initial condition  $\tau X(T) = (-p(T), q(T))$ . With a view to the present work, we can imagine a single unit, with position  $q$  and momentum  $p$ , undergoing rotational motion in a washboard potential.

Applying the time-reversal operator to the system and the original initial condition  $X(0)$  produces another possible motion of the system [133]. However, it is not always the case that these two trajectories produce average velocities that are equal in magnitude but opposite in sign. For example, its possible to envisage a potential such that a unit moving to the right will fall into a ‘trap’, while the unit moving to the left will experience unbounded motion. Clearly, the sum of the two average velocities will not equal zero. The point emerges that to produce (and guarantee that) two trajectories with zero average velocity, the first needs to be evolved to some terminal time  $t = T$  at which point the time reversal operator is applied.

It should also be mentioned that the act of selecting an initial condition can be sufficient in itself to violate time-reversibility symmetry. That is, even though the equations of motion are time-reversal symmetric, not all solutions need necessarily have this symmetry. This is the case for trajectories where the initial condition and its time reversed counterpart follow distinct paths in phase-space. As an example of such a trajectory consider a continuously rotating pendulum (cf. Fig. 28). So by creating a trajectory with time-averaged velocity  $\nu \neq 0$ , over an observation time of duration  $t = T$ , and initial condition  $X_0$ , time-reversibility symmetry has been broken, unless a second initial condition  $\hat{\tau}X_T$  is chosen that produces a trajectory with

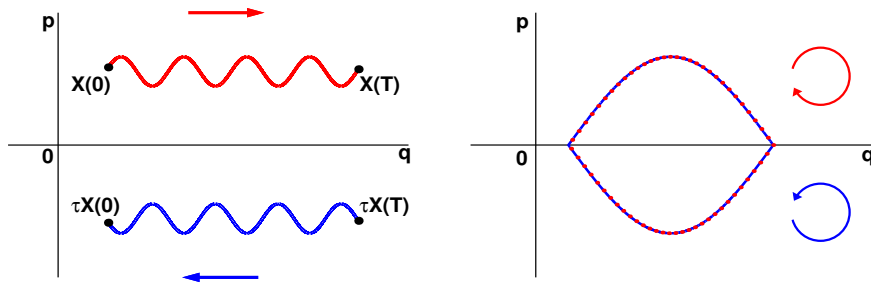


Figure 28: (Colour Online) Time reversal symmetry in the case of a simple pendulum. Left: Schematic illustration of the forward (red) and backward (blue) trajectories for a unit in the regime of rotational motion. The forward trajectory has initial condition  $X(0)$  and terminal coordinate  $X(T)$ , whereas the time-reversed trajectory has initial condition  $\tau X(T)$  and terminal coordinate  $\tau X(0)$ . Right: Schematic illustration of the forward (red) and backward (blue) trajectories for a unit in the regime of librational motion. Source: Figure taken from Ref. [119].

time-averaged velocity  $-\nu$ . This is not true for self-reversed trajectories where the initial conditions  $X_0$  and  $\hat{\tau}X_T$  produce trajectories that coincide in phase-space. The librating trajectories of a pendulum are self-reversed. See Fig. 28 for a schematic illustration of this. The same principles apply to trajectories that wander chaotically in phase-space.

Given what has just been discussed, it seems a rather hopeless situation to find a Hamiltonian of the form given in Eq. (63) that expresses a non-zero net current, because every initial condition is related to another that negates its contribution to the current. This statement is true as long as the entire energy surface is populated with initial conditions. However, for systems with an open component, i.e. unbounded in at least one of its coordinates, it is not feasible to populate an entire energy surface with initial conditions. Therefore, it is more natural to define a finite set of initial conditions which, given the infinite extent of (at least one of) the coordinates can be regarded as *localised in space*. Such sets of initial conditions are frequently used in applications (see [134] for an example), and are chosen to be physically relevant, such as for the problem of a unit flow emerging when the units are initially trapped in a single well of a spatially infinitely extended multiple well potential. Indeed this is done when the second model is further examined in a later section.

Looking more closely at the implication of choosing localised initial conditions, it is supposed that the coordinates are localised in the domain  $q_{j,l} \leq q_j(0) \leq q_{j,r}$  with  $1 \leq j \leq n$  representing the index of each degree-of-freedom (which for the present discussion is not restricted to two), and the subscripts  $l$  and  $r$  denote left and right respectively. Let a trajectory (with regard to a finite observation time  $T$ ) be *transporting* if (i) at least one of the coordinates  $q_j(t)$  escapes from the domain of the localised initial conditions in some time  $0 < t_{escape} \ll T$  and (ii) it subsequently undergoes directed motion, that is,  $\langle p_j(t) \rangle \neq 0$  for  $t_{escape} \leq t \leq T$  where  $\langle \cdot \rangle$  denotes the average with respect to time. This gives a trajectory moving away from the set of localised initial conditions such that at the end of the observation time one of the terminal coordinates obeys  $q_j(T) < q_{j,l}$  or  $q_j(T) > q_{j,r}$  for some  $j$ . Thus, the situation has arisen where the initial condition of the corresponding backward trajectory, which would compensate the contribution of the forward trajectory to the current, is not contained in the set of localised initial conditions. This seems to suggest that in systems where time-reversibility has been broken, via the use of localised initial conditions, there will be a non-zero directed current. This is not necessarily the case. In fact other symmetries need first to be violated, i.e. spatial symmetries. This is seen more clearly when the symmetry properties of the second, asymmetric model are considered. First, let us examine the conditions that allow for the occurrence of a non-zero current in the symmetric model case.

#### 3.2.4. The emergence of a non-zero current in the symmetric case

Before moving on, let us return to the previously discussed symmetric model and examine the initial conditions used there. It is worth noting that as the system is spatially symmetric and yet a non-zero current

can emerge in the ensemble dynamics, the choice of initial conditions must consequently be important. First, let us recall what these initial conditions are. Let us denote some initial condition by  $X(0)$  where  $X(0) = (p(0), q(0), P(0), Q(0))$  with  $Q(0) = P(0) = 0$ ,  $p(0) > 0$  and  $q(0) \in (-25.5, -24.5)$ . Thus, the initial dynamics will see the coordinate  $q(0)$  approach  $Q(0)$ .

Applying the time-reversal operator to  $X(0)$  yields  $\tau X(0) = \hat{X}(0) = (-p(0), q(0), -P(0), Q(0))$ . The flow, generated by the equations of motion with initial conditions  $X(0)$  and  $\hat{X}(0)$ , do not necessarily produce zero-averaging counter-propagating trajectories. This is clear when one considers that with  $X(0)$  the coordinate  $q(0)$  will approach  $Q(0)$ . However, under the flow with initial condition  $\hat{X}(0)$  the distance between these coordinates is monotonically increasing. This holds true for all such initial conditions defined above. Thus, the presence of the interaction potential breaks time-reversibility for this set of initial conditions. This echoes Loschmidt's paradox in that the underlying system obeys time-reversibility, yet some ensembles do not obey the symmetry. Thus, this system has helped to illuminate an important point, from the point of view of current generation. Namely, a system (with initial condition  $X(0)$ ) under time-reversal does not necessarily produce counter-propagating trajectories,  $X(0)$  &  $\tau X(0)$ , that combined have zero averaged current.

In fact, the appropriate initial condition  $\hat{X}(0)$  that would produce the counter-propagating trajectory negating the current contribution of the trajectory with initial condition  $X(0)$  is given by  $\hat{X}(0) = (-p(0), -q(0), 0, 0)$ . Crucially, the set of initial conditions described above does not contain  $\hat{X}(0)$ , and thus this explains the emergence of a current. It should be noted that  $\hat{X}(0)$  is not created through any time-reversal operation. Rather, this initial condition is generated from the system's spatial symmetries. Another point to note is that if the original initial conditions  $X(0)$  are evolved for any time  $T > 10$  (which the simulations exceed by far) then the time-reversed initial condition  $\tau X(T)$  is outside the set of localised initial conditions (as described above). Thus the temporal *and* spatial symmetries have been violated through the choice of initial conditions.

### 3.2.5. Time-reversal symmetry manifolds

The system Eq. (63) possesses an energy integral

$$E = \frac{1}{2}\mathbf{p}^2 + U_{\text{eff}}(\mathbf{q}). \quad (64)$$

There exists a closed maximum equipotential surface  $U_{\text{eff}}(\mathbf{q}) = E$  bounding all motions and one has  $p = P = 0$ , on this surface. Moreover, for Hamiltonian systems of the form Eq. (63) time-reversibility is manifested in coordinate-space in the symmetry features induced by reflections on the time-reversibility symmetry manifolds.

In the case of the two models discussed, or any two-degree-of-freedom system for that matter, the symmetry manifolds are represented by symmetry lines. In general, for  $n$ -degree-of-freedom systems, these symmetry manifolds are obtained by setting the velocities (momenta) equal to zero. This produces an  $n$ -dimensional 'mirror' plane,

$$M = \{\mathbf{q} \mid \mathbf{p} = \mathbf{0}\} \quad \mathbf{q}, \mathbf{p} \in \mathbb{R}^n \quad (65)$$

where the trajectories starting on this plane will follow the same path in coordinate-space in forward and backward time. This is clear when one considers the form of the Hamiltonian being even in the momenta  $\mathbf{p}$  and the fact that the time-reversal operator changes the sign of the momenta  $\mathbf{p} \rightarrow -\mathbf{p}$ . More accurately, the time reversibility manifolds are given by

$$S_k : \quad -\frac{\partial U_{\text{eff}}}{\partial q_k} = F_k(\mathbf{q}) = 0, \quad 1 \leq k \leq n. \quad (66)$$

Let us consider reflections of a trajectory, projected onto coordinate space, on the symmetry manifolds  $S_k$  induced by the corresponding operators  $\hat{R}_k$ . First note that the reflections spoken of here are not spatial reflections. Rather, these reflections map each point of a trajectory onto another,  $\mathbf{q} \rightarrow \hat{R}_k(\mathbf{q})$ , on

equipotentials,  $U_{\text{eff}}(\mathbf{q}) = U_{\text{eff}}(\prod_{k=1}^m \hat{R}_k(\mathbf{q}))$ , such that the sign on the right hand side of the equations of motion for  $\dot{p}_k$  are reversed,  $\text{sign}(F_k(\hat{R}_k(\mathbf{q}))) \neq \text{sign}(F_k(\mathbf{q}))$ , with  $1 \leq k \leq n$ .

Observe that upon reflecting on all symmetry manifolds the relation

$$U_{\text{eff}}(\mathbf{q}) = U_{\text{eff}}\left(\prod_{k=1}^m \hat{R}_k(\mathbf{q})\right), \quad 1 \leq m \leq n \quad (67)$$

is left invariant under permutations of the reflection operators. In fact, time-reversing symmetry is in coordinate-space tantamount to invariance with respect to reflections on the symmetry manifolds. In more detail, any self-reversed trajectory, projected onto coordinate-space, repeatedly crosses every symmetry manifold  $S_k$  upon which each time the sign of the corresponding force  $-\infty < F_k(\mathbf{q}) < \infty$  changes. Moreover, each crossing subsequent to the previous one occurs from the opposite direction. Thus there must be turning points for the trajectory, contained in the maximum equipotential surface  $U_{\text{eff}}(\mathbf{q}) = E$ , implying bounded motion and no directed flow can arise. Notice that no assumptions with regard to the spatial symmetries of the trajectory are needed. In contrast, as transporting (unbounded) trajectories are not invariant with respect to reflections on the symmetry manifolds, preservation of time-reversing symmetry is not possible. A transporting trajectory may escape without having crossed a symmetry manifold at all. However, if it does cross then after all such crossings of a symmetry manifold, the escaping trajectory promotes directed transport. Nevertheless, reflections on the symmetry manifolds, mapping a transporting trajectory onto another transporting one, can induce spatial symmetries such that these two trajectories mutually compensate each others contribution to the net flow. Let the point  $\mathbf{q}_O$  in coordinate-space be an initial condition associated with a transporting trajectory. Reflecting in coordinate-space on the symmetry manifolds  $S_k$  transforms an original point,  $\mathbf{q}_O$ , into its image point,  $\mathbf{q}_I$ , according to  $\hat{R}_k \mathbf{q}_O = \mathbf{q}_{I,k}$  reversing the sign on the r.h.s. in the equations of motion for  $\dot{p}_k$  according to  $\text{sign}(F_k(\mathbf{q}_O)) \neq \text{sign}(F_k(\mathbf{q}_{I,k}))$ . However, the magnitude of the gradients  $F_k = -\partial U_{\text{eff}}/\partial q_k$  is not necessarily maintained. Reflection on all of the symmetry manifolds yields

$$\prod_{k=1}^n \hat{R}_k \mathbf{q}_O = \mathbf{q}_I \quad \text{and} \quad U_{\text{eff}}(\mathbf{q}_O) = U_{\text{eff}}(\mathbf{q}_I) \quad (68)$$

reversing the sign in each of the r.h.s. of the equations of motion for the evolution of the momenta  $\text{sign}(F_k(\mathbf{q}_I)) \neq \text{sign}(F_k(\mathbf{q}_O))$ ,  $1 \leq k \leq n$ . With the time evolution of a coordinate expressed as

$$q_k(t) = q_k(0) + \int_0^t dt' \{p_k(0) + \int_0^{t'} dt'' [-F_k(\mathbf{q}(t''))]\}, \quad (69)$$

we conclude that, for the pair of trajectories emanating from  $\mathbf{q}_O$  and  $\mathbf{q}_I$ , symmetry (zero net flow) results if  $(\mathbf{p}_I, \mathbf{q}_I) = (-\mathbf{p}_O, -\mathbf{q}_O)$  so that  $F_k(\mathbf{q}_I) = -F_k(\mathbf{q}_O)$ ,  $1 \leq k \leq n$ . This is the case when the potential is even in the coordinates, that is  $U_{\text{eff}}(\mathbf{q}) = U_{\text{eff}}(-\mathbf{q})$  (the symmetric model for example). Then there exist pairs of current-annihilating *counterpropagating* trajectories,  $X(t)$ , starting from  $X(0)$ , and  $-X(t)$ , starting from  $-X(0)$ . In other words, *reversion symmetry* under reflections on the symmetry manifolds is needed for zero net flow which, together with invariance with respect to changes of the sign of the momenta, amounts to parity-symmetry of the system  $H(\mathbf{p}, \mathbf{q}) = H(-\mathbf{p}, -\mathbf{q})$ . Conversely, violation of reversion symmetry with respect to at least one of the coordinates  $q_k$  establishes a prerequisite for the occurrence of directed flow.

### 3.2.6. The effect of broken symmetries

It is useful to see how the above theory on spatio-temporal symmetries can be applied in practice, and in particular to observe the effects of breaking these symmetries. For this reason, the spatio-temporal symmetry properties of the asymmetric model are next examined. Particular attention is given to the phase-space dynamics and to current generation where the effects of broken symmetries is most clearly visible.

The asymmetric model has an effective potential given (in short) by

$$U_{\text{eff}}(\mathbf{q}) = U(q) + V(Q) + H_{\text{int}}(q, Q) \quad (70)$$

where  $U(q)$  is the washboard potential,  $V(Q)$  is the anharmonic (deposit) potential, and  $H_{\text{int}}(q, Q)$  is the interaction potential. Some properties of the washboard and interaction potentials were discussed in the introduction to Sec. 3. However, it is worth reiterating those that are relevant in this section. The washboard potential is of period one and observes the coordinate symmetry  $U(q) = U(-q)$ . This amounts to symmetry with respect to  $q_n = n/2$  for every integer  $n$ . Likewise, the interaction potential is invariant under reflections of its argument, namely  $(q - Q) \leftrightarrow -(q - Q)$ . In contrast, the deposit degree-of-freedom  $V(Q)$  does not obey such a reflection symmetry. That is,  $V(Q) \neq V(-Q)$  resulting in equations of motion (cf. Eq. (60) & Eq. (61)) that do not remain invariant under reflections in  $Q$ .

Even with the anharmonic part  $V(Q)$ , which breaks a reflection symmetry of the system, the asymmetric model case still possesses time-reversal invariance. Thus, if the phase-space is entirely populated with initial conditions, then the system will produce a zero net current. This raises the question of what effect localised initial conditions imply for the system's current output.

At this point it is worthwhile describing exactly the set of initial conditions that were used in the numerical analysis of the asymmetric model. These initial conditions were chosen such that the washboard unit was at rest at the origin, with the system's energy initially residing in the deposit degree-of-freedom and the interaction potential. In more detail, at time  $t = 0$ , the washboard unit's position and velocity were given by  $q(0) = \dot{q}(0) = 0$ . Thus the washboard unit begins its time evolution with zero energy. Assuming system energy  $E$ , the set of initial conditions for the remaining degrees-of-freedom are chosen to populate uniformly and densely the level curve

$$E = \frac{1}{2}\dot{Q}^2 + V(Q) + H_{\text{int}}(0, Q) \quad (71)$$

in the  $(Q, \dot{Q})$ -plane. This set is topologically a circle. Importantly, these initial conditions are unbiased in the velocity, i.e.  $\dot{Q} \leftrightarrow -\dot{Q}$ .

Returning to the symmetry analysis we now turn our attention to the time-reversal symmetry manifolds. As this is a two-degree-of-freedom system, the symmetry manifolds will exclusively be termed symmetry lines. Setting the velocities in Eq. (60) & Eq. (61) equal to zero obtains Ref. [130]

$$S_1 : \quad \sin(2\pi q) + D \frac{\tanh(q - Q)}{\cosh(q - Q)} = 0, \quad (72)$$

$$S_2 : \quad \exp(-Q) - 1 + D \frac{\tanh(q - Q)}{\cosh(q - Q)} = 0. \quad (73)$$

The symmetry line  $S_1$  exhibits the following symmetry:

$$Q \rightarrow -Q, \quad \frac{n}{2} + q \rightarrow -\frac{n}{2} - q : \quad S_{1,n} \rightarrow -S_{1,-n} \quad (74)$$

with  $n$  labelling the branches of the symmetry line as  $S_{1,n}$ . The occurrence of the multiple branches of the  $S_1$  symmetry line can be understood by considering the symmetries of the washboard potential. In contrast,  $S_2$  yields a single branch containing no apparent symmetries.

The two cases, coupled and uncoupled, result in markedly different dynamics. Notably, uncoupling the two subsystems produces integrable dynamics. The dynamics becomes non-integrable (chaotic) when the two subsystems are coupled. This complexity is also manifested in the symmetry lines  $S_1$  and  $S_2$ . To see this, consider first the uncoupled case. With the coupling parameter  $D = 0$ , the equations representing the symmetry lines are simplified and solutions take the form  $q = n/2$  for all  $n \in \mathbb{Z}$  and  $Q = 0$ . For  $D \neq 0$  the solutions to the equations for  $S_1$  and  $S_2$  become more complicated. This point is illustrated in Fig. 29 which shows the time-reversal symmetry lines when  $D = 0.75$ . For illustration, only the branches of the symmetry line  $S_{1,n}$ , with  $n = -1, 0, 1$ , related to the starting potential well are shown. The direction of flow, as determined by the sign of the forces  $-\partial U_{\text{eff}}/\partial q$  and  $-\partial U_{\text{eff}}/\partial Q$ , is indicated by arrows in the different regions in the coordinate plane. Boundaries of the energetically-allowed region in coordinate-space are represented by the two lines labelled  $B_e$ . Reflections of a trajectory, projected onto coordinate space, on

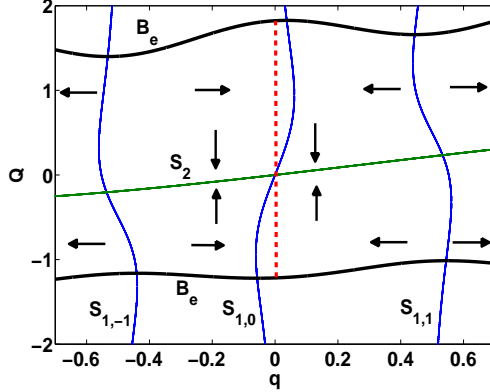


Figure 29: (Colour Online) Time-reversal symmetry lines in the coordinate plane  $(q, Q)$  - see Eqs. (72)-(73). The coupled particle (conservative) dynamics take place in a spatially asymmetric potential. The system's energy is  $E = 1.5$  and the energetically accessible region is bounded by the two curves indicated by  $B_e$ . The dashed (red) line corresponds to the location of the initial conditions projected onto coordinate-space. Arrows indicate the direction of flow in different regions, as determined by the sign of the forces  $-\partial U_{\text{eff}}/\partial q$  and  $-\partial U_{\text{eff}}/\partial Q$ . Source: Figure taken from Ref. [130].

the symmetry lines  $S_k$  are induced by the corresponding operators  $\hat{R}_k$  mapping each point on the trajectory to another one on equipotentials

$$U_{\text{eff}}(q, Q) = U_{\text{eff}}\left(\prod_{k=1}^2 \hat{R}_k(q, Q)\right), \quad (75)$$

such that the sign on the r.h.s. in the equations of motion is reversed, i.e.,

$$\text{sign}(\partial U_{\text{eff}}(q, Q)/\partial q) \neq \text{sign}(\partial U_{\text{eff}}(\hat{R}_1(q, Q))/\partial q) \quad (76)$$

upon reflection on  $S_1$ , and

$$\text{sign}(\partial U_{\text{eff}}(q, Q)/\partial Q) \neq \text{sign}(\partial U_{\text{eff}}(\hat{R}_2(q, Q))/\partial Q) \quad (77)$$

upon reflection on  $S_2$ . Note that the magnitude of the gradients  $\partial U_{\text{eff}}(q, Q)/\partial q$  and  $\partial U_{\text{eff}}(q, Q)/\partial Q$  is not necessarily maintained.

It is clear that the symmetry lines for the uncoupled and coupled system are significantly different. Coupling the two subsystems has the effect of contorting the symmetry lines. It should be stressed again that even though the time-reversal symmetry lines differ for each value of the coupling parameter, the result for the net current is the same when the energy surface is entirely populated by initial conditions. That is, when the energy surface is entirely populated by initial conditions, the resulting current is zero regardless of the value  $D$  which regulates the coupling strength.

Now the issue of localised initial conditions can be addressed. The initial conditions described above are shown, projected onto the  $(q, Q)$ -plane, as the red dashed line in Fig. 29 which shows the time-reversal symmetry lines for  $D = 0.75$ . Notice that one branch of the symmetry lines  $S_{1,0}$  divides the initial conditions into two segments, each promoting transport in different directions. For the segment lying to the left of  $S_{1,0}$  the flow is in the direction of positive  $q$ , while in the segment to the right of  $S_{1,0}$  the flow moves in the direction of negative  $q$ . Crucially, there is an imbalance in the size of the segments, and thus initially there is an unequal number of trajectories moving towards the two chaotic saddles located at the intersections of  $S_{1,1}$  and  $S_{1,-1}$  with  $S_2$ . This imbalance and the fact that the system contains an open component allows for the emergence of a non-zero directed current.

Previously, it has been stated that broken spatial-symmetries are of no consequence (with respect to the current) for systems with an energy surface entirely populated with initial conditions. However, the above

discussion shows that for localised initial conditions broken symmetries play an important role. Namely, the asymmetric  $V(Q)$  breaks time-reversibility for the localised initial conditions described above. Moreover, using a different potential  $V(Q)$ , which is invariant under reflections in  $Q$ , would restore the symmetry between counterpropagating trajectories, leading to a zero current.

It is worth re-emphasising that the mechanism responsible for the non-zero net current presented in this section is novel in that it doesn't require a mixed phase-space, induced by time-periodic driving, consisting of regular and chaotic components [78, 84, 51]. Rather, for the autonomous systems discussed here chaos is only needed in an initial stage of the dynamics to guide trajectories onto regular paths [96],[130],[132]. After the finite period of transient chaos, the units subsequently undergo regular rotational motion. This is in contrast to the sticking episodes close to tori, of finite duration, that provide a non-zero net current in the non-autonomous Hamiltonian case.

A step in this direction, i.e. of directed transport in autonomous systems, was taken by [135]. In a three degree-of-freedom system, modelling a molecular motor, the external time periodic driving was replaced by an autonomous degree-of-freedom that acts as an energy store. They observed that energy was able to propagate through the system resulting in directed transport. However, their results differ from the results presented in this section in two respects. Firstly, transport in the molecular motor model was aided by thermal fluctuations. Secondly, although on the one hand noise aided transport, on the other it also had the effect of destroying transport. Thus, the intervals transport (which are of finite duration) are separated by periods of bounded motion.

### 3.3. Collective transport in time-dependent driven systems

In Sec. 3.2 the Hamiltonian dynamics of autonomous systems of two coupled units were explored. This part continues in a similar vein. However, the equations of motion are augmented by the inclusion of time-dependent driving and dissipative terms, thus adding further complexity to the coupled dynamics. Further, the short range interaction potential Eq. (53) (which allows for the occurrence of certain phenomena, in particular transient chaos) is replaced by a potential that allows for long range interactions between the particles.

In Sec. 3.3.1 the driven and damped dynamics of two interacting particles evolving in a symmetric and spatially periodic potential is considered. The latter is exerted to a time-periodic modulation of its inclination. For directed particle transport mediated by rotating periodic motion, exact results regarding the collective character of the running solutions are derived. Sec. 3.3.3 reports on the cooperativity-induced negative mobility in the dynamics of two coupled particles climbing in unison against the direction of the bias force. Sec. 3.3.4 deals with the transport dynamics of systems with many degrees of freedom in form of an extended linear chains evolving in a washboard potential. By means of adiabatically slow modulations of the potential landscape the extended chain of coupled particles escapes from the confinement of a potential well, and subsequently enters a regime of long lasting transients where the entire chain transports in a ballistic fashion.

#### 3.3.1. Collective periodic running states in coupled particle dynamics

The considered systems consist of two coupled particles each evolving in a washboard potential. The particles are driven by a time periodic force and damped. These systems are nonautonomous and without conservation of energy. They possess coupled inertial dynamics of the form [136]

$$\ddot{q}_1 = -\sin(2\pi q_1) - \gamma \dot{q}_1 + F_1 \sin(\Omega t + \theta_0) - \kappa(q_1 - q_2), \quad (78)$$

$$\ddot{q}_2 = -\sin(2\pi q_2) - \gamma \dot{q}_2 + F_2 \sin(\Omega t + \theta_0) + \kappa(q_1 - q_2), \quad (79)$$

where  $\gamma$  is the strength of the damping,  $F_{1,2}$  are the driving amplitudes, and  $\Omega, \theta_0$  are the driving frequency and phase respectively.  $\kappa$  represents the strength of the linear coupling between the two particles.

The focus of this section is on how the coupling strength influences the dynamics of the system above (Eq. (78) and Eq. (79)). However, it is useful for what is to come to understand the uncoupled dynamics ( $\kappa = 0$ ) of this system [94]. That is, the dynamics of a single driven and damped particle evolving in a

washboard potential. The dissipative nature of this system means that all orbits will eventually evolve = to one of the systems, possibly coexisting, attractors. The type of attractors present will depend on the parameters used, while the particular attractor that an orbit evolves to is dependent on the initial condition. This is illustrated in Fig. 30 where two qualitatively different attractors are shown. The parameters used are  $\gamma = 0.1$ ,  $\Omega = 2.25$ ,  $\theta_0 = 0$ . The strange chaotic attractor (blue) results when the driving amplitude is  $F = 1.3$ . Increasing this driving amplitude to  $F = 1.5$  results in the periodic attractor (red). With regard to a net current the transporting orbits evolving on the periodic attractor will yield a non-zero net current, whereas the trajectories landing on the strange chaotic attractor are, on long time scales, typically expected to produce a vanishingly small contribution to the net current. However, as is seen later, it is possible for trajectories evolving on a chaotic attractor in a higher dimensional phase-space to produce a non-zero current.

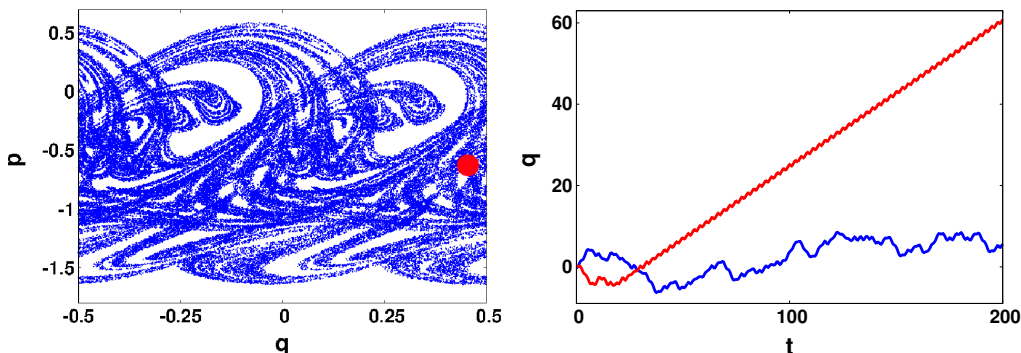


Figure 30: (Colour Online) Deterministic driven and damped dynamics of two coupled units, as defined by Eqs. (78)-(79). Left panel: Stroboscopic map with sampling rate  $2\pi/\Omega$ , with  $\Omega$  being the frequency of the two external periodic driving forces. Shown are the strange (blue) and periodic (red) attractors corresponding to driving strengths  $F_1 = 1.3$  and  $F_2 = 1.5$  respectively, in the uncoupled  $\kappa = 0.0$  regime. The remaining system parameters are the damping strength  $\gamma = 0.1$ , the driving frequency  $\Omega = 2.25$ , and the driving phase  $\theta_0 = 0$ . The coordinates  $q$  are given mod (1). The dot (red) has been enlarged for emphasis. Right panel: A corresponding example trajectory for motion on the strange (blue line) and periodic (red line) attractor. Source: Figure taken from Ref. [136].

Thus, the single particle system exhibits a rich source of interesting dynamics. The full system, Eq. (78) and Eq. (79), presents a further opportunity for new and interesting behaviours. For now consider the uncoupled case  $\kappa = 0$ . Thus, depending on the strength of the driving amplitudes  $F_1$  and  $F_2$  (with the remaining parameters as given above), there are a number of possible combinations of attractor for the underlying subsystems. For driving amplitudes  $F = 1.3$  (strange chaotic attractor) and  $F = 1.5$  (regular attractor) there are three combinations of attractors for the underlying subsystems - regular/regular, regular/strange, and strange/strange. The complexity of this system arises when the two subsystems are coupled, i.e  $\kappa \neq 0$ .

With a view to the discussion in Sec. 3.3 regarding symmetries, it is worth briefly exploring the symmetry properties of this system which now includes driving and damping terms. To begin, let us assume equal driving amplitudes  $F_1 = F_2$ . Firstly note that the particle exchange symmetry  $q_1 \rightarrow q_2$ ,  $q_2 \rightarrow q_1$  is preserved. Thus synchronous solutions, for example, are permitted. However, time-reversibility is broken here due to damping, meaning that these systems have a clear direction of time (which is easily verified by applying the time-reversal operator to the equations of motion). This is a generic feature of dissipative systems. The implication is that applying the time-reversal operator to a *forward* trajectory does not necessarily produce another trajectory that is permitted under the equations of motion. Going further, the corresponding *backward* trajectory that would cancel the forward trajectories contribution to the net current is not obtained through the time-reversal operation. In this sense, all sets of initial condition are be biased. This is only a necessary condition for the generation of a non-zero net current. The actual current is determined by the basins of attraction in which the initial conditions lie, and by extension their corresponding attractors. Finally, in the case of unequal driving amplitudes  $F_1 \neq F_2$  the above discussion

on time-reversibility is still valid. The difference now is that the particle exchange symmetry is broken, and thus synchronous motion becomes hindered (except in the range of very strong coupling between the units).

We now look at the transport features present in the system.

### 3.3.2. Features of collective driven transport

In this section we examine a very particular type of solution for the full system. This solution, which is named the *periodic running solution*, is desirable for achieving directed particle transport.

The periodic running solutions are characterised by

$$q_i(t+T) = q_i(t) + m_i, \quad \dot{q}_i(t+T) = \dot{q}_i(t), \quad i = 1, 2, \quad (80)$$

where  $T$  is the duration of the period, and the  $m_i$  are constants representing the distance travelled over the course of a period. This is a periodic running solution in that over one period the particles each travel a uniform distance, and yet the momentum variables are periodic in the standard sense. Notice that such a solution has a non-zero average velocity. That is

$$\langle \dot{q}_i \rangle = \frac{1}{T} \int_0^T dt \dot{q}_i(t) = \frac{m_i}{T} \neq 0. \quad (81)$$

Thus particle  $i$  runs to the right (left) when  $m_i > 0$  ( $m_i < 0$ ), for  $i = 1, 2$ . For the dimer the net transport may be zero if  $m_1 + m_2 = 0$ , that is  $m_1 = -m_2$  and the particles run in a counterpropagating fashion with the same average velocity. However, this solution is not possible.

The main results regarding the character of periodic running solutions are contained in a theorem in [129] and can be summarised as follows: By assuming such a solution, described by Eq. (80), it has been possible to deduce important features of transport when the particles are in a periodic running state. Firstly, in such a state the particles will travel an equal distance and counterpropagating trajectories are excluded, i.e. the particles must travel in the same direction, viz.  $m_1 = m_2$ . Further, non-trivial periodic solutions are impossible without the time-periodic external modulations. That is, all periodic running solutions must be frequency locked to certain multiples of the external time-periodic modulations. In more detail, let  $F(t) = F \sin(\Omega t + \Theta_0)$ , with period  $T_0 = 2\pi/\Omega$ , represent the external time-periodic driving of the system. For solutions that are frequency-locked to  $F(t)$ , it holds that the distance between the particles performs periodic oscillations, i.e.

$$q_1(t+T) - q_2(t+T) = q_1(t) - q_2(t) \quad (82)$$

Moreover, the period  $T$  is determined by

$$T = 2lT_0 \quad (83)$$

for some  $l \in \mathbb{Z}$ . The coordinates obey

$$q_1\left(t + \frac{1}{2}T\right) = q_2(t) + k, \quad q_2\left(t + \frac{1}{2}T\right) = q_1(t) + k, \quad (84)$$

with  $k \in \mathbb{Z} \setminus \{0\}$  and hence

$$q_i(t+T) = q_i(t) + 2k, \quad i = 1, 2. \quad (85)$$

The existence of periodic running solutions is remarkable as with the help of a multidimensional Melnikov method it can be proven that the system exhibits Smale horseshoe chaos in its dynamics and hence, is nonintegrable (for details see [129]).

Let us look closer at the periodic running solutions described by Eq. (80). It is clear that in the uncoupled regime,  $\kappa = 0$ , a periodic running solution is not possible given that both particles have trajectories that evolve on strange attractors. Turning to the coupled regime, notice then that in the case of identical particle motion, or in-phase motion, the particles effectively decouple. Thus the dynamics is determined by two independent units which evolve on strange chaotic attractors. This holds for all values of  $\kappa$  showing that

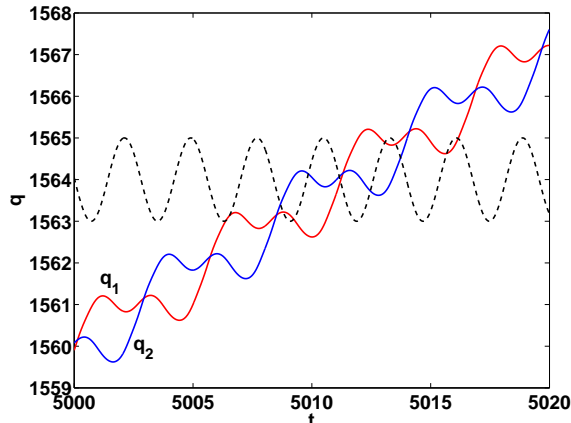


Figure 31: (Colour Online) Time evolution of the coordinates  $q_{1,2}(t)$  of the two interacting driven and damped units in a periodic running state that is frequency-locked to the external time-periodic modulation. The system dynamics are defined by Eqs. (78)-(79). The parameter values are given by  $\Omega = 2.25$ ,  $F_1 = F_2 = 1.3$ ,  $\theta_0 = 0$ ,  $\gamma = 0.1$ , and  $\kappa = 0.46$ . For comparison,  $\sin(\Omega t)$  oscillating around  $q = 1564$  with unit amplitude and frequency  $\Omega = 2.25$  is shown (dashed line). Source: Figure taken from Ref. [129].

transporting in-phase (synchronous) motion supported by a regular periodic attractor is excluded. However, this does not exclude the possibility of a periodic running solution where the two particles have motions that are out of phase. Such a solution can be seen in Fig. 31 where the time evolution of the coordinates  $q_{1,2}$  is shown, and the coupling strength is chosen as  $\kappa = 0.46$ . It is apparent that both are frequency locked to the external driving. This is also illustrated in Fig. 31 by the inclusion of the function  $F(t) = \sin(2.25t)$  oscillating around  $q = 1564$ . This figure highlights the *cooperation* between the particles which allows directed transport to take place. One unit will move backward in order for both units to move forward. In an alternating manner, one unit will sacrifice for the benefit of the dimer.

Importantly, from Fig. 31 it can be deduced that the temporal behaviour of the coordinates follows the relations given in Eqs. (82)-(85).

Concerning the influence of the coupling, let us take as example coupling strengths  $\kappa = 0$ , where there exist strange attractors for both particles, and  $\kappa = 0.46$ , where the motion can be periodic, it seems that the coupling strength plays a key role for the dynamics of the system. The fact that the system exhibits rich and complex dynamics is expected given that the phase-space is five dimensional. Conversely, the fact that the two chaotic subsystems can combine to produce regular periodic motion is less expected. This is quite important as it confirms that there is a phenomenon in which *chaos combines with chaos to form regular periodic motion*. By this, it is meant that in the uncoupled regime both subsystems support chaotic motion, but in the coupled regime there exist periodic solutions.

With regard to the emergence of a non-zero current, the favourable coupling strengths are those that are associated with motion on periodic attractors in phase space. It may be the case though that there are multiple coexisting attractors, each contributing to overall dynamics with a different weight, and it is these weights that determine the strength of the resulting net current. These weights can of course be related to the size of the corresponding basin of attraction [129]. Conversely, there exist values of the coupling strength yielding symmetry between coexisting attractors which take trajectories in opposite directions. Thus an equal number of trajectories travel in the range of positive and negative coordinates, i.e. the basins of attraction, promoting motion in different directions, are of the same size. This results in a zero current.

### 3.3.3. Interaction-induced negative mobility

Here we review work on the driven and damped dynamics of two coupled units evolving in a symmetric and periodic substrate potential which is subjected to a static bias force of magnitude  $F_0$  serving to tilt the

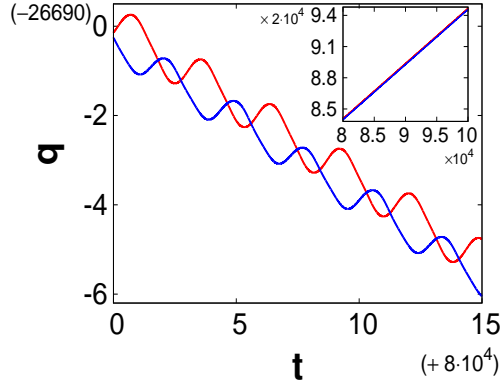


Figure 32: (Colour Online) Example trajectories of two driven and damped units in a biased periodic potential with dynamics given by Eqs. (86)-(87) (red and blue curves respectively). Inset: Time evolution of the two uncoupled units ( $\kappa = 0$ ), travelling with the bias force. Although not visible on the scale of this figure, the two curves do not overlap due to the individual units experiencing different initial transient dynamics before they enter the periodic regime with motion in the direction of the bias force. Main panel: Time evolution of the two coupled units ( $\kappa = 0.327$ ) which are travelling in the opposite direction to the bias force. The two lines represent the trajectories of the individual units. The remaining parameters are as follows: the constant external bias force  $F_0 = 0.1$ , damping  $\gamma = 0.11$ , periodic driving strength  $F = 1.3$ , driving frequency  $\Omega = 2.22$ , and driving phase  $\theta_0 = 0$ . Note the different time scales. Source: Figure adapted from Ref. [111].

potential landscape such that unit motion to the right is favoured [111]. In addition, each unit is driven by an external time-dependent modulation of amplitude  $F$ , frequency  $\Omega$ , and phase  $\theta_0$  with the same magnitude, but out-of-phase, to its counterpart. It is shown that, within a range of coupling strengths, the coupled units can become self-organised and go, as periodic running states, frequency locked with the driving, against the direction of the bias force.

The equations of motion for this system are given by [111]

$$\ddot{q}_1 = -\sin(2\pi q_1) - \gamma \dot{q}_1 - F \sin(\Omega t + \theta_0) - \kappa(q_1 - q_2) + F_0, \quad (86)$$

$$\ddot{q}_2 = -\sin(2\pi q_2) - \gamma \dot{q}_2 + F \sin(\Omega t + \theta_0) + \kappa(q_1 - q_2) + F_0. \quad (87)$$

Notice the out-of-phase character of the periodic modulation of the two units expressed by the different sign of the modulation amplitude  $F$ . The additional parameters  $\gamma$  and  $\kappa$  regulate the strength of the damping and coupling respectively.

We stress that in our system the two units, forming a dimer, are supposed to perform one-dimensional motion in parallel directions each of them in a washboard potential. That is, for equal coordinates  $q_1 = q_2 = q$  the axis of the dimer (virtual line connecting the two units) is perpendicular to the  $q$ -direction.

In general, the system will exhibit a rich and varied behaviour as a function of its parameters  $\gamma$ ,  $F$ ,  $\kappa$ ,  $\omega$ ,  $\theta_0$ , and  $F_0$ . However, one of our main objectives, as was previously mentioned, is to explore coupling phenomena within the system, and therefore in much of this study we will fix the remaining parameters while varying the coupling parameter  $\kappa$ .

Fig. 32 displays the existence of negative mobility, i.e. solutions in which the motion goes against the direction of bias. Below we demonstrate that the mechanism allowing for such motion is cooperation between the units where they pull each other over consecutive potential barriers. In more detail, a coordinated energy exchange between the units allows them to collectively climb against the direction of the tilt.

As an explanation of this phenomena, we describe the mechanism that makes negative mobility possible. Fig. 33 shows snapshots of a two-unit compound moving in the opposite direction of the bias force where

the units move in the respective potential landscape given by

$$U(q_1, t) = \frac{1}{2\pi}(1 - \cos(2\pi q_1)) + F \sin(\Omega t + \theta_0)q_1 - F_0 q_1, \quad (88)$$

$$U(q_2, t) = \frac{1}{2\pi}(1 - \cos(2\pi q_2)) - F \sin(\Omega t + \theta_0)q_2 - F_0 q_2. \quad (89)$$

(Note that the potential energy as given above relates to the on-site potential not containing the unit interaction part). These seven snapshots, taken over one period of the driving, show the relative position of each unit (henceforth unit 1 - left panels and unit 2 - right panels) versus its position in the potential landscape. In addition, arrows where present indicate the direction and magnitude of momentum for the respective units, with no visible arrow indicating a vanishing momentum. It can be seen that negative mobility is the product of coupling between the units and the effect of the time modulated potential. For example, at the beginning of the period unit 1 has a positive momentum in the direction of the bias force. However, this is countered by the height of the potential barrier, and by the coupling to unit 2 which has an even stronger negative momentum. Thus motion in the direction of bias is hindered. Regarding negative mobility we underline that the opposite time-periodic forces make it only possible that for one unit the current inclination of the washboard potential is of such form that the unit is temporarily locked in a potential well (thus hampering its dragging influence on the other unit in the unwanted direction of the tilt) while the other unit experiences a washboard potential whose current inclination favours motion against the static tilt force  $F_0$ . These phases of temporary locking and running against the tilt alternate between the units. This cooperative effect between the units, together with the finely tuned modulations of the potential combine, for the duration of the period, aiding motion against the bias force. Consequently, in one period of the driving, the dimer moves one spatial period against the bias force.

We remark here that in the work [111] we have also demonstrated the robustness of the motion against the bias of the tilt force with respect to additionally present thermal fluctuations.

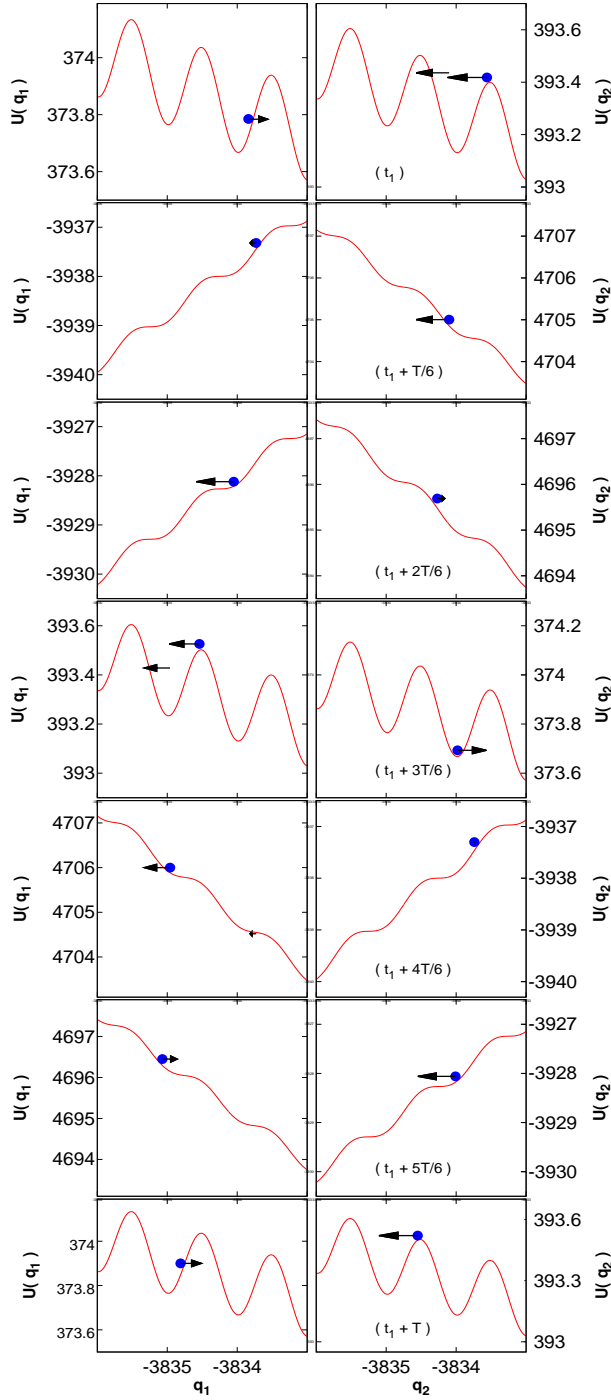


Figure 33: (Colour online) Snapshots of driven and damped dimer motion going against the bias force, taken over a period  $T$  of the external time-periodic modulation. The corresponding equations of motion are Eqs. (86)-(87). Reading from top to bottom, each row shows the evolution advanced by a time  $T/6$  starting from an initial time  $t = t_1$ . The bottom axis is  $q$  and the left/right axes  $U(q)$ . Arrows indicate direction and magnitude of a units momentum. Left (right) column: unit 1 (2). The parameters are set as  $F_0 = 0.1$ ,  $\gamma = 0.11$ ,  $F = 1.3$ ,  $\Omega = 2.22$ ,  $\theta_0 = 0$ , and  $\kappa = 0.372$ . Source: Figure adapted from Ref. [111].

### 3.3.4. Adiabatic driving and directed transport in many unit systems

Here we report on the Hamiltonian dynamics of a one-dimensional chain of linearly coupled units in a spatially periodic potential which is subjected to a slowly varying time-periodic, mono-frequency external force. The average over time and space of the related force vanishes and hence, the system is effectively without bias which excludes any ratchet effect. We pay special attention to the escape of the entire chain when initially all of its units are distributed in a potential well. Moreover for an escaping chain we explore the possibility of the successive generation of a directed flow based on large accelerations.

### 3.3.5. The driven chain system of interacting units

We study a one-dimensional chain system consisting of linearly coupled units with Hamiltonian of the following form [137]

$$H = \sum_{n=1}^N \left[ \frac{p_n^2}{2} + U_0(q_n) + U_1(q_n, t) \right] + \frac{\kappa}{2} \sum_{n=1}^{N-1} (q_{n+1} - q_n)^2, \quad (90)$$

wherein  $p_n$  and  $q_n$  denote the canonically conjugate momenta and positions of the units evolving in the periodic, spatially-symmetric (washboard) potential of unit period, i.e.,

$$U_0(q) = U_0(q + 1) = -\cos(2\pi q)/(2\pi). \quad (91)$$

The external, time-dependent forcing field

$$U_1(q, t) = -F \sin(\Omega t + \Theta_0)q \quad (92)$$

causes time-periodic modulations of the slope of the potential. It has to be stressed that there is no additional bias force involved in the sense that the following average over time and space vanishes, i.e.

$$\int_0^1 dq \int_0^{T=2\pi/\Omega} dt \frac{\partial U(q, t)}{\partial q} = 0, \quad (93)$$

with  $U(q, t) = U_0(q) + U_1(q, t)$ . The units interact linearly with coupling strength  $\kappa$ . Remarkably, as pointed out in prior literature [78] in the limiting case of uncoupled units, i.e.  $\kappa = 0$ , there results an (unexpected) asymmetry of the flux of units, emanating from one potential well, and flowing to the left and right potential wells which indicates the existence of directed transport without breaking the reflection symmetry in space and time in this system. One reason for the occurrence of phase-dependent directed transport is the lowering of the symmetry of the flow in phase space by the ac-field where this asymmetry vanishes only for specific values of the initial phase  $\Theta_0$  [78]. In Ref. [138] the authors report further on this exceptional situation and show that directed transport is sustained on fairly long time scales despite the presence of chaos. In particular it has been demonstrated that for sufficiently small forcing frequencies,  $\Omega \ll 1$ , the width of the arising chaotic layer diverges leading to a strong enhancement of the chaotic transport [138].

The equations of motion derived from the Hamiltonian in Eq. (90) read as

$$\frac{d^2 q_n}{dt^2} + \sin(2\pi q_n) = F \sin(\Omega t + \Theta_0) + \kappa[q_{n+1} + q_{n-1} - 2q_n]. \quad (94)$$

The analysis here deals with zero initial phase of the external force term, viz.  $\Theta_0 = 0$ . The influence of the phase  $\Theta_0$  on the generation of directed motion in the periodic potential  $U_0(q)$  has been studied under adiabatically slow driving in detail in Ref. [139]. We stress that averaging over the initial phase  $\Theta_0$  yields vanishing net current in the periodically driven system.

### 3.3.6. Extremely long transients of directed transport

In our dynamical studies the initial conditions are chosen such that the units are initially contained in a potential well. Furthermore, in the uncoupled case, i.e.  $\kappa = 0$ , escape from the potential well induced by the driving force, as discussed in [139], is excluded. To ensure trapping in the driven but uncoupled dynamics the orbits have to lie fairly deep inside the separatrix, yielding there a large island of stability with dynamics that is still regular.

Likewise, without the *weak* external ac-field and when the units are coupled the chain is supposed to remain trapped in the potential well despite the arising chaotic motion.

In terms of phase space structure we recall that in the case of individual units, i.e.  $\kappa = 0$ , in the corresponding adiabatically driven system of one-and-a-half degree of freedom there arises a broad stochastic layer from the connection of various zones of instability due to resonance overlap. Non-contractible KAM tori confine the stochastic layer from below and above and form impenetrable barriers for motion in phase space. For the weakly nonintegrable system the chaotic sea contains still islands of regular motion. Provided these islands possess non-zero winding numbers orbits with initial condition inside such an island facilitate transport. Moreover, the motion around these islands is characterised by the stickiness to them that can lead to trapping of the trajectory for a long time [127, 75, 140, 80]. This is due the intricate structure of the stochastic layer where close to resonances at the boundary between regular and chaotic regions there exists a hierarchy of smaller and smaller islands and surrounding cantori. The latter can severely restrict the transport in phase space and thus effectively partition the chaotic layer [75, 77].

It seems that the cantori are the less leaky the smaller the modulation frequency  $\Omega$ . Hence they form almost impenetrable barriers that confine trajectories for a very long but *transient* period. One should remark that eventually this transient period of directed motion terminates because the trajectory escapes through one of the holes in the cantori and accesses other regions of the chaotic layer. Therefore the motion does not necessarily proceed unidirectionally and unless the trajectory becomes captured by ballistic channels [122, 85, 86] it iterates within the chaotic layer going along with changes of the direction of motion.

For nonlinear Hamiltonian systems with  $N \geq 2$  degrees of freedom only a few numerical results addressing the existence of an enhanced trapping regime are known [141],[142]. It is supposed that the role played by cantori in driven systems with  $N = 1$  is played by families of  $N$ -dimensional tori, constituting partial barriers in the  $2N$ -dimensional phase space, where the chaotic trajectory can stick to [141],[142]. On the other hand Arnold diffusion is possible and hence in principle a chaotic trajectory, wandering along the entire stochastic layer, can explore the whole phase space [143],[144]. However, due to stickiness to higher dimensional invariant tori Arnold diffusion can be suppressed so that certain stochastic regions are distinguished in which the trajectories become trapped for longer times [141].

We demonstrate that it is possible to generate directed motion with adiabatic periodic modulations of the slope of the spatially periodic potential.

Concerning the initial conditions we proceed in the following way: Initially an amount of energy  $E_n = 0.5p_n^2 + U_0(q_n) \langle \Delta E$  is applied per unit such that the whole chain is elongated homogeneously along a fixed position  $\tilde{q}_0$  near the bottom of the well. Then, the position and/or momenta of all units are randomised. The random position values are chosen from a bounded interval  $|q_n(0) - \tilde{q}_0| \leq \Delta q$  and, likewise, the random initial momenta,  $|p_n(0) - \tilde{p}_0| \leq \Delta p$ . The whole chain is thus initialised close to an almost homogeneous state, but yet sufficiently displaced ( $\Delta q \neq 0$ ) in order to generate non-vanishing interactions, entailing the exchange of energy among the coupled units.

First we note that in the case without external modulation of the slope there occurs the formation of a pattern of localised states due to modulational instability (not depicted here). Due the irregular dynamics it happens that occasionally a unit overcomes the potential barrier but no coordinated motion of the chain results.

Remarkably, applying the adiabatic modulation the entire chain not only escapes from the potential well but manages also to travel freely and unidirectionally over a giant distance as seen from the spatio-temporal evolution of  $q_n(t)$  in Fig. 34. In comparison for faster modulations no directed motion of the chain is obtained. The chain consists of 100 coupled units and open boundary conditions are imposed. The profile of the chain continuously undergoes changes with ensuing deviations from a flat state. Nevertheless the intriguing feature

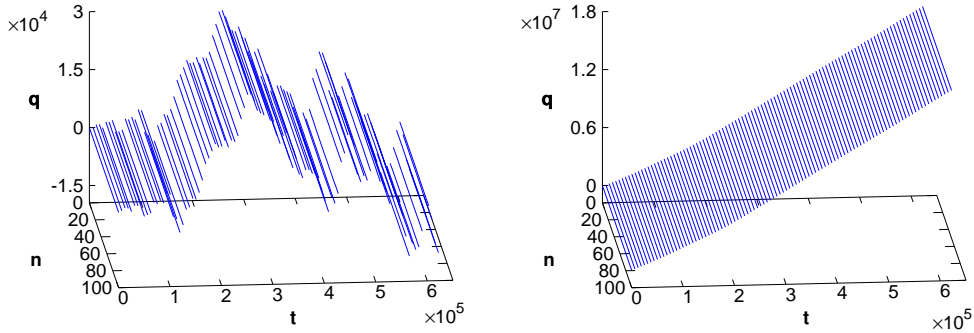


Figure 34: (Colour online) Typical spatio-temporal evolution of the coordinates  $q_n(t)$  for a chain of  $N = 100$  coupled driven units, each evolving in a periodic potential - see Eq. (94). Initially the coordinates are uniformly distributed within the interval  $|q_n(0) - \tilde{q}_0| < \Delta q$  with an average  $\tilde{q}_0 = -0.35$  and width  $\Delta q = 0.01$  and zero momenta, i.e.  $p_n(0) = \tilde{p}_0 = \Delta p = 0$ . The coupling strength is  $\kappa = 0.3$  and the periodic external driving strength and phase are  $F = 0.05$  and  $\Theta_0 = 0$ , respectively. In the left (right) panel, the driving frequency is  $\Omega = 10^{-1}$  ( $\Omega = 10^{-3}$ ). Source: Figure adapted from Ref. [137].

of transients of extremely long-range transport of the chain is provided by collective motion which is also reflected in the temporal behaviour of the mean value of the coordinate  $\langle q \rangle = \langle \frac{1}{N} \sum_{n=1}^N q_n \rangle$  shown in Fig. 35. Ensemble averages, denoted by  $\langle \cdot \rangle$  were performed over 100 realisations of trajectories whose initial condition lie in the range given in the caption of Fig. 34. Note that while for driving with  $\Omega \lesssim 10^{-2}$  on average no directed motion results for sufficiently slow modulations (here illustrated for  $\Omega = 10^{-3}$ ) a large directed current is observed. Conclusively, concerning transport, the many unit system exhibits features equivalent to that observed in the system of individual units [139].

In fact, our findings imply that in the driven  $N$ -unit system the motion takes place in ballistic channels [122] associated with stickiness to  $N$ -dimensional invariant tori. Notably, in the  $N$ -unit system the mean value  $\langle q \rangle$  evolves in the same manner as the single coordinate in the individual unit counterpart, viz. it exhibits effective growth. Thus, the collective directed motion of the numerous microscopic degrees of freedom is manifested at a collective level in the evolution of the mean value of  $q$ .

#### 4. Summary and outlook

This review has considered systems of coupled oscillatory units, both in the absence and presence of time-dependent forcing and/or environmental noise sources. The main focus was on the objective of dynamics driven escape events and in the case of non-confining potential landscapes on the possibility of undergoing an escape driven directed transport. By use of both analytical and numerical means, the main goal has been to develop a thorough understanding of the coupled nonlinear dynamics in such systems. Of particular interest were the conditions under which collective escape and/or directed transport may emerge. Sometimes this is a trivial artefact of the initial conditions, including the choice of suitable parameter regimes. Given the case, for example, that there is insufficient energy available for the particles to overcome the potential barriers, would then imply a vanishing transport and consequently no emerging directed current. It may also be the case that there is sufficient energy available, but the coupling between the particles is rather weak so that the initial direction of motion may be maintained, yielding a non-zero current. However, quite often it is the case that escape and subsequent directed transport can only emerge within a synergy where the particles work together. That is, cooperative effects become then prominent in yielding possible escape and/or finite transport.

A key point that has been evident throughout this review is that the constructive cooperation between the particles allows for novel escape mechanisms and transport scenarios that are absent in the case of a single particle dynamics. Consider three examples; a first one elaborated in Sec. 2.1.1, a second one from Sec. 3.2, and yet another from Sec. 3.3. In Sec. 2.1.1, we elucidated the case of a noise-free, i.e. a purely

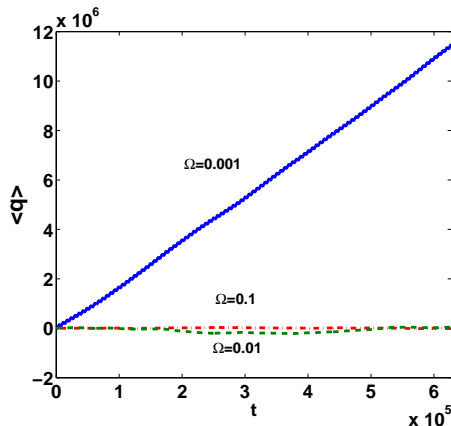


Figure 35: (Colour Online) Temporal evolution of the mean value  $\langle q \rangle = \langle \frac{1}{N} \sum_{n=1}^N q_n \rangle$  for chains of  $N = 100$  coupled units, each evolving in a periodic potential, driven with different driving frequencies as indicated in the plot. The corresponding equations of motion are described by Eq. (94). Ensemble averages, denoted by  $\langle \cdot \rangle$  were performed over 100 realisations of the initial conditions: Initially the coordinates of each unit are uniformly distributed within the interval  $|q_n(0) - \tilde{q}_0| < \Delta q$  with an average  $\tilde{q}_0 = -0.35$  and width  $\Delta q = 0.01$  and zero momenta, i.e.  $p_n(0) = \tilde{p}_0 = \Delta p = 0$ . The coupling strength is  $\kappa = 0.3$  and the periodic external driving strength and phase are  $F = 0.05$  and  $\Theta_0 = 0$ , respectively. Source: Figure adapted from Ref. [137].

deterministic scenario, as well as a thermally activated, noise-assisted escape process of a chain of coupled units out of a metastable potential well. Strikingly, in the noise-free situation the chain is not only able to generate a critical elongation in a very efficient self-organised manner, thereby successfully surpassing the potentials local maximum, but generally can also outperform its thermally activated counterpart by achieving (especially for smaller energies) a considerably enhanced escape. In the deterministic (noise-free) case, a substantial cooperation between the units expedites the formation of the critical configuration, viz. the transition state, whereas thermal noise may impinge on such cooperativity. In Sec. 3.2 it was observed that a resting particle is able to escape from its initial confining well and undergo directed transport, after a transient period of chaotic energy exchange with a second particle. If the particles were uncoupled, this initially dwelling particle would remain trapped indefinitely as this system obtains no assistance from external perturbations. Therefore, it is exclusively cooperation between the particles that allows the initially resting particle to become transporting. Conversely, the process of a permanent bond formation (dimerisation) may result, as a consequence of the coupling, yielding no net transport. In view of a potential for beneficial applications, this process may be seen as a filter, capturing/blocking a particle by impeding its movement. As a second example, let us turn to Sec. 3.3.1. For the particular model considered there, if the subsystems are uncoupled, then the dynamics is chaotic with the individual particles exploring strange attractor dynamics. However, when the particles are coupled, it is possible that the motion can become regular and periodic, cf. Fig. 31. Therefore, working synergetically together the particles can suppress the effects of chaos. This effect of suppression of chaos has been observed in [136], where the systems only positive Lyapunov exponent (in the uncoupled limit) decreased almost to zero as a result of coupling between the particles.

This review also examined two different coupling regimes. In Sec. 3.2 the coupling was short-range in nature, allowing for the effective decoupling of the particles (through increasing distance between the particles). In contrast, the coupling used in Sec. 3.2 was such that the particles remain coupled even when the distance between them is large. It is worth (briefly) discussing the differences between these regimes.

The conservative Hamiltonian systems of Sec. 3.2 were endowed with an initial small energy. Using a long range coupling regime in this case would preclude the unbounded directed motion of a single particle, as the energy would quickly become usurped by the interaction potential. Thus, many of the transport scenarios discussed in Sec. 3.2 would not occur. Therefore, it is preferable to work with a short range coupling in this case.

For the time-dependent driven and damped systems of Sec. 3.3 the external driving force can cause the rapid separation of the particles. For short-range couplings this results in effectively decoupling the particle dynamics after short periods of time, even for relatively strong coupling strengths. The dynamics in this case are not of potential use. This, however, no longer holds true for long-range coupling where the dynamics have proven to be beneficial.

While the second part of this review looked mainly at systems of two coupled oscillators, it is certainly worthwhile to extend these results to similar systems with an arbitrary number of degrees-of-freedom. One of the challenges is to develop (reduction) tools, alternative to the method of Poincaré maps, with which the underlying geometrical phase space structures such as invariant hypertori in higher-dimensional phase-spaces can be visualized appropriately. However, this task becomes hopeless rather quickly with increasing particle number  $N$  (or, more generally increasing number of degrees-of-freedom). This feature is a consequence of the Froschlé conjecture [145]. Therefore, it is appropriate to have a gradual approach to dimensional increase (as suggested by [146] for the problem of chaotic scattering in higher dimensional systems). Work in this direction has already been carried out; see, for example, in Ref. [147]. Those authors used a technique known as *colour and rotation*, where 3D projections of a 4D space are produced and the fourth dimension is represented by colour. While this approach does provide useful information, it is not applicable to large dimensional systems.

Furthermore, the transition from regular to chaotic motion in higher-dimensional phase-spaces, assisted by unstable periodic orbits needs to be investigated. That is, in order to gain insight into the transition from stability to complex instability the structure of invariant manifolds associated with unstable periodic orbits needs to be explored. In particular with regard to the emergence of transport scenarios in higher-dimensional phase-spaces, the question of whether the phenomenon of stickiness of chaotic orbits to the vicinity of periodic orbits is exhibited by higher-dimensional dynamical systems is of interest. Moreover, diffusive features in higher dimensional systems entailed by motion along unstable invariant manifolds, corresponding to unstable periodic orbits with distinct magnitudes of eigenvalues of the linearised systems merit to be addressed. A question of interest is whether multiple channels supporting diffusive behaviour coexist, or whether there emerges a single dominant channel that prevails.

Further, it is worth considering the stochastic counterpart of the systems considered in the second part of this review. The introduction of noise to a system affects the dynamics in numerous ways, depending on the type of noise and its strength. With regard to solutions of a system, particularly periodic solutions, noise can be added to test the solutions stability. However, of interest is the study of how trajectories that are close to a separatrix, which separates bounded from unbounded motion, behave. For example, can those trajectories that are in bounded regions of phase-space (or at a localisation/de-localisation transition in parameter space) be subsequently kicked, under the influence of noise, into unbounded regions of phase-space? Conversely, for those trajectories in unbounded regions of phase-space, is noise enhanced trapping [148] a feature of the stochastic system?

Last but not least, our review here has been restricted to an interacting classical nonlinear dynamics. The inclusion of quantum effects are much more demanding, both analytically and numerically. On the other hand, the phenomenon of quantum tunneling and chaos assisted tunneling does reveal new routes for escape that are not classically available. This may well enrich the characteristics for escape and directed and driven quantum transport [149]. In this spirit there remains plentiful space and time for exciting future developments.

## 5. Acknowledgements

The authors thank Sergej Flach and Anna Deluca Silberberg for constructive and insightful discussions. Further, we would like to give acknowledgement to former coauthors including S. Fugmann, S. Martens, T. Gross, A.D. Brubanks, and A.H. Osbaldestin. This research was supported by the Volkswagen-Foundation projects I/80425 (L.S.-G.) and I/80424 (P.H.) the DFG Sachbeihilfen HA1517/31-2, and HA1517/35 (P.H.). This work was partially supported by the European Union, Seventh Framework Programme (FP7-REGPOT-2012-2013-1) under grant agreement 316165 (G.T.). L.S-G would like to acknowledge DFG-IRT1740 for financial support.

## 6. References

### References

- [1] P. Hänggi, P. Talkner, M. Borkovec, [Reaction-rate theory - 50 years after Kramers](#), *Rev. Mod. Phys.* 62 (1990) 251.
- [2] E. Pollak, P. Talkner, [Reaction rate theory: What it was, where is it today, and where is it going?](#), *Chaos* 15 (2005) 026116.
- [3] P. Hänggi, [Escape from a metastable state](#), *J. Stat. Phys.* 42 (1986) 105.
- [4] P. Hänggi, [Addendum and erratum](#), *J. Stat. Phys.* 44 (1986) 1003.
- [5] J. S. Langer, [Statistical theory of the decay of metastable states](#), *Ann. Phys.* 54 (1969) 258.
- [6] B. V. Petukhov, V. L. Pokrovskii, [Quantum and classical dislocation motion in a Peierls potential relief](#), *Zh. Eksp. Teor. Fiz.* 63 (1972) 634, [English translation: Sov. Phys. JETP](#) 36 (1973) 336.
- [7] M. Büttiker, R. Landauer, [Nucleation theory of overdamped soliton motion](#), *Phys. Rev. A* 23 (1981) 1397.
- [8] P. Hänggi, F. Marchesoni, P. Sodano, [Nucleation of thermal sine-Gordon solitons: Effect of many-body interactions](#), *Phys. Rev. Lett.* 60 (1988) 2563.
- [9] P. Hänggi, F. Marchesoni, [Breathers and kink-antikink nucleation](#), *Phys. Rev. Lett.* 77 (1996) 787.
- [10] F. Marchesoni, L. Gammaitoni, A. R. Bulsara, [Spatiotemporal stochastic resonance in a  \$\varphi^4\$  model of kink-antikink nucleation](#), *Phys. Rev. Lett.* 76 (1996) 2609.
- [11] W. Sung, P. J. Park, [Polymer translocation through a pore in a membrane](#), *Phys. Rev. Lett.* 77 (1996) 783.
- [12] P. J. Park, W. Sung, [Polymer release out of a spherical vesicle through a pore](#), *Phys. Rev. E* 57 (1998) 730.
- [13] K. L. Sebastian, A. K. R. Paul, [Kramers problem for a polymer in a double well](#), *Phys. Rev. E* 62 (2000) 927.
- [14] S. Lee, W. Sung, [Coil-to-stretch transition, kink formation, and efficient barrier crossing of a flexible chain](#), *Phys. Rev. E* 63 (2001) 021115.
- [15] K. Lee, W. Sung, [Barrier crossing of a semiflexible ring polymer](#), *Phys. Rev. E* 64 (2001) 041801.
- [16] P. Kraikivski, R. Lipowsky, J. Kierfeld, [Barrier crossing of semiflexible polymers](#), *Europhys. Lett.* 66 (2004) 763.
- [17] M. T. Downton, M. J. Zuckermann, E. M. Craig, M. Plischke, H. Linke, [Single-polymer Brownian motor: A simulation study](#), *Phys. Rev. E* 73 (2006) 011909.
- [18] P. Hänggi, F. Marchesoni, F. Nori, [Brownian motors](#), *Ann. Phys. (Leipzig)* 14 (2005) 51.
- [19] R. D. Astumian, P. Hänggi, [Brownian motors](#), *Physics Today* 55 (11) (2002) 33.
- [20] P. Reimann, P. Hänggi, [Introduction to the physics of Brownian motors](#), *Appl. Phys. A* 75 (2002) 169.
- [21] C. Cattuto, F. Marchesoni, [The kink-counting problem: Equilibrium densities and nucleation rates](#), *Europhys. Lett.* 62 (2003) 363.
- [22] P. Hänggi, F. Marchesoni, [Artificial Brownian motors: Controlling transport on the nanoscale](#), *Rev. Mod. Phys.* 81 (2009) 387.
- [23] P. Reimann, G. J. Schmid, P. Hänggi, [Universal equivalence of mean first-passage time and Kramers rate](#), *Phys. Rev. E* 60 (1999) R1.
- [24] J. Lehmann, P. Reimann, P. Hänggi, [Surmounting oscillating barriers](#), *Phys. Rev. Lett.* 84 (2000) 1639.
- [25] R. S. Maier, D. L. Stein, [Noise-activated escape from a sloshing potential well](#), *Phys. Rev. Lett.* 86 (2001) 3942.
- [26] J. Lehmann, P. Reimann, P. Hänggi, [Activated escape over oscillating barriers: The case of many dimensions](#), *Phys. Stat. Sol. (b)* 237 (2003) 53.
- [27] P. Talkner, L. Machura, M. Schindler, P. Hänggi, J. Luczka, [Statistics of transition times, phase diffusion and synchronization in periodically driven bistable systems](#), *New J. Phys.* 7 (2005) 14.
- [28] W. Forst, *Theory of Unimolecular Reaction*, Academic Press, New York, 1971.
- [29] M. Remoissenet, *Waves called solitons: Concepts and Experiments*, Springer-Verlag, Berlin, 1999.
- [30] R. S. MacKay, S. Aubry, [Proof of existence of breathers for time-reversible or Hamiltonian networks of weakly coupled oscillators](#), *Nonlinearity* 7 (1994) 1623.
- [31] S. Aubry, [Breathers in nonlinear lattices: Existence, linear stability and quantization](#), *Physica D* 103 (1997) 201.
- [32] S. Flach, C. R. Willis, [Discrete breathers](#), *Phys. Rep.* 295 (1998) 181.
- [33] P. Marquié, J. M. Bilbault, M. Remoissenet, [Observation of nonlinear localized modes in an electrical lattice](#), *Phys. Rev. E* 51 (1995) 6127.
- [34] H. S. Eisenberg, Y. Silberberg, R. Morandotti, A. R. Boyd, J. S. Aitchison, [Discrete spatial optical solitons in waveguide arrays](#), *Phys. Rev. Lett.* 81 (1998) 3383.
- [35] P. Binder, D. Abramov, A. V. Ustinov, S. Flach, Y. Zolotaryuk, [Observation of breathers in Josephson ladders](#), *Phys. Rev. Lett.* 84 (2000) 745.
- [36] M. Peyrard, A. R. Bishop, [Statistical mechanics of a nonlinear model for DNA denaturation](#), *Phys. Rev. Lett.* 62 (1989) 2755.
- [37] T. Dauxois, M. Peyrard, A. R. Bishop, [Dynamics and thermodynamics of a nonlinear model for DNA denaturation](#), *Phys. Rev. E* 47 (1993) 684.
- [38] M. Barbi, S. Cocco, M. Peyrard, [Helicoidal model for DNA opening](#), *Phys. Lett. A* 253 (1999) 358.
- [39] S. Cocco, R. Monasson, [Statistical mechanics of torque induced denaturation of DNA](#), *Phys. Rev. Lett.* 83 (1999) 5178.
- [40] M. Barbi, S. Cocco, M. Peyrard, S. Ruffo, [A twist opening model for DNA](#), *J. Bio. Phys.* 24 (1999) 97.
- [41] J. L. Marín, S. Aubry, [Breathers in nonlinear lattices: Numerical calculation from the anticontinuous limit](#), *Nonlinearity* 9 (1996) 1501.
- [42] D. Hennig, [Periodic, quasiperiodic, and chaotic localized solutions of a driven, damped nonlinear lattice](#), *Phys. Rev. E* 59 (1999) 1637.

- [43] A. Vanossi, K. Ø. Rasmussen, A. R. Bishop, B. A. Malomed, V. Bortolani, [Spontaneous pattern formation in driven nonlinear lattices](#), Phys. Rev. E 62 (2000) 7353.
- [44] P. Maniadis, S. Flach, [Mechanism of discrete breather excitation in driven micro-mechanical cantilever arrays](#), Europhys. Lett. 74 (2006) 452.
- [45] S. Nosé, [A unified formulation of the constant temperature molecular dynamics methods](#), J. Chem. Phys. 81 (1984) 511.
- [46] M. Peyrard, [The pathway to energy localization in nonlinear lattices](#), Physica D 119 (1998) 184.
- [47] G. P. Tsironis, S. Aubry, [Slow relaxation phenomena induced by breathers in nonlinear lattices](#), Phys. Rev. Lett. 77 (1996) 5225.
- [48] M. I. Rabinovich, P. Varona, A. I. Selverston, H. D. I. Abarbanel, [Dynamical principles in neuroscience](#), Rev. Mod. Phys. 78 (2006) 1213.
- [49] M. Sato, B. E. Hubbard, A. J. Sievers, [Colloquium: Nonlinear energy localization and its manipulation in micromechanical oscillator arrays](#), Rev. Mod. Phys. 78 (2006) 137.
- [50] S. Takeno, G. P. Tsironis, [Energy localization and molecular dissociation](#), Phys. Lett. A 343 (2005) 274.
- [51] S. Denisov, S. Flach, P. Hänggi, [Tunable transport with broken space-time symmetries](#), Phys. Rep. 538 (2014) 77.
- [52] R. Eichhorn, P. Reimann, P. Hänggi, [Brownian motion exhibiting absolute negative mobility](#), Phys. Rev. Lett. 88 (2002) 190601.
- [53] R. Eichhorn, P. Reimann, P. Hänggi, [Paradoxical motion of a single Brownian particle: Absolute negative mobility](#), Phys. Rev. E 66 (2002) 066132.
- [54] R. Eichhorn, P. Reimann, B. Cleuren, C. Van Den Broeck, [Moving backward noisily](#), Chaos 15 (2005) 026113.
- [55] L. Machura, M. Kostur, P. Talkner, J. Luczka, P. Hänggi, [Absolute negative mobility induced by thermal equilibrium fluctuations](#), Phys. Rev. Lett. 98 (2007) 040601.
- [56] M. Kostur, L. Machura, P. Talkner, P. Hänggi, J. Luczka, [Anomalous transport in biased ac-driven Josephson junctions: Negative conductances](#), Phys. Rev. B 77 (2008) 104509.
- [57] T. Gross, D. Hennig, L. Schimansky-Geier, [Self-organized Escape Processes of Linear Chains in Nonlinear Potentials](#), World Scientific, 2014.
- [58] D. Hennig, S. Fugmann, L. Schimansky-Geier, P. Hänggi, [Self-organized escape of oscillator chains in nonlinear potentials](#), Phys. Rev. E 76 (2007) 041110.
- [59] D. Hennig, L. Schimansky-Geier, P. Hänggi, [Self-organized, noise-free escape of a coupled nonlinear oscillator chain](#), EPL 78 (2007) 20002.
- [60] G. Henkelman, H. Jónsson, [A dimer method for finding saddle points on high dimensional potential surfaces using only first derivatives](#), J. Chem. Phys. 111 (1999) 7010.
- [61] Y. S. Kivshar, M. Peyrard, [Modulational instabilities in discrete lattices](#), Phys. Rev. A 46 (1992) 3198.
- [62] I. Daumont, T. Dauxois, M. Peyrard, [Modulational instability: First step towards energy localization in nonlinear lattices](#), Nonlinearity 10 (1997) 617.
- [63] S. Fugmann, D. Hennig, L. Schimansky-Geier, P. Hänggi, [Deterministic escape dynamics of two-dimensional coupled nonlinear oscillator chains](#), Phys. Rev. E 77 (2008) 061135.
- [64] T. Gross, D. Hennig, L. Schimansky-Geier, [Modulational instability and resonant wave modes act on the metastability of oscillator chains](#), Phys. Rev. E 90 (2014) 032919.
- [65] S. Dos Santos, V. Sánchez-Morcillo, N. Jiménez, A.-P. Abellard, A. Bouakaz, [Modulational instability of microbubbles surface modes](#), AIP Conf. Proc. 1433 (2012) 311.
- [66] D. Hennig, L. Schimansky-Geier, P. Hänggi, [Surmounting collectively oscillating bottlenecks](#), EPL 83 (2008) 60008.
- [67] D. Hennig, C. Mulhern, A. D. Burbanks, L. Schimansky-Geier, [Nonlinear response of a linear chain to weak driving](#), Phys. Rev. E 89 (2014) 012906.
- [68] E. Bright Wilson Jr., J. C. Decius, P. C. Cross, [Molecular vibrations: The theory of infrared and Raman vibrational spectra](#), McGraw-Hill, New York, 1955.
- [69] M. L. Sage, J. Jortner, [Bond Modes](#), John Wiley & Sons, Inc., 1981.
- [70] R. H. Page, Y. R. Shen, Y. T. Lee, [Local modes of benzene and benzene dimer, studied by infrared-ultraviolet double-resonance in a supersonic beam](#), J. Chem. Phys. 88 (1988) 4621.
- [71] D. Hennig, G. P. Tsironis, H. Gabriel, [Hamiltonian approach to the dissociation of a coupled nonlinear exciton-vibron system](#), Phys. Rev. E 49 (1994) 3653.
- [72] A. J. Sievers, S. Takeno, [Intrinsic localized modes in anharmonic crystals](#), Phys. Rev. Lett. 61 (1988) 970.
- [73] G. Kopidakis, S. Aubry, G. P. Tsironis, [Targeted energy transfer through discrete breathers in nonlinear systems](#), Phys. Rev. Lett. 87 (2001) 165501.
- [74] N. J. Zabusky, [Computational synergetics and mathematical innovation](#), J. Comp. Phys. 43 (1981) 195.
- [75] R. S. MacKay, J. D. Meiss, I. C. Percival, [Transport in Hamiltonian systems](#), Physica D 13 (1984) 55.
- [76] L. E. Reichl, [The transition to chaos in conservative systems: Quantum manifestations](#), Springer-Verlag, Berlin, 1992.
- [77] G. Radons, T. Geisel, J. Rubner, [Classical chaos versus quantum dynamics: Kam tori and cantori as dynamical barriers](#), Adv. Chem. Phys. 73 (1989) 891.
- [78] O. Yevtushenko, S. Flach, K. Richter, [ac-driven phase-dependent directed diffusion](#), Phys. Rev. E 61 (2000) 7215.
- [79] S. Denisov, S. Flach, A. A. Ovchinnikov, O. Yevtushenko, Y. Zolotaryuk, [Broken space-time symmetries and mechanisms of rectification of ac fields by nonlinear \(non\)adiabatic response](#), Phys. Rev. E 66 (2002) 041104.
- [80] S. Denisov, S. Flach, P. Hänggi, [Stationary Hamiltonian transport with dc bias](#), Europhys. Lett. 74 (2006) 588.
- [81] H. Schanz, M. F. Otto, R. Ketzmerick, T. Dittrich, [Classical and quantum Hamiltonian ratchets](#), Phys. Rev. Lett. 87 (2001) 070601.
- [82] H. Schanz, T. Dittrich, R. Ketzmerick, [Directed chaotic transport in Hamiltonian ratchets](#), Phys. Rev. E 71 (2005)

- 026228.
- [83] P. Cvitanović, R. Artuso, R. Mainieri, G. Tanner, G. Vattay, [Chaos: Classical and quantum](#), Niels Bohr Institute, Copenhagen, 2012.
  - [84] S. Flach, O. Yevtushenko, Y. Zolotaryuk, [Directed current due to broken time-space symmetry](#), Phys. Rev. Lett. 84 (2000) 2358.
  - [85] S. Denisov, J. Klafter, M. Urbakh, S. Flach, [DC currents in Hamiltonian systems by Lévy flights](#), Physica D 170 (2002) 131.
  - [86] S. Denisov, J. Klafter, M. Urbakh, [Ballistic flights and random diffusion as building blocks for Hamiltonian kinetics](#), Phys. Rev. E 66 (2002) 046217.
  - [87] J. B. Gong, P. Brumer, [Directed anomalous diffusion without a biased field: A ratchet accelerator](#), Phys. Rev. E 70 (2004) 016202.
  - [88] P. Hänggi, R. Bartussek, [Brownian rectifiers: How to convert Brownian motion into directed transport](#), Lect. Notes Phys. 476 (1996) 294.
  - [89] X. Z. Cheng, M. B. A. Jalil, H. K. Lee, [Analytical solution to transport in Brownian ratchets via the gambler's ruin model](#), Phys. Rev. Lett. 99 (2007) 070601.
  - [90] M. O. Magnasco, [Forced thermal ratchets](#), Phys. Rev. Lett. 71 (1993) 1477.
  - [91] R. Bartussek, P. Hänggi, J. G. Kissner, [Periodically rocked thermal ratchets](#), Europhys. Lett. 28 (1994) 459.
  - [92] P. Malgaretti, I. Pagonabarraga, J. M. Rubí, [Cooperative rectification in confined Brownian ratchets](#), Phys. Rev. E 85 (2012) 010105.
  - [93] H. Risken, [The Fokker-Planck-equation \(2nd ed.\): Methods of solution and applications.](#), Springer-Verlag, 1989.
  - [94] D. Hennig, L. Schimansky-Geier, P. Hänggi, [Directed transport of an inertial particle in a washboard potential induced by delayed feedback](#), Phys. Rev. E 79 (2009) 041117.
  - [95] E. Heinsalu, M. Patriarca, F. Marchesoni, [Dimer diffusion in a washboard potential](#), Phys. Rev. E 77 (2008) 021129.
  - [96] D. Hennig, A. D. Burbanks, A. H. Osbaldestin, [Directed transport of two interacting particles in a washboard potential](#), Physica D 238 (2009) 2273.
  - [97] S. Fugmann, D. Hennig, S. Martens, L. Schimansky-Geier, [Deterministic escape of a dimer over an anharmonic potential barrier](#), Physica D 237 (2008) 3179.
  - [98] D. Hennig, S. Martens, S. Fugmann, [Transition between locked and running states for dimer motion induced by periodic external driving](#), Phys. Rev. E 78 (2008) 011104.
  - [99] P. Jung, J. G. Kissner, P. Hänggi, [Regular and chaotic transport in asymmetric periodic potentials: Inertia ratchets](#), Phys. Rev. Lett. 76 (1996) 3436.
  - [100] J. L. Mateos, [Chaotic transport and current reversal in deterministic ratchets](#), Phys. Rev. Lett. 84 (2000) 258.
  - [101] J. L. Mateos, [Current reversals in chaotic ratchets](#), Acta Phys. Polonica B 32 (2001) 307.
  - [102] J. L. Mateos, [Current reversals in chaotic ratchets: The battle of the attractors](#), Physica A 325 (2003) 92.
  - [103] U. E. Vincent, A. Kenfack, D. V. Senthilkumar, D. Mayer, J. Kurths, [Current reversals and synchronization in coupled ratchets](#), Phys. Rev. E 82 (2010) 046208.
  - [104] D. Cubero, V. Lebedev, F. Renzoni, [Current reversals in a rocking ratchet: Dynamical versus symmetry-breaking mechanisms](#), Phys. Rev. E 82 (2010) 041116.
  - [105] L. Machura, M. Kostur, J. Luczka, [Inertial Brownian motors driven by biharmonic signals](#), Chem. Phys. 375 (2010) 445.
  - [106] A. L. R. Bug, B. J. Berne, [Shaking-induced transition to a nonequilibrium state](#), Phys. Rev. Lett. 59 (1987) 948.
  - [107] M. E. Möbius, B. E. Lauderdale, S. R. Nagel, H. M. Jaeger, [Brazil-nut effect: Size separation of granular particles](#), Nature 414 (2001) 270.
  - [108] M. Kostur, L. Machura, P. Hänggi, J. Luczka, P. Talkner, [Forcing inertial Brownian motors: Efficiency and negative differential mobility](#), Physica A 371 (2006) 20.
  - [109] D. Speer, R. Eichhorn, P. Reimann, [Brownian motion: Anomalous response due to noisy chaos](#), EPL 79 (2007) 10005.
  - [110] D. Speer, R. Eichhorn, P. Reimann, [Transient chaos induces anomalous transport properties of an underdamped Brownian particle](#), Phys. Rev. E 76 (2007) 051110.
  - [111] C. Mulhern, D. Hennig, [Current reversals of coupled driven and damped particles evolving in a tilted potential landscape](#), Phys. Rev. E 84 (2011) 036202.
  - [112] D. Speer, R. Eichhorn, M. Evstigneev, P. Reimann, [Dimer motion on a periodic substrate: Spontaneous symmetry breaking and absolute negative mobility](#), Phys. Rev. E 85 (2012) 061132.
  - [113] W. Acevedo, T. Dittrich, [Directed transport in a spatially periodic magnetic billiard](#), Prog. Theor. Phys. Supp. 150 (2003) 313.
  - [114] H. Schanz, M. Prusty, [Directed chaos in a billiard chain with transversal magnetic field](#), J. Phys. A 38 (2005) 10085.
  - [115] M. Horvat, T. Prosen, [Uni-directional transport properties of a serpent billiard](#), J. Phys. A 37 (2004) 3133.
  - [116] L. A. Bunimovich, [Mushrooms and other billiards with divided phase space](#), Chaos 11 (2001) 802.
  - [117] E. G. Altmann, A. E. Motter, H. Kantz, [Stickiness in mushroom billiards](#), Chaos 15 (2005) 033105.
  - [118] E. G. Altmann, A. E. Motter, H. Kantz, [Stickiness in Hamiltonian systems: From sharply divided to hierarchical phase space](#), Phys. Rev. E 73 (2006) 026207.
  - [119] C. Mulhern, [Collective induced phenomena in systems of coupled oscillators](#), Ph.D. thesis, University of Portsmouth, UK (December 2012).
  - [120] H. Kantz, [Billiards \(Online source\)](#).
  - [121] S. J. Lade, [Directed transport without net bias in physics and biology](#), Ph.D. thesis, The Australian National University, Australia (2010).
  - [122] S. Denisov, S. Flach, [Dynamical mechanisms of dc current generation in driven Hamiltonian systems](#), Phys. Rev. E 64

- (2001) 056236.
- [123] O. E. Rossler, [An equation for hyperchaos](#), Phys. Lett. A 71 (1979) 155.
  - [124] S. Bleher, C. Grebogi, E. Ott, [Bifurcation to chaotic scattering](#), Physica D 46 (1990) 87.
  - [125] G. Contopoulos, H. E. Kandrup, D. Kaufmann, [Fractal properties of escape from a two-dimensional potential](#), Physica D 64 (1993) 310.
  - [126] M. Zaslavsky, Chaos in dynamical systems, Harwood, New York, 1985.
  - [127] M. Zaslavsky, Physics of chaos in Hamiltonian systems, Imperial College Press, London, 1998.
  - [128] C. Mulhern, D. Hennig, A. D. Burbanks, A. H. Osbaldestin, [Current reversals and current suppression in an open two-degree-of-freedom system](#), Phys. Rev. E 83 (2011) 066207.
  - [129] D. Hennig, A. D. Burbanks, A. H. Osbaldestin, C. Mulhern, [From collective periodic running states to completely chaotic synchronised states in coupled particle dynamics](#), Chaos 21 (2011) 023132.
  - [130] D. Hennig, A. D. Burbanks, A. H. Osbaldestin, C. Mulhern, [Transient-chaos induced directed transport in a spatially-open Hamiltonian system](#), J. Phys. A 43 (2010) 345101.
  - [131] E. Ott, Chaos in dynamical systems, Cambridge University Press, Cambridge, 1992.
  - [132] D. Hennig, A. D. Burbanks, C. Mulhern, A. H. Osbaldestin, [Emergence of continual directed flow in Hamiltonian systems](#), Phys. Rev. E 82 (2010) 026210.
  - [133] J. S. W. Lamb, J. A. G. Roberts, [Time-reversal symmetry in dynamical systems: A survey](#), Physica D 112 (1998) 1.
  - [134] D. Hennig, A. D. Burbanks, A. H. Osbaldestin, [Directed current in the Holstein system](#), Phys. Rev. E 83 (2011) 031121.
  - [135] T. Dittrich, N. A. Naranjo, [Directed transport in a ratchet with internal and chemical freedoms](#), Chem. Phys. 375 (2010) 486.
  - [136] C. Mulhern, D. Hennig, A. D. Burbanks, [The coupled dynamics of two particles with different limit sets](#), Eur. Phys. J. B 86 (2013) 185.
  - [137] D. Hennig, [Directed transient long-range transport in a slowly driven Hamiltonian system of interacting particles](#), Phys. Lett. A 372 (2008) 6260.
  - [138] S. M. Soskin, O. M. Yevtushenko, R. Mannella, [Divergence of the chaotic layer width and strong acceleration of the spatial chaotic transport in periodic systems driven by an adiabatic ac force](#), Phys. Rev. Lett. 95 (2005) 224101.
  - [139] D. Hennig, L. Schimansky-Geier, P. Hänggi, [Slowly rocking symmetric, spatially periodic Hamiltonians: The role of escape and the emergence of giant transient directed transport](#), Eur. Phys. J. B 62 (2008) 493.
  - [140] J. D. Meiss, E. Ott, [Markov tree model of transport in area-preserving maps](#), Physica D 20 (1986) 387.
  - [141] H. Kantz, P. Grassberger, [Chaos in low-dimensional Hamiltonian maps](#), Phys. Lett. A 123 (1987) 437.
  - [142] E. G. Altmann, H. Kantz, [Hypothesis of strong chaos and anomalous diffusion in coupled symplectic maps](#), EPL 78 (2007) 10008.
  - [143] V. I. Arnold, [Instability of dynamical systems with several degrees of freedom](#), Sov. Math. Dokl. 5 (1964) 581.
  - [144] B. V. Chirikov, [A universal instability of many-dimensional oscillator systems](#), Phys. Rep. 52 (1979) 263.
  - [145] A. J. Lichtenberg, M. A. Leiberman, Regular and chaotic dynamics, Springer-Verlag, New York, 1983.
  - [146] C. Jung, O. Merlo, T. H. Seligman, W. P. K. Zapfe, [The chaotic set and the cross section for chaotic scattering in three degrees of freedom](#), New J. Phys. 12 (2010) 103021.
  - [147] M. Katsanikas, P. A. Patsis, [The structure of invariant tori in a 3-D galactic potential](#), Int. J. Bifurcation Chaos 21 (2011) 467.
  - [148] E. G. Altmann, A. Endler, [Noise-enhanced trapping in chaotic scattering](#), Phys. Rev. Lett. 105 (2010) 244102.
  - [149] S. Kohler, J. Lehmann, P. Hänggi, [Driven quantum transport on the nanoscale](#), Phys. Rep. 406 (2005) 379.